EBOOK-ASTROINFORMATICS SERIES

MACHINE LEARNING IN ASTRONOMY: A WORKMAN'S MANUAL

November 23, 2017

Snehanshu Saha, Kakoli Bora, Suryoday Basak, Gowri Srinivasa,
Margarita Safonova, Jayant Murthy and Surbhi Agrawal

PESIT South Campus
Indian Institute of Astrophysics, Bangalore
M. P. Birla Institute of Fundamental Research, Bangalore

Preface

The E-book is dedicated to the new field of Astroinformatics: an interdisciplinary area of research where astronomers, mathematicians and computer scientists collaborate to solve problems in astronomy through the application of techniques developed in data science. Classical problems in astronomy now involve the accumulation of large volumes of complex data with different formats and characteristic and cannot now be addressed using classical techniques. As a result, machine learning algorithms and data analytic techniques have exploded in importance, often without a mature understanding of the pitfalls in such studies.

The E-book aims to capture the baseline, set the tempo for future research in India and abroad and prepare a scholastic primer that would serve as a standard document for future research. The E-book should serve as a primer for young astronomers willing to apply ML in astronomy, a way that could rightfully be called "Machine Learning Done Right" borrowing the phrase from Sheldon Axler ((Linear Algebra Done Right)! The motivation of this handbook has two specific objectives:

- develop efficient models for complex computer experiments and data analytic techniques which can be used in astronomical data analysis in short term and various related branches in physical, statistical, computational sciences much later (larger goal as far as memetic algorithm is concerned).

- develop a set of fundamentally correct thumb rules and experiments, backed by solid mathematical theory and render the marriage of astronomy and Machine Learning stability and far reaching impact. We will do this in the context of specific science problems of interest to the proposers: the classification of exoplanets, classification of nova, separation of stars, galaxies and quasars in the survey catalogs, and the classification of multi-wavelength sources.

We hope the E-book serves its purpose and inspires scientists across communities to collaborate and develop a very promising field.

.....

Sincerely,

Authors

Contents

1 INTRODUCTION

While developing methodologies for of Astroinformatics, during the next three to five years, we anticipate a number of applied research problems to be addressed. These include:

- Decision-theoretical model addressing exoplanet habitability using the power of convex optimization and algorithmic machine learning: we will focus here on the applicability and efficacy of various machine learning algorithms to the investigation of planetary habitability. There are several different methods available, namely, K-Nearest Neighbor (KNN), Decision Tree (DT), Random Forest (RF), Support Vector Machine (SVM), Na"ive Bayes, and Linear Discriminant Analysis (LDA). We plan to evaluate their performance in the determination of the habitability of exoplanets. PHL's Exoplanet Catalog (PHL-EC) is one of the most complete catalogs which contains observed and estimated stellar and planetary parameters for a total of 3415 (July 2016) currently confirmed exoplanets, where the estimates of the surface temperature are given for 1586 planets. We will test the machine learning algorithms on this and other catalogs to derive the Habitability Index for each planet. Through this, we expect to develop a unified scheme to determine the habitability index of an exoplanet. We will implement a standalone or web-based software package to be applied to any new planets found. Exoplanets are one of the most exciting problems in astrophysics, and we expect large volumes of new data to become available with Gaia and the next generation of dedicated planet hunting missions, including WFIRST and JWST.

- Variational Approaches to eccentricity estimation: The problem of determining optimal eccentricity as a feature in computing the habitability score- Variational Calculus and the theory of Optimal control (Variational Methods in Optimization By Donald R. Smith) will be used.

- Star-Galaxy Classification using Machine Learning: Using the data from Super COSMOS Sky Survey (SSS), we intend to demonstrate the efficiency of gradient boosted methods, particularly that of the XGBoost algorithm, to be able to produce results which can compete with those of other ensemble based machine learning methods in the task of star galaxy classification. Extensive experiments involving cost sensitive learning and variable subset selection shall be carried out which in turn should help resolve some intrinsic problems with the data. The improvisations are expected to work well in handling the complexity of the data set which otherwise has not been attempted in the literature.

- ML Driven Mining and Automatic Labeling of the Habitability Catalog: Classical problems in astronomy are compounded by accumulation of large volume of complex data, rendering the task of classification and interpretation incredibly laborious. The presence of noise in the data makes analysis and interpretation even more arduous. Machine learning algorithms and data analytic techniques provide the right platform for the challenges posed by these problems. Novel Meta-heuristic (Cross culture Evolution based) clustering and probabilistic herding based clustering algorithms will be proposed to investigate the potential habitability of exoplanets by using information from PHL's Exoplanet Catalog (PHL-EC). Accuracy of such predictions is evaluated. The machine learning algorithms are integrated to analyze data from PHL's Exoplanet Catalog (PHL-EC) with specific examples being presented and discussed. Exoplanet, a software for analyzing data obtained from PHL's Exoplanet Catalog via machine learning, will also be developed and deployed in public domain.

- Nova Classification using Machine Learning: We propose a completely novel and never attempted before classification scheme, based on the shape of the light curves obtained from the AAVSO database. Nova eruptions discovered by Payne-Gaposhkin in 1964 occur on the surface of white dwarf stars in interacting binaries, generically called cataclysmic variables by Warner in 1995. They usually have a red dwarf companion star, where material accumulates on the surface until the pressure and temperature become high enough for a thermonuclear runaway reaction to occur. We obtain the light curves for the V-band from the AAVSO database. The AAVSO database has photometric magnitude estimates from amateur and professional astronomers all around the world. This database has magnitudes for roughly 200 novas. A catalog of 93 very well-observed nova light curves has been formed, in which light curves were constructed from numerous individual measured magnitudes and 26 of the light curves following the eruption all the way to quiescent. An automatic classification scheme of nova, not attempted before, is a fundamental contribution beyond reasonable doubt.

2 A Comparative Study in Classification Methods of Exoplanets: Machine Learning Exploration via Mining and Automatic Labeling of the Habitability Catalog

2.1 Introduction

For centuries, astronomers, philosophers and other scientists have considered possibilities of the existence of other planets that could support life as it is on Earth or in different forms. The fundamental question that remains unanswered is: are other extrasolar planets (exoplanets) or moons (exomoons) capable of supporting life? Exoplanet research is one of the newest and most active areas in astrophysics and astroinformatics. In the last decade, thousands of planets were discovered in our Galaxy alone. The inference is that stars with planets are a rule rather than exception, with estimates of the actual number of planet exceeding the number of stars in our Galaxy by orders of magnitude [Strigari et al.(2012)].

Led by the NASA Kepler Mission [Batalha 2014], around 3416 planets have been confirmed, and 4900+ celestial objects remain as candidates, yet to be confirmed as planets. **The discovery and characterization of exoplanets requires both, extremely accurate instrumentation and sophisticated statistical methods to extract the weak planetary signals from the dominant starlight or very large samples. Stars and galaxies can be seen directly in telescopes, but exoplanets can be observed only after advanced statistical analysis of the data. Consequently, statistical methodology is at the heart of almost every exoplanet science result. - from https://www.iau.org/science/events/1135/ - IAU Focus Meetings (GA) FM 8: Statistics and Exoplanets** Different exoplanet detection methods [Fischer et al.2014] include radial velocity based detection, astrometry, transits, direct imaging, and microlensing. Each of these methods posses their own advantages and difficulties [Danielski2014]. For example, detection through radial velocity cannot determine accurately the mass of a distant object [Ridden-Harper et al.2016] but only estimate the minimum mass of a planet, whereas mass is the primary criterion for exoplanet confirmation. Similarly, each method entails its own disadvantages for detection, confirmations and analysis. This requires a careful study and analysis of light curves.

Characterization of Kepler's different planets is important to judge their habitability [Swift et al.2013]. Detailed modeling of planetary signals to extract information of the orbital or atmospheric properties is even more challenging. Moreover, there is also the challenge of inferring the properties of the underlying planet population from incomplete and biased samples. In previous work, measurements have been performed in order to estimate habitability

or *earth similarity* such as Earth Similarity Index (ESI) [Schulze-Makuch et al.2011], Biological Complexity Index (BCI) [Irwin et al.2014], Planetary Habitability Index (PHI) [Schulze-Makuch et al.2011] and Cobb-Douglas Habitability Score (CDHS) [Bora et al.2016]. The increased importance of statistical methodology is a trend that extends across the domain of astronomy. Naturally, a need for software to process complex astronomical data and collaborative engagement among astronomers, astrostatisticians and computer scientists emerges. These problems fall into the new field of *astroinformatics*: an interdisciplinary area of research where astronomers, mathematicians and computer scientists collaborate to solve problems in astronomy through the application of techniques developed in data science. Classical problems in astronomy now involve the accumulation of large volumes of complex data with different formats and characteristics and cannot now be addressed using classical techniques. As a result, machine learning algorithms and data analytic techniques have exploded in importance, often without a mature understanding of the pitfalls in such studies (for example, [Peng, Zhang & Zhao2013] reported remarkable accuracy but accomplished on unbalanced data thereby handicapped by the inherent bias in the data, unfortunately)

Planetary Habitability Laboratory's (University of Puerto Rico) Exoplanet Catalog (PHL-EC) [Méndez2015, Méndez2016] contains several features which may be analyzed in the process of detection and classification of exoplanets [Fischer et al.2014] based on habitability. These include the composition of the planets (*P. Composition Class*), the climate of the planets (*P. Zone Class*) and the surface pressure of the planets (*P. Surf Press*) among others. The ecological conditions in any exoplanet must be suitable in order for life (like on Earth) to exist. Hence, in the data set, the *classes* of planets broadly include planets which are habitable, and planets which are not habitable. A typical data set is derived from either photometry or spectroscopy, which is calibrated and analyzed in the form of light curves [Soutter2012]. Classification of these light curves and identification of the source producing dips in the light curve are essential for detection through the transit method. A dip in the light curve represents the presence of an exoplanet but this phenomenon may also be due to the presence of eclipsing binaries, pulsating stars, red giants etc. Similarly, significant challenges to the process of classification is posed by varying intensities of light curves, presence of noise, etc.

The purpose of this research is to understand the following: given the features of habitable planets, whether it may be feasible to automate the task of determining the habitability of a planet that has not previously been classified. The planet's ecological conditions such as presence of water, pressure, gravitational force, magnetic field etc have to be studied in detail [Heller & Armstrong2014] in order to adequately determine the na-

ture of habitability of a planet. For example, the presence of water may increase the likelihood for an exoplanet to be a potential habitable candidate [Irwin et al.2014], but this cannot be affirmed until other parameters are considered. These factors not only explain the existence of life on a planet, but also its evolution such that life can be sustained [Irwin & Schulze-Makuch2011, Irwin et al.2014]. The goal of the current work is to classify the exoplanets into the different categories of habitability on the basis of their atmospheric, physical, and chemical conditions [Gonzalez, Brownlee & Ward2001], or more aptly, based on whether the respective planet is located in the *comfortable habitable zone* (CHZ) of planet's parent star. If a planet resides in the CHZ of their parent star, it is considered to be a potential candidate for being habitable as the atmospheric conditions in these zones are more likely to support life [Kaltenegger et al.2011]. A planet's atmosphere is the key to establishing its identity, allowing us to guess the formation, development and sustainability of life [Kasting1993]. Numerous features such as planet's composition, habitable zone [Huang1959], atmosphere class, mass, radius, density, orbital period, radial velocity, just to name a few, have to be considered for a complete atmospheric study of an exoplanet.

Machine learning (ML) is a field of data analysis that evolved from studies of classical *pattern recognition* techniques. Statistics is at the heart of ML algorithms, which is why it is generally treated differently from related fields such as artificial intelligence (AI). The areas of data analytics, pattern recognition, artificial intelligence and machine learning have a lot in common; ML stems out as a convergence of statistical methods and computer science. The phrase *machine learning* almost literally signifies its purpose: to enable machines to learn trends and features in data. In the current study, existing machine learning techniques have been used to explore solutions to the problem of habitability. ML techniques have proved to be effective for the task of classification in important data sets and extracting necessary information and interesting patterns from large amount of data. ML algorithms are classified into *supervised* and *unsupervised* methods, also known as *predictive* and *descriptive* methods respectively. According to [Ball & Brunner2010], supervised methods rely on a training set of objects (with both features and labels) for which the target property is known with confidence. An algorithm is *trained* on this set of objects; *training* refers to the process of discerning between classes (for tasks of classification) of data based on the feature set (in astrophysics, a *feature* should be considered the same as an *observable*). The mapping resulting from training is applied to other objects for which the target property, or the *class label* is not available, in order to estimate which class of data they belong to. In contrast, unsupervised methods do not label data into classes; the task of an unsupervised ML technique is to generally find underlying trends in data, which are not explicitly stated or mentioned in the respective data

set. Unsupervised algorithms usually require an initial input to one or more of the adjustable parameters and the solution obtained depends on this input [Waldmann & Tinetti2012].

In the atmosphere of exoplanets, the desired accuracy of flux is 10^{-4} to 10^{-5}, which is difficult to achieve. An improved version of independent component analysis (ICA) has been proposed [Waldmann & Tinetti2012], where the noise due to instrumental, systematic and other stellar sources was filtered using an unsupervised learning approach; a wavelet filter was used to remove noise even in low signal-to-noise (SNR) conditions. This is achieved for HD189733b spectrum obtained through Hubble/NICMOS. In another supervised ML approach [Debray & Wu2013], stellar light curves were used to determine the existence of an exoplanet; this was accomplished by representing light curves as time series data, which was then combined with feature selection to obtain the appropriate outcome. Through a dynamic time warping algorithm, each light curve was compared to a baseline light curve, elucidating the similarity between the two. Other models which utilize alternate sequential minimal optimization (SMO) and multi-layer perceptron (MLP) have been implemented with the accuracy of 83% and 82.2% respectively. In [Abraham2014], a data set based on light curves, obtained from Kepler observatory was used for classification of stars as potentially harboring exoplanets or not. The pre-processing of the large data set of Kepler light curves removed the initial noise from the light curves and strong peaks (most likely transiting planets) were identified by calculating standard deviations and means for certain threshold values; these thresholds were selected from the percentage change metric. Next, feature extraction was performed to help capture the information regarding consistency of the peaks and transit time, which are otherwise relatively short. Principal component analysis (PCA) on these extracted features was used as a measure towards dimensionality reduction. Furthermore, four different supervised learning algorithms: k-nearest neighbor classifier (K-NN), logistic regression, softmax regression, and support vector machine (SVM) were applied. Softmax regression produced the best result for the training data set. The overall accuracy was boosted by applying k-means clustering and further application of softmax regression and PCA to 85% on the test data. NASA's catalog provides recent information about the planetary data, where certain celestial bodies are considered as Kepler's Object of Interest (KOI). Analysis and classification of KOIs is done in [McCauliff et al.2014], via a supervised machine learning approach that automates the categorization of the raw threshold crossing events (TCE) into a set of three classes namely planet candidate (PC), astrophysical false positive (AFP) and non-transiting phenomena (NTP), otherwise carried out manually by NASA's Kepler TCE Review (TCERT) team. Random forest classifier was proposed and the classification function was decided based on the statistical distribution of the attributes of each TCE like SNR, angular

offset, etc. The labels of training data were obtained by matching ephemeris contained in KOI to TCE catalog. Data imputation was carried out by using sentinel values to fill in missing attribute values; sensitivity analysis was carried out for the same operations. The precision of 95% for PC, 93% for AFP and 99% for NTP was observed. Further analysis with different classification algorithms (naïve Bayes, K-NN) was carried out, which proves greater effectiveness of Random forests.

In the process of conducting experiments, the authors developed a software called *Exo-Planet* [Theophilus, Reddy & Basak2016]. ExoPlanet served as a platform for conducting the experiments and is an open source software. In all future works, the authors will use it as a platform for analyzing data and testing algorithms.

2.2 Motivation

Today, many observatories all over the world survey and catalog astronomical data. For any newly discovered exoplanet, or a planet for which data is more recently collected, many attributes must be carefully considered before it may be appropriately classified. Manually completing this task is extremely cumbersome. Recently, the Kepler Habitable Zone Working Group submitted their *Catalog of Kepler Habitable Zone Exoplanet Candidates* for publication. Notably absent from this initial list are any true *Earth twins*: Earth-size planets with Earth-like orbits around Sun-like stars. While the search for Earth-twins continues as increasingly sophisticated software searches through Kepler's huge database, extrapolations from earlier statistical studies suggest that maybe one-in-ten Sun-like stars have Earth-size rocky planets orbiting inside the Habitable Zone [Dayal et al.2015]. Several Earth-twins could still be awaiting discovery in Kepler's data. A method that could rapidly find Earth-twins from Kepler's database is desirable. There are some salient features of the PHL-EC data set which make it an attractive option for machine learning based analysis. Eccentricity is assumed to be 0 when unknown; the attributes of equilibrium and surface temperature for non-gaseous planets show a linear relationship: this makes PHL-EC remarkably different from other data sets. Further, the data set exhibits a huge *bias* towards one of the classes (the *non-habitable* class of exoplanets: this poses significant challenges which needed to be properly addressed by using appropriate machine learning approaches, in order to prevent *over-fitting* and to avoid the problem of false positives.

ML techniques for analyzing data have become popular over the past two decades due to an increase in computational power. Despite this, ML techniques are not known to be applied to automate the task of classifying exoplanets. This prompted the authors to explore

the data set with various ML algorithms. Several mathematical techniques were explored and improvisations are proposed and implemented to check reliability of the classification methods. Much later in the manuscript, the effectiveness of the algorithms to accurately classify the exoplanets considered as *most likely habitable* in the optimistic and conservative lists of habitable planets of PHL-EC have been verified. The authors were keen to test the goodness of different classification algorithms and reconcile the data driven approach with the discovery and subsequent physics based inferences about habitability. This has been a very strong motivation and helped the authors go through painstaking and elaborate experimentation. Later in the paper, the results of classification performed on artificially augmented data (based on the samples naturally present in the catalog) have been presented to demonstrate that ML can be effectively used to handle large volumes of data. The authors believe that using machine learning as a *black box* should be strongly discouraged and instead, its treatment should be rigorous. The word *exploration* in the title indicates a thorough surveying of appropriate methods to solve the problem of exoplanet classification. This paper presents the results of SVM, K-NN, LDA, Gaussian naïve Bayes, decision trees, random forests and XGBoost. The performance of each classifier is examined and is correlated with the nature of the data.

2.3 Methods

The advancement of technology and sophisticated data acquisition methods generates a plethora of moderately complex to very complex data exist in the field of astronomy. Statistical analysis of this data is hence a very challenging and important task [Saha et al.2016]. Machine learning based approaches can carry out this analysis effectively [Ball & Brunner2010]. ML based approaches are broadly categorized into two main types: supervised and unsupervised techniques. The authors studied some of the most important work which used ML techniques on astronomical data. This motivated them to revisit important machine learning techniques and to discover their potential in the field of astronomical data analysis. The goal of the current work is to determine whether a given exoplanet can be classified as potentially habitable or not. These will be elaborated in detail later. Different algorithms were investigated in this context using data obtained from PHL-EC.

Classification techniques may also be classified into *metric* and *non-metric* classifiers, based on their working principles. Metric classifiers generally apply measures of geometric similarity and distances of feature vectors, whereas non-metric classifiers should be applied in scenarios where there are no definitive notions of similarity between feature vectors.

The results from metric and non-metric methods of classification have been enunciated separately for better understanding of suitability of these approaches in the context of the given data set. The classifier whose performance is considered as a threshold is naïve Bayes, considered as the gold standard in data analytics.

2.3.1 Naïve Bayes

Naïve Bayes classifier is based on Bayes' theorem. It can perform the classification of an arbitrary number of independent variables and is generally used when data has many attributes. Consequently, this method is of interest since the data set used, PHL-EC, has a large number of attributes. The data to be classified may be either *categorical*, such as P.Zone Class or P.Mass Class, or *numerical*, such as P.Gravity or P.Density. A small amount of training data is sufficient to estimate necessary parameters [Rish2001]. The method assumes independent distribution for attributes and thus estimates class conditional probability as in Equation.

$$P(X \mid Y_i) = P(X_1 \mid Y_i) \times P(X_2 \mid Y_i) \times ... \times P(X_n \mid Y_i) \tag{1}$$

As an example from the data set used in this work, consider two attributes: P. Sem Major Axis and P. Esc Vel. Assuming *independent* distribution between these attributes implies that the distribution of P. Sem Major Axis does not depend on the distribution of P. Esc Vel, and vice versa (albeit this assumption is often violated in practice; regardless, this algorithm is used and is known to produce good results). The naïve Bayes algorithm can be expressed as:

Step 1: Let $X = \{x_1, x_2, ..., x_d\}$ and $C = \{c_1, c_2, ..., c_d\}$ be the set of feature vectors corresponding to each entity in the data set, and the set of corresponding class labels (each class label can have one of three unique values here: *mesoplanet*, *psychroplanet*, and *non-habitable planets*, discussed) respectively. Reiterating, the attributes in the PHL-EC data set are mass of the planet, surface temperature, pressure etc., of each cataloged planet.

Step 2: Using Bayes' rule and applying naïve Bayes' assumption of *class conditional independence*, the *likelihood* that a given feature vector x belongs to a class c_j to a product of terms as in Equation.

$$p(x \mid c_j) = \prod_{k=1}^{d} p(x_k \mid c_j) \tag{2}$$

Class conditional independence in this context means that the output of the classifiers are independent of the classes. For example, if a data set has two classes c_a and c_b, then

for a feature vector x, the outcomes $p(c_a|x)$ and $p(c_b|x)$ are independent of each other, that is, there is no relationship between the classes.

Step 3: Recompute the posterior probability as shown in Equation .

$$p(c_j \mid x) = p(c_j) \prod_{k=1}^{d} p(x_k \mid c_j) \tag{3}$$

The *posterior probability* is the conditional probability that a given feature vector x belongs to the class c_j.

Step 4: Using Bayes' rule, the class label c_j which achieves highest probability is assigned to a new pattern x. Since the pattern in this context refers to the feature vector of a planet, the class labels mesoplanet, psychroplanet, or non-habitable will be assigned as the class label of the sample being classified based on whichever class has highest probability score for a particular planet.

2.3.2 Metric Classifiers

1. *Linear Discriminant Analysis* (LDA): The LDA classifier attempts to find a linear boundary that best separates the different classes in the data. This yields the optimal Bayes' classification (i.e. under the rule of assigning the class having highest *a posteriori* probability) under the assumption that the covariance is the same for all classes. The authors implemented an enhanced version of LDA (often called regularized discriminant analysis). This involves eigen decomposition of the sample covariance matrices and transformation of the data and class centroid. Finally, the classification is performed using the nearest centroid in the transformed space considering prior probabilities into account [Welling2005]. The algorithm is expressed as:

   Step 1: Compute mean vectors, μ_i for $i = 1, 2, ..., c$ classes from the data set, where each mean vector is d-dimensional; d is the number of attributes in the data. This aspect is similar to what has been stated in the subsection on Naïve Bayes'. Hence, μ_i is the mean vector of class i, where an element at position j in μ_i is the average of all the values of the j^{th} attribute for the class i.

   Step 2: Compute scatter matrices between classes and within class as shown in Equations .

$$S_B = \sum_{i=1}^{c} M_i(\mu_i - m)(\mu_i - m)^T \tag{4}$$

where S_B represents scatter matrix between classes, M_i is size of the respective class, m is the overall mean, considering values from all the classes for each attribute, and μ_i is the sample mean.

$$S_w = \sum_{i=1}^{c} S_i \tag{5}$$

where S_w is the scatter matrix within class w, and S_i is the scatter matrix for the i^{th} class and is given as

$$S_i = \sum_{x \in D_i}^{n} (x_i - \mu_i)(x_i - \mu_i)^t \tag{6}$$

Step 3: Compute eigen vectors and eigen values corresponding to scatter matrices.

Step 4: Select k eigen vectors that corresponds to largest eigen values and frame a matrix M whose dimensions are $d \times k$.

Step 5: Apply transformation $X \times M$, where the dimensions of X are $n \times d$, and i^{th} row is the i^{th} sample. Every row in the matrix X corresponds to an entity in the data set.

This method is found to be unsuitable for the classification problem. The reasons are explained in nezt section.

2. *Support Vector Machine* (SVM): SVM classifiers are effective for binary class discrimination [Hsu, Chang & Lin2016]. The basic formulation is designed for the linear classification problem; the algorithm yields an optimal hyperplane i.e. one that maintains the largest minimum distance from all the training data; it is defined as the margin for separating entities from different classes. For instance, if the two classes are the ones belonging to habitable and non-habitable planets respectively, the problem is a binary classification problem and the hyper-plane must maintain the largest possible distance from the data-points of either class. It can also perform non-linear classification by using *kernels*, which involves the computation of inner products of all pairs of data in the feature space. This implicitly transforms the data into a different space where

a separating hyperplane may be found. The algorithm for classification using SVM, stated briefly, is as follows:

Step 1: Create a support vector set S using a pair of points from different classes.

Step 2: Add the points to S using Kuhn-Tucker conditions, while there are violating points, add every violating point V to S.

$$S = S \cup V \tag{7}$$

If any of the coefficients, a_p is negative due to addition of V to S then prune all such points.

3. *K-Nearest Neighbor* (K-NN): K-nearest neighbors is an instance-based classifier that compares new incoming instance with the data stored in memory [Cai, Duo & Cai2010]. K-NN uses a suitable distance or similarity function and relates new problem instances to the existing ones in the memory. K neighbors are located and majority vote outcome decides the class. For example, let us assume K to be 7. Suppose the test entity has 4 out of the nearest 7 entities belonging to class habitable and the remaining 3 out of the 7 nearest entities belonging to class non-habitable. In such a scenario, the test entity is classified as habitable. However, if the choice of K is 9 and the number of nearest neighbors belonging to class non-habitable is 5, instead of 3, then the test entity will be classified as non-habitable. Occasionally, the high degree of local sensitivity makes the method susceptible to noise in the training data. If $K = 1$, then the object is assigned to the class of that single nearest neighbor. A shortcoming of the K-NN algorithm is its sensitivity to the local structure of the data. K-NN can be understood in an algorithmic way as:

Step 1: Let X is the set of training data, Y be the set of class labels for X, and x be the new pattern to be classified.

Step 2: Compute the Euclidean distance between x and all other points in X.

Step 3: Create a set S containing K smallest distances.

Step 4: Return majority label for Y_i, where $i \in S$.

Surveying various machine learning algorithms was a key motivation even though some methods and algorithms could easily suffice. This explains the reason for describing methods such as SVM, K-NN or LDA even though the results are not very promising for obvious

reasons explained. We reiterate that any learning method is as good as the data and without a balanced data set, there could not exist any reasonable scrutiny of the efficiency of the methods used in the manuscript or elsewhere. In the next subsection, non-metric classifiers which include decision trees, random forests, and extreme gradient boosted trees (XGBoost), would bolster the logic behind discouraging *black box* approaches in data analytics in the context of this problem or otherwise. Readers are advised to pay special attention to the following section.

2.3.3 Non-Metric Classifiers

1. *Decision Tree*: A decision tree constructs a tree data structure that can be used for classification or regression [Quinlan1986]. Each of the nodes in the tree splits the training set based on a feature; the first node is called the *root node*, which is based on the feature considered to be the best predictor. Every other node of the tree is then split into child nodes based on a certain splitting criteria or decision rule which determines the allegiance of the particular object (data) to the feature class. A node is said to be more *pure* if the likelihood to classify a given feature vector belonging to class c_i in comparison with any other class c_j, for $i \neq j$ is greater. The leaf nodes must be pure nodes, i.e., whenever any data sample that is to be classified reaches a leaf node, it should be classified into one of the classes of the data with a very high accuracy. Typically, an *impurity measure* is defined for each node and the criterion for splitting a node is based on the increase in the *purity* of child nodes as compared to the parent node. In other words, splits that produce child nodes having significantly less impurity as compared to the parent node are favored. The *Gini index* and *entropy* are two popular impurity measures. Gini index interprets the reduction of error at each node, whereas entropy is used to interpret the information gained at a node. One significant advantage of decision trees is that both categorical and numerical data can be dealt with. However, decision trees tend to over-fit the training data. The algorithm used to explain the working of decision trees is as follows:

   Step 1: Begin tree construction by creating a node T. Since this is the first node of the tree, it is the root node. Classification is of interest only in cases with multiple classes and a root node may not be sufficient for the task of classification. At the root node, all the entities in the training set are considered and a single attribute which results in the least error when used to discern between classes is utilized to *split* the entity set into subsets.

Step 2: Before the node is split, the number of child nodes needs be determined. Let us considering a binary valued attribute such as P. Habitable, the resulting number of child nodes after a split will simply be two. In the case of discrete valued attributes, if the number of possible values is more than two, then the number of child nodes may be more than two depending on the DT algorithm used. In the case of continuous valued attributes, a threshold needs to be determined such that minimum error in classification is effected.

Step 3: In each of the child nodes, the steps 1 and 2 should be repeated, and the tree should be subsequently grown, until it provides for a satisfactory classification accuracy. An impurity measure such as the Gini impurity index or entropy must be used to determine the best attribute on which the split should be based between any two subsequent levels in the decision tree.

Step 4: *Pruning* may be done, while constructing the tree or after the tree is constructed, in order to prevent over-fitting.

Step 5: For the task of classification, a test entity is traced to an appropriate leaf node from the root node of the tree.

It is important to observe here and in the later part of the manuscript that DT and other tree based algorithms yield significantly better results for balanced as well as biased data.

2. *Random Forest*: A random forest is an ensemble of multiple decision trees. Each tree is constructed by selecting a random subset of attributes from the data set. Each tree in turn performs a regression or a classification and a decision is taken based on mean prediction (regression) or majority voting (classification) [Breiman2001]. The task of classifying a new object from the data set is accomplished using randomly constructed trees. Classification requires a *tree voting* for a class i.e. the test entity is classified as class c_i if a majority of the decision trees in the forest classified the entity into class c_i. For example, if a random forest consists of ten decision trees, out of which six trees classified a feature vector x as belonging to the class of psychroplanets, and the remaining four trees classified x as being non-habitable, then we may conclude that the random forest classified x as a psychroplanet.

   Random forests work efficiently with large data sets. The training algorithm for random forests applies the general technique of bootstrap aggregation or *bagging* to tree learn-

ers. Given a training set $X = \{x_1, x_2, ..., x_n\}$ with class labels $Y = \{y_1, y_2, ..., y_n\}$, bagging selects random samples from the training set with iterative replacement and fits trees to these samples subsequently. The algorithm for classification may be described as:

Step 1: For $a = 1, ..., N$ and for $b = 1, 2, ..., M$ sample with replacement, n training samples from X with the corresponding set of Y_m features from Y; let this subset of samples be denoted as X_a, Y_b.

Step 2: Next, the i^{th} decision tree is trained: f_i on X_a, Y_b. Steps 1 and 2 are repeated for as many trees as desired in the random forest.

Step 3: After training, predictions for unseen samples x' can be made by considering the majority votes from all the decision trees in the forest.

The brief primer on non-metric classifiers is terminated by including a recently developed boosted-tree machine learning algorithm, XGBoost.

3. *XGBoost*: XGBoost [Chen & Guestrin2016] is another method of classification that is similar to random forests: it uses an ensemble of decision trees. The major departure from random forest lies in how the trees in XGBoost are trained. XGBoost uses *gradient boosting*. Unlike random forests, an objective function is minimized and each leaf has an associated score which determines the class membership of any test entity. Subsequent trees constructed in a forest of XGBoosted trees must minimize the chosen objective function so that there is measured improvement in classification accuracy as more trees are constructed. The steps in XGBoosted trees are as follows:

   Step 1: For $a = 1, ..., N$ and for $b = 1, 2, ..., M$ sample with replacement, n training samples from X with the corresponding set of Y_m features from Y; let this subset of samples be denoted as X_a, Y_b.

   Step 2: Next, the i^{th} decision tree is trained: f_i on X_a, Y_b. Steps 1 and 2 are repeated for as many trees as desired in the random forest.

   Step 3: Steps 1 and 2 are repeated by considering more trees. Subsequent trees must be chosen carefully so as to minimize the value of a chosen objective function. The results from each tree are added, that is each tree then contributes to the decision.

   Step 4: Once the model is trained, the prediction can be done in a way similar to random forests, but by making use of structure scores.

For more details on the working principles of XGBoost and a brief illustrative example, the reader should refer to Appendix.

2.4 Framework and Experimental Set Up

2.4.1 Data Acquisition: Web Scraping

The data is retrieved from Planetary Habitability Laboratory, University of Puerto Rico which is regularly updated with new data and discovery. Therefore, web scraping helps to easily update any local repository on a remote computer. Web scraping is a method of extracting data from web pages, given the structure of the web page is known a prior. The positioning of HTML tags and meta-data in a web page may be used for developing a scraper.

Figure 1 presents the outline of the scraper used to retrieve data from the website of the Planetary Habitability Laboratory. Modern web browsers are equipped with utilities for exploring structures of web pages. By using such inspection tools to understand the structure of web pages, scrapers may be developed to retrieve data present in HTML pages already. The steps in developing a scraper are explained below:

1. **Explore Website Structure**

   The first step in the process of developing a scraper is to understand the structure of the web pages. The position of HTML tags is carefully studied and patterns are discovered that may help define the placement of desired data.

2. **Create Scraping Template**

   Based on the knowledge gained in the first step, a template is designed that allows a program to extract data from a web page. In essence, a web page is a long string of characters. A set of web pages which display similar data may have similar characteristic structure and hence a single template may be used to extract data from similar web pages.

3. **Automate Navigation and Extraction**

   Once a template is developed, a scraper may be deployed to automatically collect data from web pages. It may be scheduled to update a local catalog or may be run as and when required. The authors did not schedule the scraper to run at regular intervals since that was not needed. The necessity may arise in future and scheduling may be acted upon.

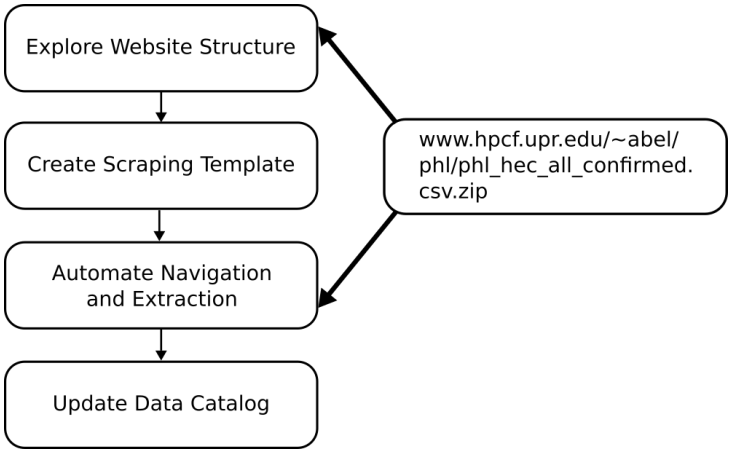

Figure 1: Steps in scraper

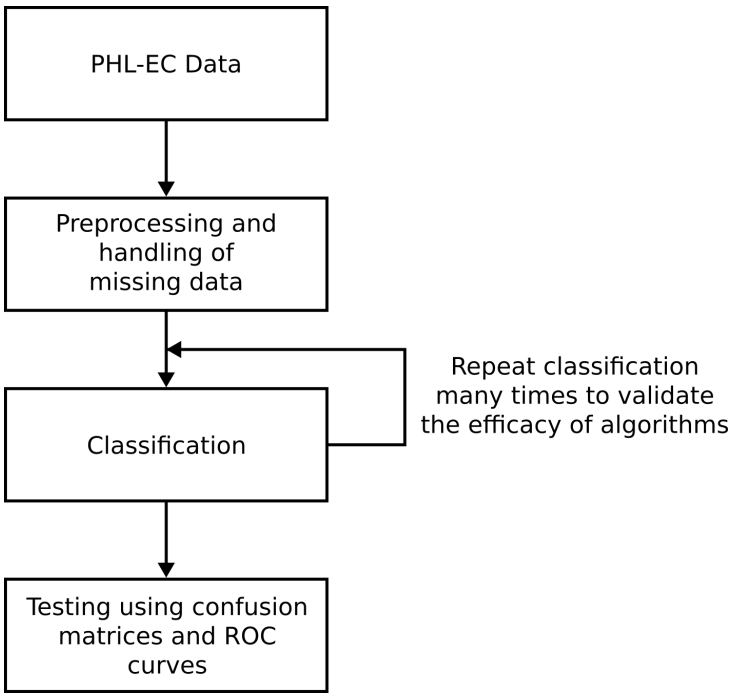

Figure 2: Overview of the steps in the analysis of data.

4. **Update Data Catalog**

   As a good practice, most scrapers update a local catalog. As the scraping process progresses, newly added or altered data should be updated thus avoiding redundant data handling. As and when a new or altered element is discovered, it should be immediately updated in the local catalog before retrieving the next element in sequence.

2.4.2 Classification of Data

PHL-EC has been derived from the Hipparcose catalog which contains 118,219 stars. PHL-EC was created from the Hipparcose Catalog by examining the information on distances, stellar variability, multiplicity, kinematics, and spectral classification for the stars contained therein. In this study, PHL-EC has been used because it provides an expanded target list for use in the search for extraterrestrial intelligence by Project Phoenix of the SETI Institute. PHL-EC data set consists of a total of 68 features and about 3500 confirmed exoplanets (at the time of writing of this paper). The reason behind selecting PHL-EC as the source of data is that it combines measures and modeled parameters from various sources. Hence, it provides a good metric for visualization and statistical analysis [Méndez2011]. Statistical machine learning approaches have not been applied on this data set, to the best of the authors' knowledge, providing good reasons to explore and exploit accuracy of different machine learning algorithms.

The PHL-EC data set possesses 13 categorical features and 55 continuous features. There are three classes in the data set, namely non-habitable, mesoplanets, and psychroplanets on which the ML methods have been tried (there do exist other classes in the data set on which the methods cannot be tried the reasons for which has been explained in Section 2.6.1. These three labels or classes or types of planets (for the purpose of classification) can be defined on the basis of their thermal properties as follows:

1. **Mesoplanets** [Asimov1989]: The planetary bodies whose sizes lie between Mercury and Ceres falls under this category (smaller than Mercury and larger than Ceres). These are also referred to as M-planets [Méndez2011]. These planets have mean global surface temperature between 0°C to 50°C, a necessary condition for complex terrestrial life. These are generally referred as Earth-like planets.

2. **Psychroplanets** [Méndez2011]: These planets have mean global surface temperature between -50°C to 0°C. Hence, the temperature is colder than optimal for sustenance of terrestrial life.

3. **Non-Habitable**: Planets other than mesoplanets and psychroplanets do not have thermal properties required to sustain life.

The catalog includes features like atmospheric type, mass, radius, surface temperature, escape velocity, earth's similarity index, flux, orbital velocity etc. Online data source for the current work is available at http://phl.upr.edu/projects/habitable-exoplanets-catalog/data/database.

The data flow diagram of the entire system is depicted in Figure 2. As a first step, data from PHL-EC is pre-processed (the authors have tried to tackle the missing values by taking mean for continuous valued attribute and mode for categorical attributes). Certain attributes from the database namely P.NameKepler (planet's name), Sname HD and Sname Hid (name of parent star), S.constellation (name of constellation), Stype (type of parent star), P.SPH (planet standard primary habitability), P.interior ESI (interior earth similarity index), P.surface ESI (surface earth similarity index), P.disc method (method of discovery of planet), P.disc year (year of discovery of planet), P. Max Mass, P. Min Mass, P.inclination and P.Hab Moon (flag indicating planet's potential as a habitable exomoons) were removed as these attributes do not contribute to the nature of classification of habitability of a planet. Interior ESI and surface ESI, however, together contribute to habitability, but since the data set directly provides P.ESI, these two features were neglected. Following this, classification algorithms were applied on the processed data set. In all, 51 features are used.

Initially, a ten-fold cross-validation procedure was carried out, that is, the entire data set was divided into ten bins in which one of the bins was considered as test-bin while the remaining 9 bins were taken as training data. In this method the data is sampled without replacement. Later, upon careful exploration of the data, more robust *artificial balancing* methods were used. The details are enunciated in Sections 2.5.2 and 2.5.3.

Scikit-learn [Pedregosa et al.2011] was used to perform these experiments. A brief overview of the classifiers used and their respective settings (in Scikit-learn) are provided below:

1. *Gaussian Naïve Bayes* evaluates the classification labels based on class conditional probabilities with class apriori probabilities, class count, mean and variance set to default values.

2. The *k-nearest neighbor* classifier was used with the k value being set to 3 while the weights are assigned uniform values and the algorithm was set to auto.

3. *Support vector machines*, a binary classifier was used with a penalty parameter C of the error term, initialized to default 1.0 while the kernel used was that of a radial basis function (RBF) [Powell1977] and the gamma parameter (kernel coefficient) was assigned to 0.0 and coefficient of the kernel was set to 0.0 as well.

4. The parameters setup for *linear discriminant analysis* classifier was implemented by the decomposition strategy similar to *SVM* [Eckart & Young1936, Hestenes1958]. No shrinkage metric was specified and no class prior probabilities were assigned.

5. *Decision trees* build tree based structures by using a split criterion namely Gini impurity, with measure of split being selected as best split and no max-depth and min-depth were specified whereas a *random forest* is an ensemble of decision trees with estimator value set up to 100 trees; the remaining parameters were set to the same as the decision tree.

6. *XGBoost* is a recent ensemble tree-based method which optimizes the tree being built. For this algorithm, the maximum number of estimators chosen to develop a classifier was 1000 and the maximum permissible depth of each tree bound at 8. The objective function used was that of a multinomial softmax.

2.5 Complexity of the data set used and Results

2.5.1 Classification performed on an unbalanced and smaller Data Set

Initially, 664 planets were considered, as their surface temperature was known out of which 9 planets were mesoplanets and 7 planets were psychroplanets, from the data set scraped in June 2015 [Méndez2015]. These planets selected for classification at this stage were rocky planets, deemed more habitable than planets of other terrain. The accuracy of all classifiers are documented in Table 1.

The PHL-EC data set is too complex for an immediate application of classifiers. The cause of the initial high accuracy is due to the *data bias* of a single class: The non-habitable class dominates over all the other classes. The sensitivity and specificity using this method were both very close to 1, for all classifiers.

Table 1: Accuracy of each algorithm executed on unbalanced PHL-EC data set

Algorithm	Accuracy (%)
Naïve Bayes	98.7
Decision Tree	98.61
LDA	93.23
K-NN	97.84
Random Forest	98.7
SVM	97.84

2.5.2 Classification performed on a balanced and smaller data set

Unbelievably high accuracy for all methods, metric and non-metric in the unbalanced data set and unreasonable sensitivity and specificity values were recorded. Bias towards a particular class, as evident from the number of samples across the different classes in the data set, was responsible for this. The efficacy of ML algorithms can not be judged when such a bias is present. Therefore, the data set needed to be balanced artificially so that dominance of one particular class samples is removed from the and the real picture emerges regarding the appropriateness of a particular machine learning algorithm, metric or otherwise.

To counter the problems faced in the first phase of research with regard to data bias, smaller data sets were constructed by selecting all planets belonging to mesoplanet and psycroplanet classes and selecting 10 planets which belonged to the non-habitable class at random, resulting in 26 planets in a smaller, artificially balanced data set. Classification and testing was then performed on each artificially balanced data set. In every iteration of testing on a smaller data set, the test data was formed by selecting one entity from mesoplanet, one from psychroplanet and two from non-habitable; the remaining entities from all classes were used as training data for that respective training-testing cycle. All possible combinations of training and test data were used, resulting in $\binom{8}{1} \times \binom{7}{1} \times \binom{10}{2} = 2835$ training and testing cycles for each smaller data set. Five hundred iterations, or artificially balanced data sets, were formed and tested for each classifier. The data set used by the authors can be obtained by clicking on the link: $https://github.com/SuryodayBasak/exoplanets\_data$. It should be noted that this method is not the same as that of blatant *undersampling* to counter the effects of bias. Rather, after the artificial balancing is done, a large number of iterations of the experiments are performed. As the process of selecting random non-habitable samples is stochastic in nature, by increasing the number of training-testing iterations and averaging the classification accuracy, the test results become more reliable and representative of the performance of the ML classifiers.

Table 2: Accuracy of each algorithm executed on pre-processed and artificially balanced PHL-EC data set.

Algorithm	Curve Color	Accuracy(%)
Random Forest	Green	96.667
Decision Tree	Red	96.697
Naïve Bayes	Cyan	91.037
LDA	Magenta	84.251
K-NN	Blue	72.191
SVM	Yellow	79.055

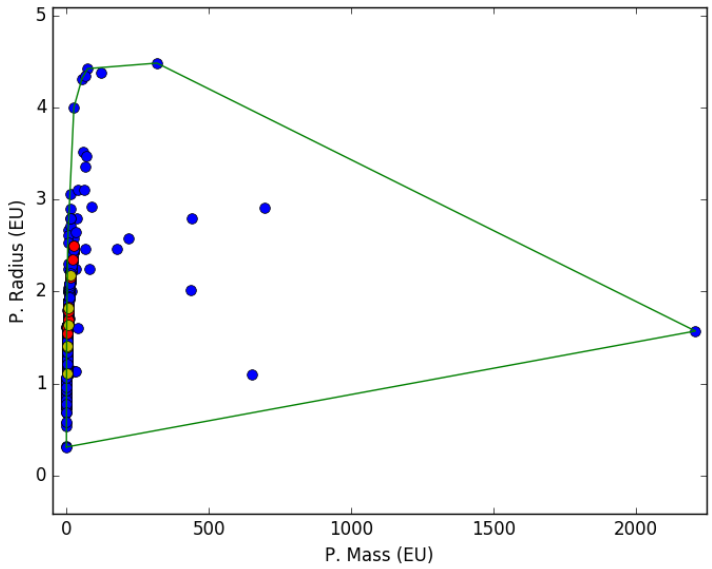

Figure 3: Convex hull shown across two dimensions.

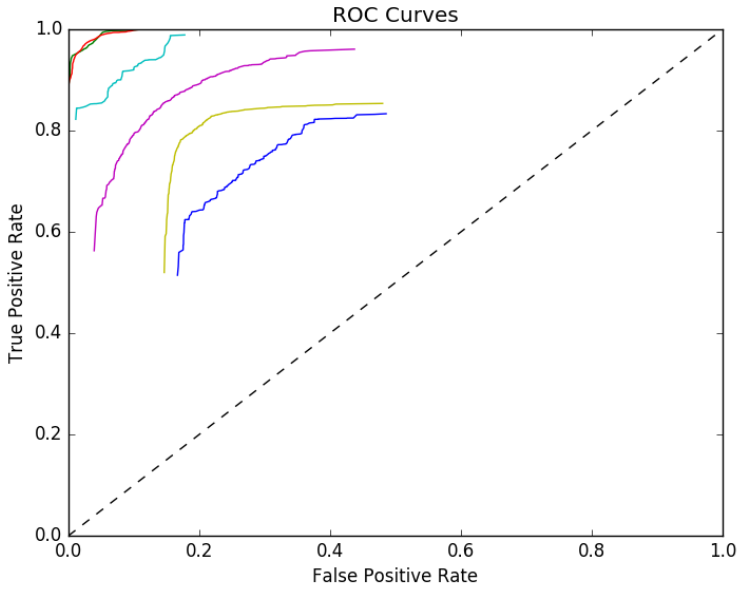

Figure 4: ROC curves for each method used on artificially balanced data sets.

A *separability test* was also performed on the data in order to determine if the data set is linearly separable or not. If the different classes in data are not linearly separable, certain classifiers may not work well or may not be appropriate for the respective application. The *convex hull* of different classes in the data provides us with an indication of separability: the convex hull of a given set of points is the smallest n dimensional polygon which can adequately envelop all the points in the respective set, where n is the number of attributes of the points. If the convex hull of any two or more classes intersect or overlap, then it may be concluded that the classes of data are not linearly separable. Figure 3 depicts the convex hull of data across two dimensions (P. Mass vs P. Radius). Although only the convex hull test considering all the dimensions of the data is completely representative of separability, a graph across two dimensions is depicted for simplicity as it is difficult to plot the convex hull for all pairs of features for a data set with many dimensions. The data points in blue represent the entities belonging to the non-habitable class, red represents mesoplanets and yellow represents psychroplanets. It is observed that the data belonging to the classes of mesoplanet and psychroplanet are present within the convex hull of the class non-habitable. Thus, the three classes in the data set are linearly inseparable.

The accuracy and ROC curves of the different classifiers after artificially balancing the data set are shown in Table 2 and Figure 4 respectively. The receiver operating characteristics (ROC) curve is created by plotting the true positive rate (TPR) against the false positive rate (FPR). The ROC curve is a useful tool for visualizing and analyzing the performance of a classifier and selecting the classifier with the best performance for a given data set. Simply stated, the closer the points in a curve are towards the top left corner, the better the performance of a classifier is, and vice-versa.

2.5.3 Classification performed on a balanced and larger data set

An updated version of the data set was scraped on 20th May 2016. This data set had 3411 entries: 24 mesoplanets, 13 psychroplanets, and 3374 non-habitable planets. At this stage, after the preliminary explorations described in Sections 2.5.1 and 2.5.2, the authors decided not to leave out any of the planets from the ML analysis: all of the 3411 entities were considered for determining the habitability. The number of items in this data set was significantly more than the older data set used to have. Hence, the artificial balancing method was modified. In the new balancing method, all 13 psychroplanets were considered in a smaller data set and 13 random and unique entities from each of the other two classes were also considered. Thus, in this case, the number of entities in a smaller, artificially balanced data set was 39. Following this, each smaller data set was divided in the ratio of 9:4 (training:testing) and 500

Table 3: Accuracy of each algorithm executed on pre-processed, artificially balanced and updated PHL-EC data set without seven attributes

Algorithm	Accuracy(%)
Random Forest	96.466
Decision Tree	95.1376
Naïve Bayes'	91.3
LDA	84.251
K-NN	59.581
SVM	39.7792

iterations of training and testing were performed on each such data set. 500 such data sets were framed for analysis. To sum it up, 2,50,000 iterations of training-testing were performed for each classifier.

1. **First Iteration of the Experiment**

   Initial analysis using the updated data set did not include the attributes such as P.SFlux Min, P.SFlux Max, P.Teq Min, P.Teq Max, P.Ts Min, P.Ts Max, and P.Omega. For temperature and flux, the corresponding average values were considered as the authors tried to make do with a lesser number of attributes by considering just the mean of the equilibrium and surface temperatures. The accuracy observed at this phase is recorded in Table 3.

2. **Second Iteration of the Experiment**

   In the next step, all the seven attributes initially not considered were included in the data set for analysis. This is considered to be a complete analysis and the accuracy achieved at this stage is reported in three separate sub-subsections.

   (a) **Naïve Bayes**

   The accuracy achieved using the Gaussian naïve Bayes Classifier is 92.583%. The ROC curve for this is given in Figure 5. The results of naïve Bayes is given in Table 4.

   (b) **Metric Classifiers**

   The accuracy using metric classifiers is given in Table 5. The corresponding color of curves in the ROC is present as a column. The ROC curve for all the metric classifiers is given in Figure 6.

Table 4: Sensitivity, accuracy, precision, and specificity achieved using naïve Bayes

Class	Sensitivity	Accuracy	Precision	Specificity
Non-Habitable	0.9999	0.9883	0.9999	0.9649
Psychroplanet	0.8981	0.9173	0.8243	0.9558
Mesoplanet	0.9691	0.9173	0.9295	0.8136

Table 5: Accuracy and ROC curve colors for metric classifiers

Algorithm	Curve Color	Accuracy(%)
SVM	Blue	36.489
K-NN	Green	68.607
LDA	Red	77.396

(c) **Non-Metric Classifiers** The accuracy using non metric classifiers is given in Table 9. The corresponding color of curves in the ROC is present as a column. The ROC curve for all the non metric classifiers is given in Figure **??**.

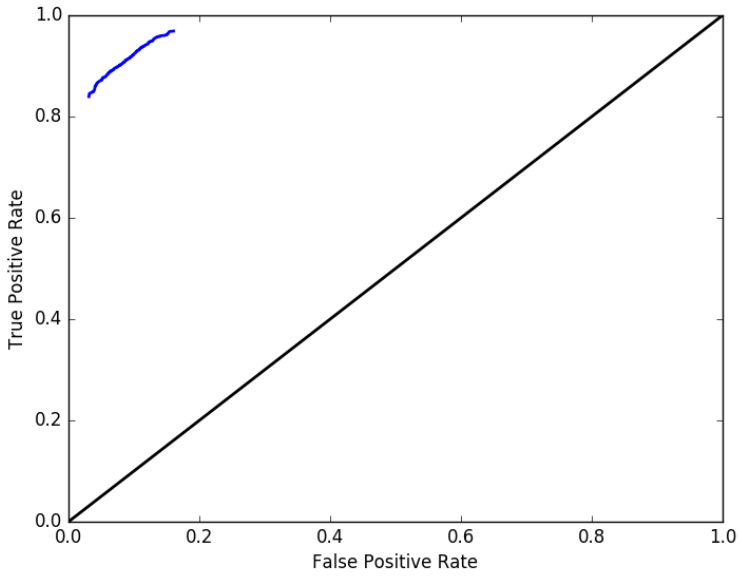

Figure 5: ROC for Gaussian naïve Bayes Classifier

As the data is linearly inseparable, classifiers utilizing the separability of data naturally performed less efficiently. Such classifiers are metric classifiers and include SVM, LDA, and K-NN as discussed before. SVM and LDA both work by constructing a hyperplane between classes of data: LDA constructs a hyper-plane by assuming the data from each

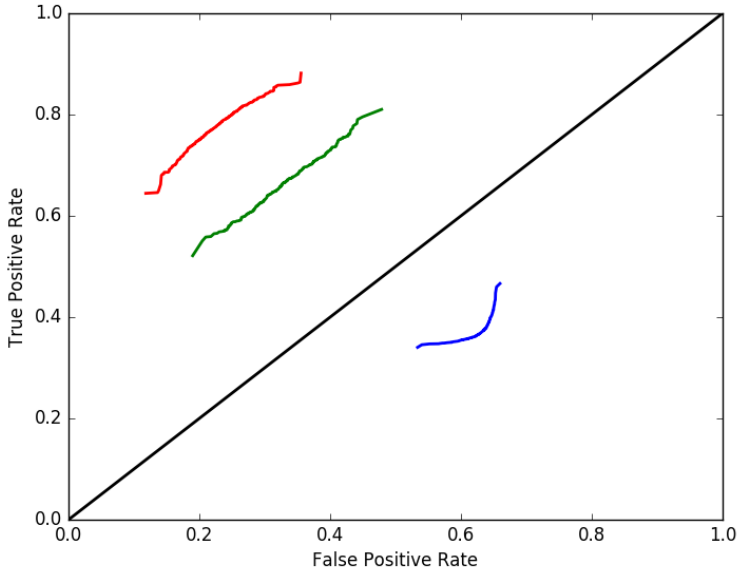

Figure 6: ROC curves for metric classifiers

Table 6: Sensitivity, accuracy, precision, and specificity achieved using SVM classifier

Class	Sensitivity	Accuracy	Precision	Specificity
Non-Habitable	0.8216	0.6151	0.3617	0.2022
Psychroplanet	0.7517	0.6268	0.4316	0.3771
Mesoplanet	0.4869	0.5050	0.3453	0.5412

Table 7: Sensitivity, accuracy, precision, and specificity achieved using K-NN classifier

Class	Sensitivity	Accuracy	Precision	Specificity
Non-Habitable	0.9998	0.9585	0.9996	0.8759
Psychroplanet	0.7200	0.6962	0.5366	0.6486
Mesoplanet	0.7797	0.6779	0.5184	0.4744

Table 8: Sensitivity, accuracy, precision, and specificity achieved using LDA classifier

Class	Sensitivity	Accuracy	Precision	Specificity
Non-Habitable	0.9935	0.9417	0.9847	0.8382
Psychroplanet	0.8520	0.8030	0.7042	0.7050
Mesoplanet	0.8155	0.8032	0.6785	0.7787

Table 9: Accuracy and ROC curve colors for non-metric classifiers

Algorithm	Curve Color	Accuracy(%)
Decision Tree	Blue	94.542
Random Forests	Green	96.311
XGBoost	Red	93.960

Table 10: Sensitivity, accuracy, precision, and specificity achieved using decision tree classifier

Class	Sensitivity	Accuracy	Precision	Specificity
Non-Habitable	0.9926	0.9691	0.9843	0.9220
Psychroplanet	0.9610	0.9578	0.9242	0.9512
Mesoplanet	0.9479	0.9419	0.8993	0.9299

class to be normally distributed with the parameters of mean and co-variance for the respective classes; SVM is a relatively recent kernel based method. Considering binary classification, in both cases, the hyperplane defines a threshold and the classes are assigned based on the response of a function $g(x)$, which may be higher or lower than the threshold. For example, if the output of $g(x)$ is greater than the corresponding threshold for any data point x_1, then the associated class may be *Class-1* and if it is lower than the threshold, then the associated class may be *Class-0*. For tasks involving multi-class classification, an appropriate set of thresholds is defined (based on the number of required hyperplanes) and the function $g(x)$ then has to find the class to which the data corresponds best by considering appropriate conditions for membership to each class. If data is linearly inseparable, it becomes nearly impossible to appropriately define a hyperplane which may adequately separate the different classes of data in a vector space. The K-NN classifier works on the basis of similarity to nearest neighbors. Even in this case, chances of error increases as the method works based on geometric similarity to singular regions in a vector space corresponding to each class.

Decision trees, random forests, and XGBoost, on the other hand, are non-metric classifiers. These classifiers do not work by constructing hyperplanes or consider kernels. These classifiers are able to divide the feature space into multiple regions corresponding

Table 11: Sensitivity, accuracy, precision, and specificity achieved using random forest classifier

Class	Sensitivity	Accuracy	Precision	Specificity
Non-Habitable	0.9990	0.9811	0.9978	0.9452
Psychroplanet	0.9617	0.9681	0.9276	0.9809
Mesoplanet	0.9757	0.9661	0.9513	0.9468

Table 12: Sensitivity, accuracy, precision, and specificity achieved using XGBoost classifier

Class	Sensitivity	Accuracy	Precision	Specificity
Non-Habitable	0.9993	0.9677	0.9984	0.9046
Psychroplanet	0.9613	0.9599	0.9252	0.9572
Mesoplanet	0.9489	0.9515	0.9034	0.9569

to a single class and the same is done for all the classes. This is a measure to overcome the limitation of the requirement of separability among classes of data in a classifier. Hence, the results from these classifiers are the best. A probabilistic classifier, Gaussian naïve Bayes performs better than the metric classifiers due to the strong independence assumptions between the features.

Different specificity and sensitivity values, along with the precision are given in Tables 4, 6, 7, 8, 10, 11 and 12 for the classification algorithms.

2.6 Discussion

2.6.1 Note on new classes in PHL-EC

Two new classes appeared in the augmented data set scraped on 28th May 2016. These two new classes are:

1. **Thermoplanet**: A class of planets, which has a temperature in the range of 50°C-100°C. This is warmer than the temperature range suited for most terrestrial life [Méndez2011].

2. **Hypopsychroplanets**: A class of planets whose temperature is below −50°C. Planets belonging to this category are too cold for the survival of most terrestrial life [Méndez2011].

   The above two classes have two data entities each in the augmented data set used. This number is inadequate for the task of classification, and hence the total of four entities were excluded from the experiment.

2.6.2 Missing attributes

It can be expected in any data set for feature values to be missing. The PHL-EC too has attributes with missing values.

1. The attributes of P. Max Mass and P. SPH were dropped as they had too few values for some algorithms to consider them as strong features.

2. All other named attributes such as the name of the parent star, planet name, the name in Kepler's database, etc. were not included as they do not have much relevance in a data analytic sense.

3. For the remaining, if a data sample had a missing value for a continuous valued attribute, then the mean of the values of all the available attributes for the corresponding class was substituted. In the case of discrete valued attributes, the same was done, but using the mode of the values.

After the said features were dropped, about 1% of all the values of the the data set used for analysis were missing. Most algorithms require the optimization of an objective function. Tree based algorithms also need to determine the importance of features as they have to optimally split every node till the leaf nodes are reached. Hence, ML algorithms are equipped with mechanisms to deal with important and non-important attributes.

2.6.3 Reason for extremely high accuracy of classifiers before artificial balancing of data set

Since the data set is dominated by the non-habitable planets class, it is essential that the training sets used for training the algorithms be artificially balanced. The initial set of results achieved were not based on artificial balancing and are described in Table 1. Most of the classifiers resulted in an accuracy between 97% and 99%.

In the data set, the number of entities in the non-habitable class is greater than 1000 times the number of entities in both the other classes put together. In such a case, voting for the dominating class naturally increases as the number of entities belonging to this class is greater: the number test entities classified as non-habitable are far greater than the number of test entities classified into the other two classes. The extremely high accuracies depicted in Table 1 is because of the dominance of one class and not because the classes are correctly identified. In such a case, the sensitivity and specificity are also close to 1. Artificial balancing is thus a necessity unless a learning method is designed specifically which auto corrects the imbalance in the data set. Performing classification on the given data set straightaway is not an appropriate methodology and artificial balancing is a must. Artificial balancing was done by selecting 13 entities from each class. This number corresponds to the number of total entities in the class of psychroplanets.

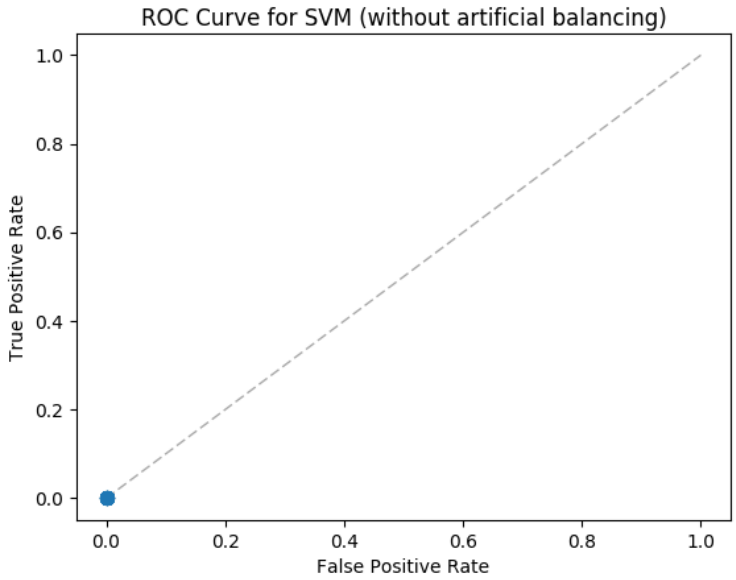

Figure 7: ROC for SVM without artificial balancing

2.6.4 Demonstration of the necessity for artificial balancing

Predominantly in the case of metric classifiers, an imbalanced training set can lead to misclassifications. The classes which are underrepresented in the training set might not be classified as well as the dominating class. This can be easily analyzed by considering the *area under the curve* (AUC) of the ROC of the metric classifiers in the case of balanced and imbalanced training sets. As an illustration: the AUC of SVM for the unbalanced training set (tested using a a balanced test set) is 0%, but after artificial balancing, it comes up to approximately 37%. The ROC for the unbalanced case is shown in Figure 7. The marker at (0,0) shows the only point in the plot; the FPR and TPR are observed to be constantly zero for SVM without artificial balancing. Similarly, in the case of other metric classifiers, classification biases can be eliminated using artificial balancing.

2.6.5 Order of importance of features

In any large data set, it is natural for certain features to contribute more towards defining the characteristics of the entities in that set. In other words, certain features contribute more towards class belongingness than certain others. As a part of the experiments, the authors wanted to observe which features are more important. The ranks of features and the percentage importance for random forests and for XGBoosted trees are presented in Tables

13 and 14 respectively. Every classifier uses the features in a data set in different ways. That is why the ranks and percentage importances observed using random forests and XGBoosted trees are different. The feature importances were determined using artificially balanced data sets.

2.6.6 Why are the results from SVM, K-NN and LDA relatively poor?

As the data set has been improving since the first iteration of the classification experiments, the authors were able to understand the nature of the data set better with time. With the continuous augmentation of the data set, it is easier to understand why some methods work poorer compared to others.

As mentioned in Section 2.5.2, the data entities from different classes are not linearly separable. This is proved by finding the data points from the classes of mesoplanets and psychroplanets within the convex hull of the non-habitable class. Classifiers such as SVM and LDA rely on data to be separable in order to optimally classify test entities. Since this condition is not satisfied by the data set, SVM and LDA have not performed as well as other classifiers such as random forest or decision trees.

SVM with radial basis kernels performed poorly as well. The poor performance of LDA and SVM may be attributed to the similar trends that entities from all the classes follow as observed from Figure 3. Apart from a few outliers, most of the data points follow a logarithmic trend and classes are geometrically difficult to discern.

K-NN also classifies based on geometric similarity and has a similar reason for poor performance: the nearest entities to a test entity may not be from same class as the test class. K-NN is observed to perform best when the value of k is between 7 and 11 [Hassanat et al.2014]. In our data set, these numbers almost correspond to the number of entities present in the classes of mesoplanets and psychroplanets; the number of entities belonging to mesoplanets and psychroplanets are inadequate for the best performance.

2.6.7 Reason for better performance of decision trees

A decision tree algorithm can detect the most relevant features for splitting the feature space. A decision tree may consequently be pruned while growing or after it is fully grown. This prevents over-fitting of the data and yields good classification results.

In decision trees, an n-dimensional space is partitioned into multiple parts corresponding to a single class. Unlike SVM or LDA, there isn't a single portion of the n-dimensional space corresponding to a single class. The advantage of this is that this can handle non-linear trends.

Table 13: Ranks of features based on random forests

Rank	Attribute	Percent Importance
1	P. Ts Mean (K)	6.731
2	P. Ts Min (K)	6.662
3	P. Teq Min (K)	6.628
4	P. Teq Max (K)	6.548
5	P. Ts Max (K)	6.49
6	S. Mag from Planet	6.399
7	P. Teq Mean (K)	6.393
8	P. SFlux Mean (EU)	6.366
9	P. SFlux Max (EU)	6.292
10	P. SFlux Min (EU)	6.264
11	P. Mag	4.216
12	P. HZD	3.822
13	P. Inclination (deg)	3.732
14	P. Min Mass (EU)	3.571
15	P. ESI	3.177
16	S. No. Planets HZ	3.014
17	P. Habitable	3.005
18	P. Zone Class	2.82
19	P. HZI	1.627
20	S. Size from Planet (deg)	1.376
21	P. Period (days)	1.034
22	S. Distance (pc)	0.54
23	S. [Fe/H]	0.42
24	P. Mean Distance (AU)	0.379
25	S. Teff (K)	0.251
26	P. Sem Major Axis (AU)	0.227
27	S. Age (Gyrs)	0.17
28	S. Luminosity (SU)	0.156
29	S. Appar Mag	0.145
30	S. Mass (SU)	0.134
31	S. Hab Zone Max (AU)	0.128
32	P. Appar Size (deg)	0.12
33	S. Hab Zone Min (AU)	0.118
34	S. Radius (SU)	0.097
35	P. Radius (EU)	0.095
36	P. Eccentricity	0.089
37	P. HZC	0.088
38	P. Density (EU)	0.083
39	S. No. Planets	0.08
40	P. Gravity (EU)	0.078
41	P. Mass (EU)	0.076
42	P. HZA	0.074
43	S. DEC (deg)	0.066
44	P. Surf Press (EU)	0.065
45	P. Mass Class	0.055
46	P. Esc Vel (EU)	0.049
47	S. RA (hrs)	0.045
48	P. Omega (deg)	0.018

Table 14: Ranks of features based on XGBoost

Rank	Attribute	Percent Importance
1	S. HabCat	25.0
2	P. Ts Mean (K)	25.0
3	P. Mass (EU)	25.0
4	P. SFlux Mean (EU)	25.0

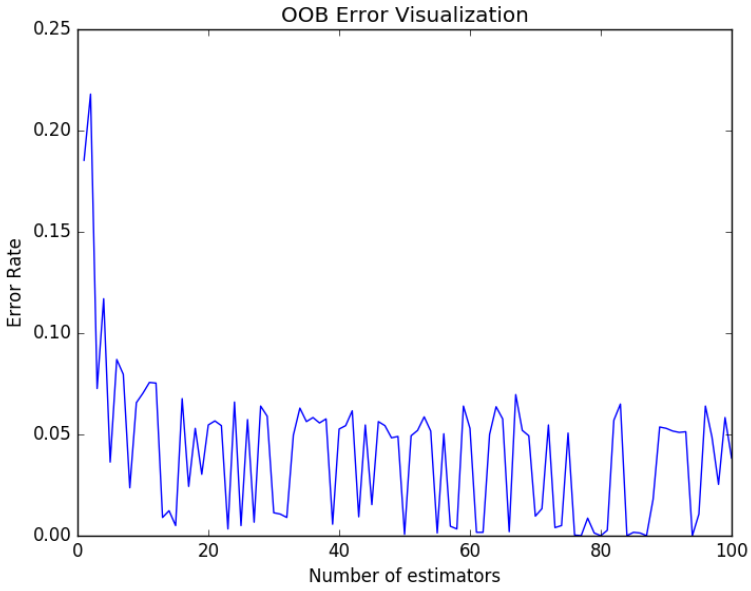

Figure 8: Decrease in OOB error with increase in number of trees in RF

This kind of an approach is appropriate for the PHL-EC data set as the trends in the data are not linear and classes are difficult to discern. Hence, multiple partitions of the feature space can greatly improve classification accuracy.

2.6.8 Explanation of OOB error visualization

Figure 8 shows the decrease in error rate as the number of tree estimators increase. After a point, the error rate fluctuates between approximately 0% and 6%. The decrease in the error rate with an increase in the number of trees to a smaller range of error testifies convergence in random forests.

2.6.9 What is remarkable about random forests?

Decision trees are often encountered with the problem of over-fitting i.e. ignorance of a variable in case of small sample size and large p-value (however, in the context of the work presented in this paper, this is not observed since unnecessary predictor variables are pruned). In contrast, random forests bootstrap aggregation or *bagging* [Breiman2001] which is particularly well-suited to problems with small sample size and large p-value. The PHL-EC data set is not large by any means. Random forest, unlike decision trees, do not require split sampling method to assess accuracy of the model. Self-testing is possible even if all the data is used for training as $2/3^{rd}$ of available training data is used to grow any one tree and the remaining one-third portion of the training data is used to calculate out-of-bag error. This helps assess model performance.

2.6.10 Random forest: mathematical representation of binomial distribution and an example

In random forests, approximately $2/3^{rd}$ of the total training data is used for growing each tree, and the remaining $1/3^{rd}$ of the cases are left out and not used in the construction of trees. Each tree returns a classification result or a *vote* for a class corresponding to each sample to be classified. The forest chooses the classification having the majority votes over all the trees in the forest. For a binary dependent variable, the vote will be *yes* or *no*; the number of affirmative votes is counted: this is the RF score and the percentage of affirmative votes received is the predicted probability of the outcome being correct. In the case of regression, it is the average of the responses from each tree.

In any DT which is a part of a random forest, an attribute x_a may or may not be included. The inclusion of an attribute in a Decision Tree is of the yes/no form. The binary nature of dependent variables is easily associated with *binomial distribution*. This implies that the probability of inclusion of x_a is binomially distributed. As an example, consider that a random forest consists of 10 trees, and the probability of correct classification due to an attribute x_a is 0.6. The probability mass function of the binomial distribution is given by Equation (8).

$$Pr(X = k) = \binom{n}{k} p^k (1-p)^{n-k} \tag{8}$$

It is easy to note that $n = 10$ and $p = 0.6$. The value of k indicates the number of times an attribute x_a is included in a DT in the forest. Since $n = 10$, the values of k may be $0, 1, 2, ..., 10$.

$k = 0$ implies that the attribute is never accounted for in the forest, and $k = 10$ implies that x_a is considered in all the trees.

The cumulative distribution function (CDF) for the binomial distribution is given by Equation (9).

$$Pr(X \leq m+1) = \sum_{k=0}^{n} \binom{n}{i} p^i (1-p)^{n-k} \tag{9}$$

For $n = 10$, $p = 0.6$ and $m = 10$, the probability for *s*uccess in Equation (10):

$$Pr(X \leq m+1) = \sum_{k=0}^{10} \binom{10}{k} (0.6)^k (0.4)^{n-k} = 1.0 \tag{10}$$

As k assumes a larger value, the value of the Cumulative Distribution approaches 1. This indicates a greater probability of success or correct classification. It follows that, increasing the number of decision trees consequently reduces the effect of noise and if the features are generally robust, the classification accuracy gets reinforced.

2.7 Binomial distribution based confidence splitting criteria

The binomially distributed probability of correct classification of an entity may be used as a node-splitting criteria in the constituent DT of an RF. From the cumulative binomial distribution function, the probability of k or more entities of class i occurring in a partition A of n observations with probability greater than or equal to p is given by the binomial random variable as in Equation (11).

$$X(n,p) = P[X(n,p_i) \geq k] = 1 - B(k;n,p_i) \tag{11}$$

As the value of $X(n,p)$ tends to zero, the probability of the partition A being a pure node, with entities belonging to only class i, increases. However, an extremely low value of $X(n,p)$ may lead to an over-fitting of of data, in turn reducing classification accuracy. A way to prevent this is to use a *confidence threshold*: the corresponding partition or node is considered to be a *pure* node if the value of $X(n,p)$ exceeds a certain threshold.

Let c be the number of classes in the data and N be the number of *outputs*, or *branches* from a particular node j. If n_j is the number of entities in the respective node, k_i the number of entities of class i, and p_i the minimum probability of occurrence of k_i entities in a child node, then the model for the confidence based node splitting criteria as used by the authors may be formulated as Equation (12).

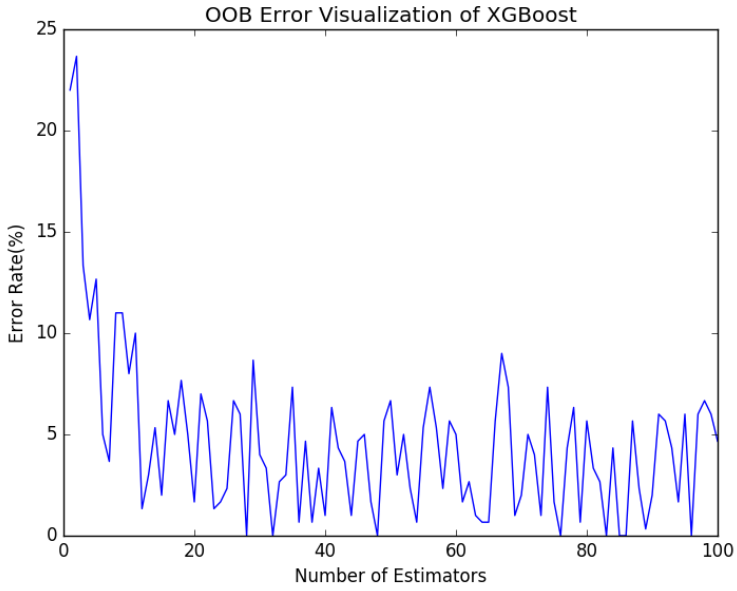

Figure 9: OOB error rate as the number of trees increases (Confidence Split)

$$var = \prod_{j=1}^{N} min\{1 - B(k_{ij}; n_j, p_j)\}$$

$$\mathscr{I} = \begin{cases} 0, & \text{if } var < \text{confidence threshold} \\ var, & \text{otherwise} \end{cases} \tag{12}$$

subject to the conditions, $c \geq 1$, $p = [0,1]$, confidence threshold $= [0,1)$, $k_{ij} \leq n_j$, $i = \{1,2,...,c\}$, $j = \{1,2,...,N\}$. Here, the i subscript represents the class of data, and the j subscript represents the output branch. So, k_{ij} represents the number of expected entities of class i in the child node j.

From the OOB error plot (Figure 9), it is observed that the classification error decreases as the number of trees increases. This is akin to the OOB plot of random forests using Gini split (Figure 8), which validates our *confidence-based* approach as a splitting criteria. For the current data set, the results obtained by using this criteria is comparable to the results obtained by using Gini impurity splitting criteria (the results are analyzed in Section 2.5.3). In the current data set, balanced data sets with 39 entities equally distributed among three

classes were used. A closer look at this method, however, reveals that it could be a difficult function to deal with as the number of samples in the data sets go on increasing, as it is in the multiplicative form. Nonetheless, it is a method worth exploring and can be considered a good method for small data sets. Hence, this method is of interest for the PHL-EC dataset. This is observed later, in the case of Proxima b (Table 23). Even otherwise, the results presented in Tables 19 and 20 indicate a comparable performance to the other tree-based classification algorithms. In the future, further work on this this method may enable it to scale up and work on large data sets.

2.7.1 Margins and convergence in random forests

The *margin* in a random forest measures the extent to which the average number of votes for $\mathbf{X}, Y$ for the right class exceeds the average vote for any other class. A larger margin thus implies a greater accuracy in classification [Breiman2001].

The generalization error in random forests converges almost surely as the number of trees increases. A convergence in the generalization error is important. It shows that the increase in the number of tree classifiers we tends to move the accuracy of classification towards near perfect (refer to Section **??** of Appendix **??**).

2.7.2 Upper bound of error and Chebyshev inequality

Accuracy is an important measure for any classification or approximation function. It is indeed an important question to be asked: *what is the error incurred by a certain classifier?* In the case of a classifier, the lower the error, the greater the probability of correct classification. It is critical that the upper bound of error be at least finite. *Chebyshev Inequality* can be related to the error bound of the random forest learner. The generalization error is bounded above by the inequality as defined by Equation 13 (refer to Section **??** of Appendix **??**).

$$Error \leq \frac{var(margin_{RF}(x,y))}{s^2} \tag{13}$$

2.7.3 Gradient tree boosting and XGBoosted trees

Boosting refers to the method of combining the results from a set of *weak learners* to produce a *strong* prediction. Generally, a weak learner's performance is only slightly better than that of a random guess. The idea is to divide the job of a single predictor across many weak predictor functions and to optimally combine the votes from all the smaller predictors. This helps enhance the overall prediction accuracy.

XGBoost [Chen & Guestrin2016] is a tool developed by utilizing these boosting principles. The word XGBoost stands for *eXtreme Gradient Boosting* as coined by the authors. XGBoost combines a large number of regression trees with a small learning rate. Subsequent trees in the forest of XGBoosted trees are grown by minimizing an objective function. Here, the word *regression* may refer to logistic or soft-max regression for the task of classification, albeit these trees may be used to solve linear regression problems as well. The boosting method used in XGBoost considers trees added early to be significant and trees added later to be inconsequential (refer to Section **??**).

XGBoosted trees [Chen & Guestrin2016] may be understood by considering four central concepts.

7.15.1: *Additive Learning*

For additive learning, functions f_i must be learned which contain the tree structure and leaf scores [Chen & Guestrin2016]. This is more difficult compared to traditional optimization problems as there are multiple functions to be considered, and it is not sufficient to optimize every tree by considering its gradient. Another overhead is with respect to implementation in a computer: it is difficult to train all the trees all at once. Thus, the training phase is divided into a sequence of steps. For t steps, the prediction value from each step, $\hat{y}_i^{(t)}$ are added as:

$$\begin{aligned}
\hat{y}_i^{(0)} &= 0 \\
\hat{y}_i^{(1)} &= f_1(x_i) = \hat{y}_i^{(0)} + f_1(x_i) \\
\hat{y}_i^{(2)} &= f_1(x_i) + f_2(x_i) = \hat{y}_i^{(1)} + f_2(x_i) \\
&\cdots \\
\hat{y}_i^{(t)} &= \sum_{k=1}^{t} f_k(x_i) = \hat{y}_i^{(t-1)} + f_t(x_i)
\end{aligned} \tag{14}$$

Central to any optimization method is an objective function which needs to be optimized. In each step. the selected tree is the one that optimizes the objective function of the learning algorithm. The objective function is formulated as:

$$\begin{aligned}
\text{obj}^{(t)} &= \sum_{i=1}^{n} l(y_i, \hat{y}_i^{(t)}) + \sum_{i=1}^{t} \Omega(f_i) \\
&= \sum_{i=1}^{n} l(y_i, \hat{y}_i^{(t-1)} + f_t(x_i)) + \Omega(f_t) + constant
\end{aligned} \tag{15}$$

Mean squared error (MSE) is used as its mathematical formulation is convenient. Logistic loss, for example, has a more complicated form. Since error needs to be minimized, the gradient of the error must be calculated: for MSE, calculating the gradient and finding a minima is not difficult, but in the case of logistic loss, the process becomes more cumbersome. In the general case, the Taylor expansion of the loss function is considered up to the term of second order.

$$\text{obj}^{(t)} = \sum_{i=1}^{n} [l(y_i, \hat{y}_i^{(t-1)}) + g_i f_t(x_i) + \frac{1}{2} h_i f_t^2(x_i)] + \Omega(f_t) + constant \tag{16}$$

where g_i and h_i are defined as:

$$\begin{aligned} g_i &= \partial_{\hat{y}_i^{(t-1)}} l(y_i, \hat{y}_i^{(t-1)}) \\ h_i &= \partial^2_{\hat{y}_i^{(t-1)}} l(y_i, \hat{y}_i^{(t-1)}) \end{aligned} \tag{17}$$

By removing the lower order terms from Equation (16), the objective function becomes:

$$\sum_{i=1}^{n} [g_i f_t(x_i) + \frac{1}{2} h_i f_t^2(x_i)] + \Omega(f_t) \tag{18}$$

which is the optimization equation of XGBoost.

7.15.2: *Model Complexity and Regularized Learning Objective*

The definition of the tree $f(x)$ may be refined as:

$$f_t(x) = w_{q(x)}, w \in R^T, q : R^d \rightarrow \{1, 2, \cdots, T\}. \tag{19}$$

where w is the vector of scores on leaves, q is a function assigning each data point to the corresponding leaf and T is the number of leaves. In XGBoost, the model complexity may be given as:

$$\Omega(f) = \gamma T + \frac{1}{2} \lambda \sum_{j=1}^{T} w_j^2 \tag{20}$$

A regularized objective is minimized for the algorithm to learn the set of functions given in the model. It is given by:

$$\mathscr{L}(\phi) = \sum_i l(\hat{y}_i, y_i) + \sum_k \Omega(f_k) \tag{21}$$

7.15.3: *Structure Score*

After the objective value has been re-formalized, the objective value of the t^{th} tree may be calculated as:

$$\begin{aligned} Obj^{(t)} &\approx \sum_{i=1}^{n} [g_i w_{q(x_i)} + \frac{1}{2} h_i w^2_{q(x_i)}] + \gamma T + \frac{1}{2}\lambda \sum_{j=1}^{T} w_j^2 \\ &= \sum_{j=1}^{T} [(\sum_{i \in I_j} g_i) w_j + \frac{1}{2} (\sum_{i \in I_j} h_i + \lambda) w_j^2] + \gamma T \end{aligned} \tag{22}$$

where $I_j = \{i | q(x_i) = j\}$ is the set of indices of data points assigned to the j^{th} leaf. In the second line of the Equation (22), the index of the summation has been changed because all the data points in the same leaf must have the same score. Let $G_j = \sum_{i \in I_j} g_i$ and $H_j = \sum_{i \in I_j} h_i$. The equation can hence be further by substituting for G and H as:

$$\text{obj}^{(t)} = \sum_{j=1}^{T} [G_j w_j + \frac{1}{2}(H_j + \lambda) w_j^2] + \gamma T \tag{23}$$

In Equation (23), every w_j is independent of each other. The form $G_j w_j + \frac{1}{2}(H_j + \lambda) w_j^2$ is quadratic and the best w_j for a given structure $q(x)$ and the best objective reduction which measures goodness of tree is:

$$w_j^* = -\frac{G_j}{H_j + \lambda} \text{obj}^* = -\frac{1}{2} \sum_{j=1}^{T} \frac{G_j^2}{H_j + \lambda} + \gamma T \tag{24}$$

7.15.4: *Learning Structure Score*

XGBoost learns tree the tree level during learning based on the equation:

$$Gain = \frac{1}{2} \left[\frac{G_L^2}{H_L + \lambda} + \frac{G_R^2}{H_R + \lambda} - \frac{(G_L + G_R)^2}{H_L + H_R + \lambda} \right] - \gamma \tag{25}$$

The equation comprises of four main parts:

- The score on the new left leaf

- The score on the new right leaf
- The score on the original leaf
- Regularization on the additional leaf

The value of $Gain$ should as high as possible for learning to take place effectively. Hence, if the value of gain is greater than γ, the corresponding branch should not be added.

A working principle of XGBoost in the context of the problem is illustrated using Figure **??**, Figure **??** and Table **??** of Appendix **??**.

2.7.4 Classification of conservative and optimistic samples of potentially habitable planets

The end objective of any machine learning pursuit is to be able to correctly analyze data as it increases with time. In the case of classifying exoplanets, the number of exoplanets in the catalog increase with time. In February 2015, the PHL-EC had about 1800 samples, whereas in January 2017, it has more than 3500 samples! This is twice the number of exoplanets as the time the authors started the current work.

The project home page of the Exoplanets Catalog of PHL (http://phl.upr.edu/projects/habitable-exoplanets-catalog) provides two lists of potentially habitable planets: the *conservative* list and the *optimistic* list. The conservative list contains those exoplanets that are more likely to have a rocky composition and maintain surface liquid water i.e. planets with 0.5 < Planet Radius ≤ 1.5 Earth radii or 0.1 < Planet Minimum Mass ≤ 5 Earth masses, and the planet is orbiting within the conservative habitable zone. The optimistic list contains those exoplanets that are less likely to have a rocky composition or maintain surface liquid water i.e. planets with 1.5 < Planet Radius ≤ 2.5 Earth radii or 5 < Planet Minimum Mass ≤ 10 Earth masses, or the planet is orbiting within the optimistic habitable zone. The tree based classification algorithms were tested on the planets in both the conservative samples' list as well as the optimistic samples' list. Out of the planets listed, Kepler-186 f is a hypopsychroplanet and was not included in the test sample (refer to Section 2.6.1). The experiment was conducted on the listed planets (except Kepler-186 f). The samples were individually isolated from the data set and were treated as the test set. The remainder of the data set was treated as the training set. The test results are presented in tables 15, 16, 21, 22, 17, 18, 19 and 20.

2.8 Habitability Classification System applied to Proxima b

On 24th August 2016, [Anglada-EscudÃl'2016] published the discovery of an apparently rocky planet(or believed to be one) orbiting Proxima Centauri, the nearest star to the Sun, named *Proxima b*. The discovery was made by Guillem Anglada-Escude, an astronomer at Queen Mary University of London along with a team. Proxima b is 1.3 times heavier than Earth. According to the PHL-EC, its radius is 1.12 EU, density is 0.9 EU, surface temperature is 262.1 K and escape velocity is 1.06 EU. These attributes are close to those of Earth. Hence, there are plausible reasons to believe that Proxima b may be a habitable planet (refer to row #3389 in the data set, *Confirmed Exoplanets: phl_hec_all_confirmed.csv* hosted at http://phl.upr.edu/projects/habitable-exoplanets-catalog/data/database).

In the PHL-EC data set, Proxima b is classified as a psychroplanet. The classification models which earlier resulted in high classification accuracy were used to classify Proxima b separately. The results are enunciated in Table 23. The results provide evidence of the strength of the system to automatically label and classify newly discovered exoplanets.

2.9 Data Synthesis and Artificial Augmentation

As mentioned earlier, the focus of the manuscript is to track the performance of the classifiers to scale. The reliability of the semi-automatic process depends on the efficacy of the classifiers if the data set grew rapidly with many entities. Since the required data is not naturally available, the authors have simulated a data generation process, albeit briefly, and performed classification experiments on the artificially generated data. The strategy has a two-fold objective: to devise a preemptive measure to check scalability of the classifiers, and to tackle classes of exoplanets with insufficient data. We elaborate the concept, theory, and model in this section and establish the equivalence of both premises.

Different kinds of simulations are seen in astrophysics. [Sale2015] modeled the extinction of stars by placing them into spatial bins and applying the Poisson point process to estimate the posterior probability of various 3D extinction maps; in this specific example, the assertion is that photometric catalogs are subject to bright and faint magnitude limits based on the instruments used for observations. This work, however, is more focused on the method of Poisson point processes instead of the specific application of it. [Sale2015] mentions that one of the assumptions is that the number of objects in a region of space (a statistical bin) follows a Poisson distribution. However, there are no quantitative metrics provided in support of this claim, such as a goodness-of-fit test, etc. But as the purpose of this work is to estimate point extinctions in a catalog that *largely* conforms to the actual physical extinctions, the

assumption that the data conforms to a Poisson distribution might be a reasonable one. [Green et al.2015] used a Markov Chain Monte Carlo (MCMC) method to create a dust map along *sightlines* (bins or discrete columns). In this work, they have assumed a Gaussian prior probability to model the dust distribution in every column. The idea of dividing the field of observations into bins is common in [Sale2015] and [Green et al.2015], however, the fundamental difference is that the posterior probability in [Sale2015] is modeled using an assumed distribution, whereas the prior probability in [Green et al.2015] is taken as Gaussian, possibly allowing the nature of the analysis to be more empirical. Thus, two methods of synthetic oversampling are explored:

1. By assuming a Poisson distribution in the data.

2. By estimating an empirical distribution from the data.

The strengths and weaknesses of each of these methods are mentioned in their respective subsections, albeit the authors would insist on the usage of empirical distribution estimation over the assumption of a distribution. Nonetheless, the first method paved way to the next, more robust method.

26 planets (data samples) belonged to the mesoplanet class and 16 samples belonged to the psychroplanet class, as of the day the analysis was done; these samples have been used for the classification experiments described in Sections 2.5 and 2.6. The naturally occurring data points are relatively less in order to describe the distribution of data by a known distribution (such as Poisson, or Gaussian). If a known distribution is estimated using this data, chances are that the distribution thus determined is not representative of the actual density of the data. As this fact is almost impossible to establish at this point in time, two separate methods of synthesizing data have been developed and implemented to gauge the efficacy of ML algorithms.

2.9.1 Generating Data by Assuming a Distribution

2.9.2 Artificially Augmenting Data in a Bounded Manner

The challenge with artificially oversampling data in PHL-EC is that the original data available is too less to estimate a reliable probability distribution which is satisfactorily representative of the probability density of the naturally occurring data. For this, a *bounding mechanism* should be used so that while augmenting the data set artificially, the values of each feature or observable does not exceed the physical limits of the respective observable, and the physical limits are analyzed from the naturally occurring data.

Table 15: Results of using decision trees (Gini impurity) to classify the planets in the conservative sample

Name	True Class	Classification Accuracy	non-habitable	psychroplanet	mesoplane
Proxima Cen b	psychroplanet	84.5	0.1	84.5	15.4
GJ 667 C c	mesoplanet	91.7	0.0	8.3	91.7
Kepler-442 b	psychroplanet	56.9	0.1	56.9	43.0
GJ 667 C f	psychroplanet	100.0	0.0	100.0	0.0
Wolf 1061 c	psychroplanet	100.0	0.0	100.0	0.0
Kepler-1229 b	psychroplanet	100.0	0.0	100.0	0.0
Kapteyn b	psychroplanet	100.0	0.0	100.0	0.0
Kepler-62 f	psychroplanet	100.0	0.0	100.0	0.0
GJ 667 C e	psychroplanet	100.0	0.0	100.0	0.0

For this purpose, we use a hybrid of SVM and K-NN to set the limits for the observables. The steps in the SVM-KNN algorithm are summarized below:

Step 1: The best boundary between the psychroplanets and mesoplanets are found using SVM with a linear kernel.

Step 2: By analyzing the distribution of either class, data points are artificially created.

Step 3: Using the boundary determined in Step 1, an artificial data point is analyzed to determine if it satisfies the boundary conditions: if a data point generated for one class falls within the boundary of the respective class, the data point is kept in it's labeled class in the artificial data set.

Step 4: If a data point crosses the boundary of its respective class, then a K-NN based verification is applied. If 3 out of the nearest 5 neighbors belongs to the class to which the data point is supposed to belong, then the data point is kept in the artificially augmented data set.

Step 5: If the conditions in Steps 3 and 4 both fail, then the respective data point's class label is changed so that it belongs to the class whose properties it corresponds to better.

Step 6: Steps 3, 4 and 5 are repeated for all the artificial data points generated, in sequence.

It is important to note that in Section **??**, the K-NN and SVM algorithms have been explained as classification algorithms; however, they are not used as classifiers in this over-sampling simulation. Rather, they are used, along with density estimation, to rectify the class-belongingness (class labels) of artificially generated random samples. If an artificially

Table 16: Results of using decision trees (Gini impurity) to classify the planets in the optimistic sample

Name	True Class	Classification Accuracy	non-habitable	psychroplanet	mesoplanet
Kepler-438 b	mesoplanet	92.5	0.2	7.3	92.5
Kepler-296 e	mesoplanet	99.8	0.2	0.0	99.8
Kepler-62 e	mesoplanet	100.0	0.0	0.0	100.0
Kepler-452 b	mesoplanet	99.6	0.4	0.0	99.6
K2-72 e	mesoplanet	99.7	0.3	0.0	99.7
GJ 832 c	mesoplanet	99.0	0.0	1.0	99.0
K2-3 d	non-habitable	0.8	0.8	0.0	99.2
Kepler-1544 b	mesoplanet	99.9	0.1	0.0	99.9
Kepler-283 c	mesoplanet	100.0	0.0	0.0	100.0
Kepler-1410 b	mesoplanet	99.9	0.1	0.0	99.9
GJ 180 c	mesoplanet	79.7	0.0	20.3	79.7
Kepler-1638 b	mesoplanet	99.4	0.6	0.0	99.4
Kepler-440 b	mesoplanet	94.8	5.2	0.0	94.8
GJ 180 b	mesoplanet	99.7	0.3	0.0	99.7
Kepler-705 b	mesoplanet	100.0	0.0	0.0	100.0
HD 40307 g	psychroplanet	87.7	0.0	87.7	12.3
GJ 163 c	psychroplanet	100.0	0.0	100.0	0.0
Kepler-61 b	mesoplanet	96.9	3.1	0.0	96.9
K2-18 b	mesoplanet	100.0	0.0	0.0	100.0
Kepler-1090 b	mesoplanet	99.7	0.3	0.0	99.7
Kepler-443 b	mesoplanet	99.5	0.3	0.2	99.5
Kepler-22 b	mesoplanet	98.4	1.6	0.0	98.4
GJ 422 b	mesoplanet	17.1	0.9	82.0	17.1
Kepler-1552 b	mesoplanet	97.3	2.7	0.0	97.3
GJ 3293 c	psychroplanet	100.0	0.0	100.0	0.0
Kepler-1540 b	mesoplanet	98.5	1.5	0.0	98.5
Kepler-298 d	mesoplanet	95.6	4.4	0.0	95.6
Kepler-174 d	psychroplanet	99.9	0.1	99.9	0.0
Kepler-296 f	psychroplanet	100.0	0.0	100.0	0.0
GJ 682 c	psychroplanet	99.2	0.8	99.2	0.0
tau Cet e	mesoplanet	99.4	0.6	0.0	99.4

Table 17: Results of using random forests (Gini impurity) to classify the planets in the conservative sample

Name	True Class	Classification Accuracy	non-habitable	psychroplanet	mesoplane
Proxima Cen b	psychroplanet	100.0	0.0	100.0	0.0
GJ 667 C c	mesoplanet	100.0	0.0	0.0	100.0
Kepler-442 b	psychroplanet	94.1	0.0	94.1	5.9
GJ 667 C f	psychroplanet	100.0	0.0	100.0	0.0
Wolf 1061 c	psychroplanet	100.0	0.0	100.0	0.0
Kepler-1229 b	psychroplanet	100.0	0.0	100.0	0.0
Kapteyn b	psychroplanet	100.0	0.0	100.0	0.0
Kepler-62 f	psychroplanet	100.0	0.0	100.0	0.0
GJ 667 C e	psychroplanet	100.0	0.0	100.0	0.0

generated random sample is generated such that it does not conform to the general properties of the respective class (which can be either mesoplanets or psychroplanets), the class label of the respective sample is simply changed such that it may belong to the class of habitability whose properties it exhibits better. The strength of using this as a rectification mechanism lies in the fact that artificially generated points which are near the boundary of the classes stand a chance to be rectified so that they might belong to the class they better represent. Moreover, due to the density estimation, points can be generated over an entire region of the feature space, rather than augmenting based on individual samples. This aspect of the simulation is the cornerstone of the novelty of this approach: in comparison to existing approaches as SMOTE (Synthetic Minority Oversampling Technique) [Chawla et al.2002], the oversampling does not depend on individual samples in the data. In simple terms, SMOTE augments data by geometrically inserting samples between existing samples; this is suitable for experiments for which there is already exist an appreciable amount of data in a data set, but reiterating, as PHL-EC has less data already (for the classes of mesoplanets and psychroplanets), an oversampling based on individual samples is not a good way to proceed. Here, it is best to estimate the probability density of the data and proceed with the oversampling in a bounded manner. For large-scale simulation tasks similar in nature to this, thus, ML-based approaches can go a long way to save time and automate the process of discovery of knowledge.

2.9.3 Fitting a Distribution to the Data Points

In this method, the mean surface temperature was selected as the core discriminating feature since it emerged as the most important feature amongst the classes in the catalog (Tables 13 and 14). The mean surface temperature for different classes of planets falls in different

Table 18: Results of using random forests (Gini impurity) to classify the planets in the optimistic sample

Name	True Class	Classification Accuracy	non-habitable	psychroplanet	mesoplanet
Kepler-438 b	mesoplanet	100.0	0.0	0.0	100.0
Kepler-296 e	mesoplanet	100.0	0.0	0.0	100.0
Kepler-62 e	mesoplanet	100.0	0.0	0.0	100.0
Kepler-452 b	mesoplanet	99.9	0.1	0.0	99.9
K2-72 e	mesoplanet	100.0	0.0	0.0	100.0
GJ 832 c	mesoplanet	100.0	0.0	0.0	100.0
K2-3 d	non-habitable	0.0	0.0	0.0	100.0
Kepler-1544 b	mesoplanet	100.0	0.0	0.0	100.0
Kepler-283 c	mesoplanet	100.0	0.0	0.0	100.0
Kepler-1410 b	mesoplanet	100.0	0.0	0.0	100.0
GJ 180 c	mesoplanet	96.2	0.0	3.8	96.2
Kepler-1638 b	mesoplanet	100.0	0.0	0.0	100.0
Kepler-440 b	mesoplanet	100.0	0.0	0.0	100.0
GJ 180 b	mesoplanet	100.0	0.0	0.0	100.0
Kepler-705 b	mesoplanet	100.0	0.0	0.0	100.0
HD 40307 g	psychroplanet	100.0	0.0	100.0	0.0
GJ 163 c	psychroplanet	100.0	0.0	100.0	0.0
Kepler-61 b	mesoplanet	100.0	0.0	0.0	100.0
K2-18 b	mesoplanet	100.0	0.0	0.0	100.0
Kepler-1090 b	mesoplanet	100.0	0.0	0.0	100.0
Kepler-443 b	mesoplanet	100.0	0.0	0.0	100.0
Kepler-22 b	mesoplanet	100.0	0.0	0.0	100.0
GJ 422 b	mesoplanet	0.0	0.0	100.0	0.0
Kepler-1552 b	mesoplanet	99.9	0.1	0.0	99.9
GJ 3293 c	psychroplanet	100.0	0.0	100.0	0.0
Kepler-1540 b	mesoplanet	100.0	0.0	0.0	100.0
Kepler-298 d	mesoplanet	100.0	0.0	0.0	100.0
Kepler-174 d	psychroplanet	100.0	0.0	100.0	0.0
Kepler-296 f	psychroplanet	100.0	0.0	100.0	0.0
GJ 682 c	psychroplanet	100.0	0.0	100.0	0.0
tau Cet e	mesoplanet	100.0	0.0	0.0	100.0

Table 19: Results of using random forests (binomial confidence split) to classify the planets in the conservative sample

Name	True Class	Classification Accuracy	non-habitable	psychroplanet	mesoplane
Proxima Cen b	psychroplanet	99.8	0.0	99.8	0.2
GJ 667 C c	mesoplanet	88.1	0.0	11.9	88.1
Kepler-442 b	psychroplanet	98.5	0.0	98.5	1.5
GJ 667 C f	psychroplanet	100.0	0.0	100.0	0.0
Wolf 1061 c	psychroplanet	100.0	0.0	100.0	0.0
Kepler-1229 b	psychroplanet	100.0	0.0	100.0	0.0
Kapteyn b	psychroplanet	100.0	0.0	100.0	0.0
Kepler-62 f	psychroplanet	100.0	0.0	100.0	0.0
GJ 667 C e	psychroplanet	100.0	0.0	100.0	0.0

ranges [Méndez2011]. The mean surface temperature was fit to a Poisson distribution; the vector of remaining features was randomly mapped to these randomly generated values of S. Temp. The resulting vectors of artificial samples may be considered to be a vector $S = (Temp_{Surface}, X)$, where X is any naturally occurring sample in the PHL-EC data set without its corresponding value of the S. Temp feature. The set of the pairs (S, c) thus becomes an entire artificial catalog, where c is the class label. The following are the steps to generate artificial data set for the mesoplanet class:

Step 1: For the original set of values pertinent to the mean surface temperature of mesoplanets, a Poisson distribution is fit. The surface temperature of the planets assumed to be randomly distributed, following a Poisson distribution. Here, an approximation may be made that the surface temperatures occur in discrete bins or intervals, without a loss of generality. As the number of samples is naturally less, a Poisson distribution may be fit to the S. Temp features after rounding off the values to the nearest decimal.

Step 2: Then, using the average value of the mesoplanets' S. Temp data, 1000 new values are generated, using the Poisson distribution:

$$Pr(X) = \frac{e^{-\lambda}\lambda^{x}}{x!} \tag{26}$$

where λ is the mean of the values of the S. Temp feature of the mesoplanet class.

Step 3: For every planet in the original data set, duplicate the data sample 40 times and replace the surface temperature value of these (total of 1000 samples) with new values of the mean surface temperature randomly, as generated in Step 2.

Table 20: Results of using random forests (binomial confidence split) to classify the planets in the optimistic sample

Name	True Class	Classification Accuracy	non-habitable	psychroplanet	mesoplanet
Kepler-438 b	mesoplanet	100.0	0.0	0.0	100.0
Kepler-296 e	mesoplanet	100.0	0.0	0.0	100.0
Kepler-62 e	mesoplanet	100.0	0.0	0.0	100.0
Kepler-452 b	mesoplanet	100.0	0.0	0.0	100.0
K2-72 e	mesoplanet	100.0	0.0	0.0	100.0
GJ 832 c	mesoplanet	99.9	0.0	0.1	99.9
K2-3 d	non-habitable	0.1	0.1	0.0	99.9
Kepler-1544 b	mesoplanet	99.7	0.0	0.3	99.7
Kepler-283 c	mesoplanet	99.8	0.0	0.2	99.8
Kepler-1410 b	mesoplanet	100.0	0.0	0.0	100.0
GJ 180 c	mesoplanet	65.10	0.0	34.9	65.1
Kepler-1638 b	mesoplanet	99.1	0.9	0.0	99.1
Kepler-440 b	mesoplanet	100.0	0.0	0.0	100.0
GJ 180 b	mesoplanet	100.0	0.0	0.0	100.0
Kepler-705 b	mesoplanet	98.6	0.0	1.4	98.6
HD 40307 g	psychroplanet	96.39	0.0	96.4	3.6
GJ 163 c	psychroplanet	100.0	0.0	100.0	0.0
Kepler-61 b	mesoplanet	100.0	0.0	0.0	100.0
K2-18 b	mesoplanet	100.0	0.0	0.0	100.0
Kepler-1090 b	mesoplanet	99.9	0.1	0.0	99.9
Kepler-443 b	mesoplanet	99.9	0.0	0.1	99.9
Kepler-22 b	mesoplanet	100.0	0.0	0.0	100.0
GJ 422 b	mesoplanet	0.0	0.0	100.0	0.0
Kepler-1552 b	mesoplanet	99.8	0.2	0.0	99.8
GJ 3293 c	psychroplanet	100.0	0.0	100.0	0.0
Kepler-1540 b	mesoplanet	100.0	0.0	0.0	100.0
Kepler-298 d	mesoplanet	99.7	0.3	0.0	99.7
Kepler-174 d	psychroplanet	100.0	0.0	100.0	0.0
Kepler-296 f	psychroplanet	100.0	0.0	100.0	0.0
GJ 682 c	psychroplanet	100.0	0.0	100.0	0.0
tau Cet e	mesoplanet	99.9	0.1	0.0	99.9

Table 21: Results of using XGBoost to classify the planets in the conservative sample

Name	True Class	Classification Accuracy	non-habitable	psychroplanet	mesoplanet
Proxima Cen b	psychroplanet	100.0	0.0	100.0	0.0
GJ 667 C c	mesoplanet	100.0	0.0	0.0	100.0
Kepler-442 b	psychroplanet	6.8	0.2	6.8	93.0
GJ 667 C f	psychroplanet	100.0	0.0	100.0	0.0
Wolf 1061 c	psychroplanet	100.0	0.0	100.0	0.0
Kepler-1229 b	psychroplanet	100.0	0.0	100.0	0.0
Kapteyn b	psychroplanet	100.0	0.0	100.0	0.0
Kepler-62 f	psychroplanet	100.0	0.0	100.0	0.0
GJ 667 C e	psychroplanet	100.0	0.0	100.0	0.0

This exercise is repeated for the psychroplanet class separately. Once the probability densities of both the classes were developed, the rectification mechanism using the algorithm described in Section 2.9.2 was used to retain only those samples in either class which conformed to the properties of the respective class. Using this method, 1000 artificial samples were generated for the mesoplanet and psychroplanet classes.

In order to generate 1000 samples for the classes with less number of samples (mesoplanets and psychroplanets), the hybrid SVM-KNN algorithm as described in Section 2.9.2 is used to rectify the class-belongingness of any non-conforming random samples. Only the top four features of the data sets from Table 13, i.e. P. Ts Mean, P. Ts Min, P. Teq Min, and P. Teq Max are considered in this rectification mechanism. This method of acceptance-rectification is self-contained in itself: the artificially generated data set is iteratively split into training and testing sets (in a ratio of 70:30). If any artificially generated sample in any iteration fails to be accepted by the SVM-KNN algorithm, its class-belongingness in the data set is changed; as this simulation is done only on two classes in the data, non-conformance to one class could only indicate the belongingness to the other class. The process of artificially generating and labeling data is illustrated using Figure 10. In Figure 10(a), a new set of data points generated randomly from the estimated Poisson distributions of both classes are plotted. The points in red depict artificial points belonging to the class of psychroplanets and the points in blue depict artificial points belonging to the class of mesoplanets. The physical limits as per the Planetary Habitability Catalog are incorporated into the data synthesis scheme and hence, in general, the number of non-conforming points generated are less. Figure 10(b) depicts three points (encircled) that should belong to the psychroplanet class but belongs to the mesoplanet class: note that these three points cross the boundary between the two classes as set by an SVM. The blue portion may contain points which belong to only

Table 22: Results of using XGBoost to classify the planets in the optimistic sample

Name	True Class	Classification Accuracy	non-habitable	psychroplanet	mesoplanet
Kepler-438 b	mesoplanet	99.9	0.1	0	99.9
Kepler-296 e	mesoplanet	100	0	0	100
Kepler-62 e	mesoplanet	100	0	0	100
Kepler-452 b	mesoplanet	100	0	0	100
K2-72 e	mesoplanet	99.2	0.8	0	99.2
GJ 832 c	mesoplanet	98.1	0	1.9	98.1
K2-3 d	non-habitable	1.2	1.2	0	98.8
Kepler-1544 b	mesoplanet	100	0	0	100
Kepler-283 c	mesoplanet	100	0	0	100
Kepler-1410 b	mesoplanet	99.6	0.4	0	99.6
GJ 180 c	mesoplanet	74	0	26	74
Kepler-1638 b	mesoplanet	99.2	0.8	0	99.2
Kepler-440 b	mesoplanet	97.9	2.1	0	97.9
GJ 180 b	mesoplanet	100	0	0	100
Kepler-705 b	mesoplanet	100	0	0	100
HD 40307 g	psychroplanet	99	0	99	1
GJ 163 c	psychroplanet	100	0	100	0
Kepler-61 b	mesoplanet	99	1	0	99
K2-18 b	mesoplanet	100	0	0	100
Kepler-1090 b	mesoplanet	100	0	0	100
Kepler-443 b	mesoplanet	99.9	0	0.1	99.9
Kepler-22 b	mesoplanet	99.9	0.1	0	99.9
GJ 422 b	mesoplanet	57.2	1.3	41.5	57.2
Kepler-1552 b	mesoplanet	99.9	0.1	0	99.9
GJ 3293 c	psychroplanet	100	0	100	0
Kepler-1540 b	mesoplanet	99.7	0.3	0	99.7
Kepler-298 d	mesoplanet	99	1	0	99
Kepler-174 d	psychroplanet	100	0	100	0
Kepler-296 f	psychroplanet	100	0	100	0
GJ 682 c	psychroplanet	99.7	0.3	99.7	0
tau Cet e	mesoplanet	99.9	0.1	0	99.9

Table 23: Accuracy of algorithms used to classify Proxima b

Algorithm	Accuracy(%)
Decision Tree	84.5
Random Forest (Gini Split)	100.0
Random Forest (Conf. Split)	100.0
XGBoost	100.0

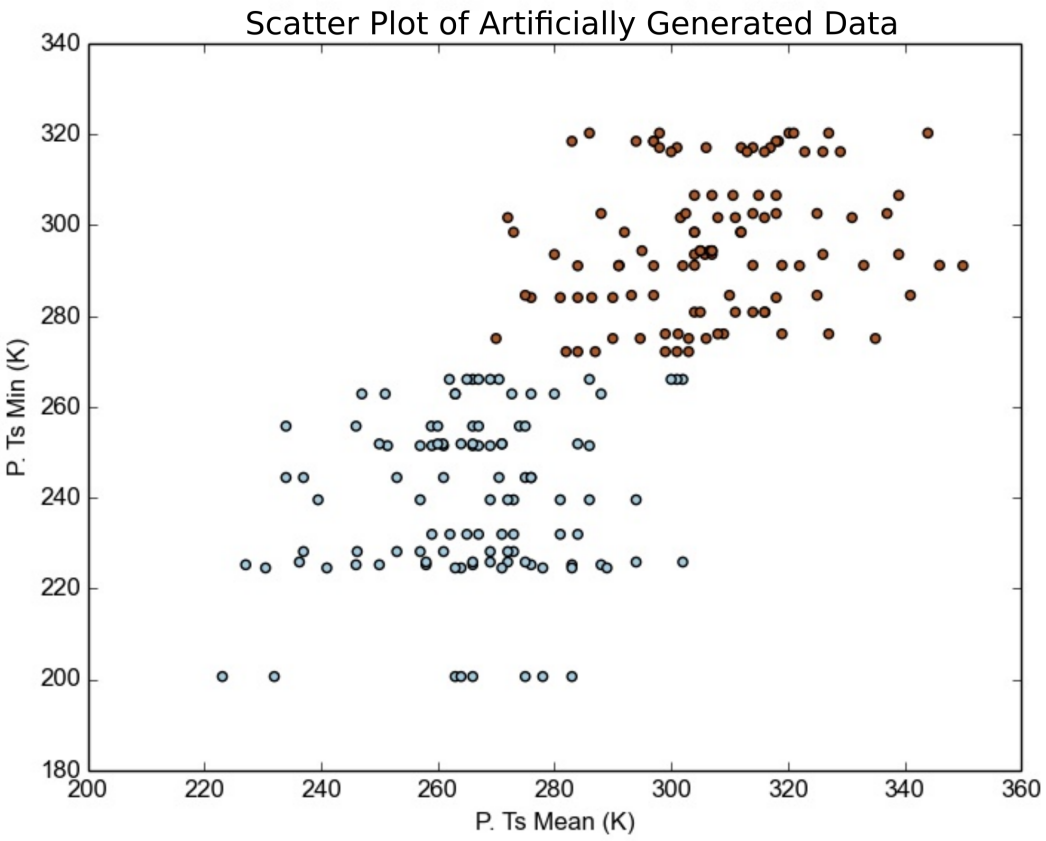

(a) Scatter plot of newly generated artificial data points in two dimensions.

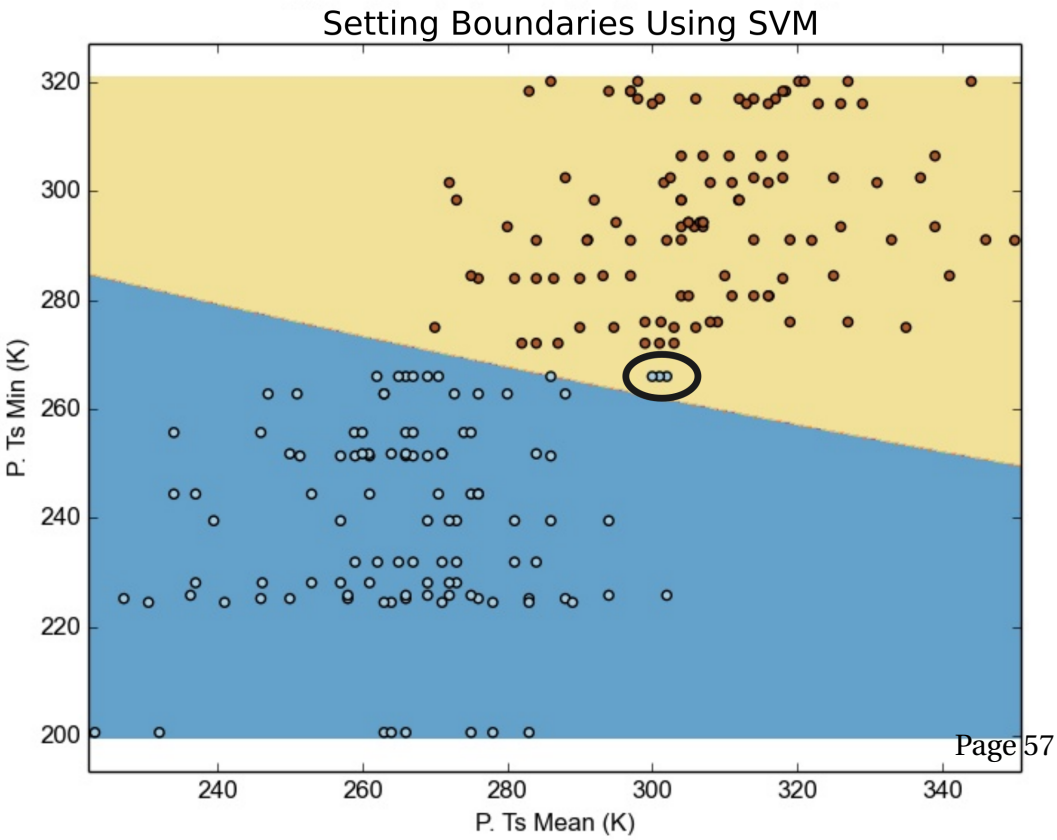

(b) Best boundaries between two classes set using SVM. Here, there are three non-conforming data points (encircled) belonging to the mesoplanets' class.

the mesoplanet class and the yellow portion may contain points which belong only to the psychroplanet class, but these three points are non-conforming according to the boundary imposed. Hence, in order to ascertain the correct labels, these three points are subjected to a K-NN based rectification. In Figure 10(c), the points in the data set are plotted after being subjected to K-NN with $k = 5$ and class labels are modified as required. The three previously non-conforming points are determined to actually belong to the class of psychroplanets, and hence their class-belongingness is changed. Figure 10(d) shows that the boundary between the two classes is altered by incorporating the rectified class-belongingness of the previously non-conforming points. In this figure, it is to be noted that all the points are conforming, and there are no points which belong to the region of the wrong class. This procedure was run many times on the artificially generated data to estimate the number of iterations and the time required for each iteration until the resulting data set was devoid of any non-conforming data points. As the process is inherently stochastic, each new run of the SVM-KNN algorithm might result in a different number of iterations (and different amounts of execution time for each iteration) required until zero non-conforming samples are achieved. However, a general trend may be analyzed for the purpose of ascertaining that the algorithm will complete in a finite amount of time. Figure 11 is a plot of the i^{th} iteration against the time required for the algorithm to execute the respective iteration (to rectify the points in the synthesized data set). From this figure, it should be noted that each successive iteration requires a smaller amount of time to complete: the red curve (a quadratic fit of the points) represents a decline in the time required for the SVM-KNN method to complete execution in successive iterations of a run. The number of iterations required for the complete execution of the SVM-KNN method ranges from one to six, with a generally declining execution time of successive iterations, proving the stability of the hybrid algorithm. Any algorithm is required to *converge*: a point beyond which the execution of the algorithm ceases. In this case, convergence must ensure that every artificially generated data point conforms to the general properties of the class to which it is labeled to belong.

The advantage of this method is that there is enough evidence of work done previously that makes use of standard probability distributions to model the occurrence of various stellar objects. This current simulation only has the added dimension of class-label rectification by using the hybrid SVM-KNN method. The method is easy to interpret. However, as the amount of data in the PHL-EC catalog are less, fitting a distribution to the data may lead to an over-fitting of the probability density estimate. To counter this point, an empirical multivariate distribution estimation was performed as a follow-through to this piece of work.

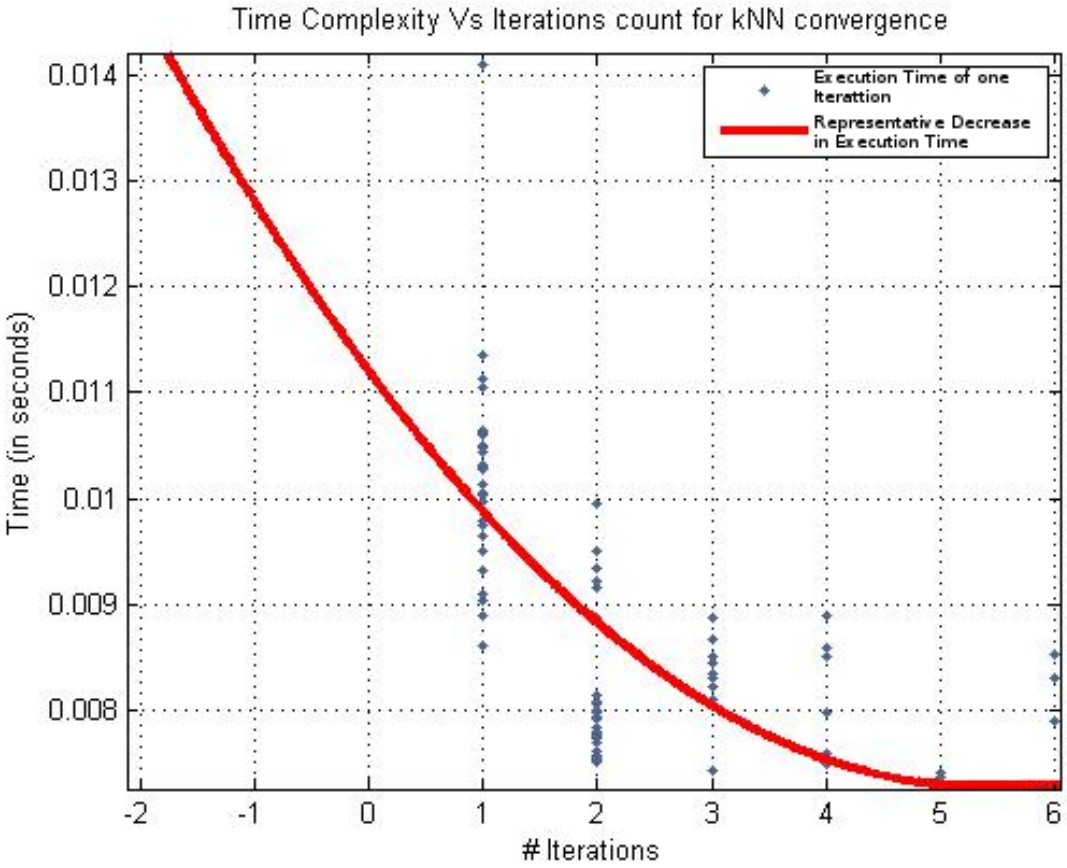

Figure 11: A quadratic curve has been fit to the execution times of successive iterations in a run of the SVM-KNN method. The time required to converge to the perfect labeling of class-belongingness of the synthetic data points reduces with each successive iteration resulting in the dip exhibited in successive iterations. This fortifies the efficiency of the proposed hybrid SVM-KNN algorithm. Accuracy is not traded with the speed of convergence.

2.9.4 Generating Data by Analyzing the Distribution of Existing Data Empirically: Window Estimation Approach

In this method of synthesizing data samples, the density of the data distribution is approximated by a numeric mathematical model, instead of relying on an established analytical model (such as Poisson, or Gaussian distributions). As the sample distribution here is sporadic, the density function itself should be approximated. The process outlined for this estimation of the population density function was described independently by [Roesnblatt1956] and [Parzen1962] and is termed Kernel Density Estimation (KDE). KDE, as a non-parametric technique, requires no assumptions on the structure of the data and further, with slight alterations to the kernel function, may also be extended to multivariate random variables.

2.9.5 Estimating Density

Let $X = x_1, x_2, \ldots, x_n$ be a sequence of independent and identically distributed multivariate random variables having d dimensions. The window function used is a variation of the uniform kernel defined on the set R^d as follows:

$$\phi(u) = \begin{cases} 1 & u_j \leq \frac{1}{2} \quad \forall\, j \in \{1,2,\ldots,d\} \\ 0 & otherwise \end{cases} \tag{27}$$

Additionally, another parameter, the edge length vector $h = \{h_1, h_2, \ldots h_d\}$, is defined, where each component of h is set on a heuristic that considers the values of the corresponding feature in the original data. If f_j is the column vector representing some feature $j \in X$ and

$$\begin{aligned} l_j &= min\{(a-b)^2 \quad \forall\ a,b \in f_j\} \\ u_j &= max\{(a-b)^2 \quad \forall\ a,b \in f_j\}, \end{aligned} \tag{28}$$

the edge length h_j is given by,

$$h_j = c\left(\frac{u_j + 2l_j}{3}\right) \tag{29}$$

where c is a scale factor.

Let $x' \in R^d$ be a random variable at which the density needs to be estimated. For the estimate, another vector u is generated whose elements are given by:

$$u_j = \frac{x_j{}' - x_{ij}}{h_j} \qquad \forall\, j \in \{1,2,\ldots,d\} \tag{30}$$

The density estimate is then given by the following equation:

$$p(x') = \frac{1}{n \prod_{i=1}^{d} h_i} \sum_{i=1}^{n} \phi(u) \tag{31}$$

2.9.6 Generating Synthetic Samples

Traditionally, random numbers are generated from an analytic density function by inversion sampling. However, this would not work on a numeric density function unless the quantile function is numerically approximated by the density function. In order to avoid this, a form of rejection sampling has been used.

Let r be a d-dimensional random vector with each component drawn from a uniform distribution between the minimum and maximum value of that component in the original data. Once the density, $p(r)$ is estimated by Equation (31), the probability is approximated to:

$$Pr(r) = p(r) \prod_{j=1}^{d} h_j \tag{32}$$

To either accept or reject the sample r, another random number is generated from a uniform distribution within the range $[0,1)$. If this number is greater than the probability estimated by Equation (32), then the sample is accepted. Otherwise, it is rejected.

Data synthesis using KDE and rejection sampling (refer to Appendix **??** for visual details) was used to generate a synthetic data set. For the PHL-EC data set, synthetic data was generated for the mesoplanet and psychroplanet classes by estimating their density by Equation (31) taking $c = 4$ for mesoplanets and $c = 3$ for psychroplanets. 1000 samples were then generated for each class using rejection sampling on the density estimate. In this method, the bounding mechanism was not used and the samples were drawn out of the estimated density. Here, the top 16 features (top 85% of the features by importance, Table 13) were considered to estimate the probability density, and hence the boundary between the two classes using SVM was not constructed. The values of the remaining features were copied from the naturally occurring data points and shuffled between the artificially augmented data points in the same way as in the method described in Section 2.9.3). The advantage of using this method is that it may be used to estimate a distribution which resembles more closely the actual distribution of the data. However, this process is more complex and takes a longer time to execute. Nonetheless, the authors would assert this as a method of synthetic oversampling than the method described in Section 2.9.2 as it is inherently unassuming and can accommodate distributions in data which are otherwise difficult to describe using the

Table 24: Results on artificially augmented data sets by assuming a distribution and augmenting in a bounded manner.

Algorithm	Class	Sensitivity	Specificity	Precision	Accuracy
Decision Trees	Non-Habitable	0.9977333333	1	1	0.9992735043
	Mesoplanet	1	0.9994227809	0.9988474837	0.9996152531
	Psychroplanet	1	0.9994768164	0.9990133202	0.9996579881
Random Forests	Non-Habitable	0.9997333333	1	1	0.9999145299
	Mesoplanet	1	0.9998717949	0.9997436555	0.9999145299
	Psychroplanet	1	1	1	1
XGBoost	Non-Habitable	0.9989333333	1	1	0.9996581197
	Mesoplanet	1	1	1	1
	Psychroplanet	1	0.9994771242	0.9990133202	0.9996581197

commonly used methods for describing the density of data.

2.10 Results of Classification on Artificially Augmented Data Sets

The results of classification experimented on the data sets generated by the methods described in Sections 2.9.1 and 2.9.4 are shown in Tables 24 and 25 respectively.

In both methods, 1000 samples were then generated for mesoplanet and psychroplanet classes; in each iteration of testing the classifiers, 1000 samples were randomly drawn from the non-habitable class. The original mesoplanet and psychroplanet data, the synthetic samples, and the samples drawn from the non-habitable class together form an augmented data set. This data set was then subjected to the non-metric classifiers to test their performance. For each iteration applied to evaluating classification accuracy, the augmented data set was split into a training and test set by randomly sampling the records of each class into the two sets at a ratio of 7:3. The classifiers were trained and their accuracy of classification estimated through the test set. The training and test sets were then re-sampled for the next iteration. This was 100 times, following which, a new set of 1000 samples were drawn from the non-habitable class to replace the previous samples. The whole process of drawing non-habitable samples and subjecting the augmented data set to 100 iterations of testing has been repeated 20 times with the averaged results presented in Tables 24 and 25. The commonly available methods available in most open source toolkits have been tried to classify the artificially augmented samples. These results indicate that the classifiers are capable of handling large data sets without any signs of diminishing performance.

The whole exercise of artificially augmenting the data set may be considered to be nothing but a simulation of the natural increase of the data points in the catalog. The methods

Table 25: Results on artificially augmented data sets by empirical analysis.

Algorithm	Class	Sensitivity	Specificity	Precision	Accuracy
Decision Trees	Non-Habitable	0.9977333333	1	1	0.9992552026
	Mesoplanet	1	0.9992102665	0.9984287024	0.9994741455
	Psychroplanet	1	0.999669159	0.9993510707	0.9997808267
Random Forests	Non-Habitable	0.9992	1	1	0.9997371188
	Mesoplanet	1	0.9999341845	0.9998688697	0.9999561769
	0.9998701299	0.9996033058	0.9992212849	0.9996933187	
XGBoost	Non-Habitable	0.9986666667	1	1	0.9995618839
	Mesoplanet	1	0.9998025406	0.9996067121	0.9998685248
	Psychroplanet	1	0.9995370983	0.9990917348	0.9996932784

described are a combination of data synthesis by density estimation as well as oversampling with replacement: the most important features were modeled using probability distributions and the values of the less important features were sampled by replacement. By incorporating the physical limits, bounding the nature of growing data points (representing planets), fitting probability densities and classifying, the authors have emulated the application of classification algorithms to the data set with a considerable growth in the number of points. Exoplanets are being discovered at a fast rate, with recent hypes on Proxima b and the TRAPPIST-1 systems. This simulation shows that even with the growing number of discovered exoplanets, machine learning classifiers can do well to segregate planets into the correct classes of habitability.

The synthetic datasets which were generated and on which classification algorithms were tried can be found at: https://github.com/SuryodayBasak/ExoplanetsSyntheticData.

2.11 Conclusion

This paper has presented statistical techniques used on the PHL-EC data set in order to explore the capability of Machine learning algorithms in determining the habitability of an exoplanet. The potential of many algorithms, namely naïve Bayes, LDA, SVM, K-NN, decision trees, random forests, and XGBoost was explored to classify exoplanets based on their habitability. Naturally, questions are bound to arise regarding the choice and use of so many classifiers. Machine learning as an emerging area has its limitations and it's not surprising that scores of manuscripts are available in the public domain. However, many of these papers have applied different machine learning algorithms without adequately justifying the motivation and limitations of these algorithms. A method is as good as the data! The authors, throughout the manuscript, wanted to highlight this and endeavored to

construct and present their work as a primer in machine learning with respect to the data set used. The goal was to discover intrinsic limitations of each learning method and document those for the benefit of readers and young researchers who wish to apply machine learning in astronomy. The performance of a classifier depends on the nature of data, the size of data etc; however, there is no guarantee that a classifier which works well on one data set will work equally well on another data set, even if both data sets are from the same domain of astronomy. The separability of data is a major factor in deciding kind of appropriate classifiers for the corresponding data set. This fact is validated in the work presented. Hence, it is imperative for any exploratory data analysis to present a comparative study of different methods used.

The novelty of the current work lies in the selection of an appropriate data set, HEC (PHL-EC catalog) that was hitherto not investigated in the existing literature. The most important difference between NASA's catalog and PHL-EC is that the former makes data available for only those planets which are Kepler's Objects of interest whereas the latter contains data for all discovered planets, KOI or not, confirmed or unconfirmed. NASA's catalog for exoplanets has around 25 features whereas PHL-EC has 68 features, including but not limited to planet's mass, radius, orbital period, planet type, flux, density, distance from star, habitable zone, Earth similarity index (ESI) [Schulze-Makuch et al.2011], habitable class, composition class, eccentricity, etc. The website of the University of Puerto Rico, Planetary Habitability Laboratory lists the number of potentially habitable exoplanets: the results of our classification correlate remarkably well with what PHL has already stated in the conservative and optimistic samples of habitable planets.

It is important to point out that the PHL-EC [Méndez2016] data set assumes circular orbits (zero eccentricity) for planets with unknown eccentricities. This could raise questions if our predictions are accurate enough to describe real systems given the initial data set. Similarly, the equilibrium temperature is measured for Earth-like planets or mainly non-gaseous planets by considering the albedo of Earth (0.367), which again may not be close to their actual equilibrium temperature. In other words, the selected data set contains several estimated stellar and planetary parameters and they have also claimed many corrections [Méndez2016] which make them different from other exoplanet databases. This is the main reason we have selected PHL-EC: since it poses such challenges. Notwithstanding these limitations in the data set, the methods and improvisations as enunciated in Section 2.6.9, have worked remarkably well and the theoretical justifications of the efficacy of those methods have been well understood and documented by the authors.

In the process of exploring the data set and the various classifiers, a software called Ex-

oPlanet [Theophilus, Reddy & Basak2016] was developed (refer to Appendix **??**). This is a follow-up to the ASTROMLS KIT [Saha et al.2015]. The goal of the software is to reduce programming overheads in research involving data analytics. The software provides a graphical user interface (GUI) to select a data set, and then a method (classification, regression, and clustering) of choice can be selected by a *point-and-click mechanism*. The results (accuracy, sensitivity, specificity, etc) and all necessary graphs (ROC, etc.) are displayed in the same window. The software is currently in its infancy. However, the authors plan to extend the functionality by including more analysis, pre-processing and post-processing methods. A cloud-based web application is on the anvil.

The accuracy of various machine learning algorithms used on the PHL-EC data set has been computed and tabulated. Random forest, decision trees, and XGBoost rank best with the highest accuracy closely followed by naïve Bayes. A separate section has been dedicated to the classification of the recently discovered exoplanet Proxima b, where the current classification system has achieved accuracy as high as 100%. However, a lot of data is not available in the PHL-EC catalog: there exists a tremendously high bias towards the non-habitable class of planets, where the number of entities is 1000 times more than that of the other classes. The number of entities available in the psychroplanet and mesoplanet classes might be deemed as insufficient for an effective classification. Despite this bias, we were able to achieve remarkable accuracy with ML algorithms by performing artificial balancing on the data. This also goes to show that deep learning (which has unfortunately grown to become a cottage industry) is not necessary for every difficult classification scenario. A careful study of the nature of the data and trends is a must and simple solutions may often suffice.

In another effort to counter the effects of bias in the data set, the underrepresented classes of mesoplanets and psychroplanets were artificially augmented using assumptions of distributions as well as empirical analysis. Though many different methods of data synthesis may be adopted, the two most common and reasonable paradigms were tried. The accuracies achieved for this were near perfect (Tables 24 and 25). From this simulation exercise, it may be expected that with the natural extension of the data set in the future, the learning algorithms will continue to infer the data better and the accuracy will remain very high.

Exoplanets are frequently discovered and categorizing them manually is an arduous task. However, the work presented here may be translated into a simple automated system. A crawler, simple enough to design, may target the major databases and can append the catalog with discovered but non-categorized exoplanets. The suite of machine learning algorithms could then perform the task of classification, as demonstrated earlier, with reasonably acceptable accuracy. A significant portion of time, otherwise invested in studying parameters and

manual labeling, could thus be saved. In future, a continuation of the present work would be directed towards achieving a sustainable and automated discrimination system for efficient and accurate analysis of different exoplanet databases.

Coupled with web scraping methods and the suite of learning algorithms, automatic labeling of newly discovered exoplanets could thus be facilitated in a fairly easy and accurate manner. In summary, the work is a detailed primer on exploratory data analysis involving algorithmic improvisations and machine learning methods applied to a very complex data set, bolstered by a comprehensive understanding of these methods as documented in the appendices. The inferences drawn fortify these methods and the effort and time invested. The software ExoPlanet is designed to achieve the ultimate goal of classifying exoplanets with the aid of a limited manual or human intervention.

3 CD-HPF: New Habitability Score Via Data Analytic Modeling

3.1 Introduction

In the last decade, thousands of planets are discovered in our Galaxy alone. The inference is that stars with planets are a rule rather than exception [Cassan et al.2012], with estimates of the actual number of planet exceeding the number of stars in our Galaxy by orders of magnitude [Strigari et al.(2012)]. The same line of reasoning suggests a staggering number of at least 10^{24} planets in the observable Universe. The biggest question posed therefore is whether there are other life-harbouring planets. The most fundamental interest is in finding the Earth's twin. In fact, *Kepler* space telescope (`http://kepler.nasa.gov/`) was designed specifically to look for Earth's analogs – Earth-size planets in the habitable zones (HZ) of G-type stars [Batalha 2014]. More and more evidence accumulated in the last few years suggests that, in astrophysical context, Earth is an average planet, with average chemistry, existing in many other places in the Galaxy, average mass and **size**. Moreover, recent discovery of the rich organic content in the protoplanetary disk of newly formed star MWC 480 [Öberg et al.2015] has shown that neither is our Solar System unique in the abundance of the key components for life. Yet the only habitable planet in the Universe known to us is our Earth.

The question of habitability is of such interest and importance that the theoretical work has expanded from just the stellar HZ concept to the Galactic HZ (Gonzales et al. 2001) and, recently, to the Universe HZ — asking a question which galaxies are more habitable than others (Dayal et al. 2015). However, the simpler question — which of thousands detected planets are, or can be, habitable is still not answered. Life on other planets, if exists, may be similar to what we have on our planet, or may be in some other unknown form. The answer to this question may depend on understanding how different physical planetary parameters, such as planet's orbital properties, its chemical composition, mass, radius, density, surface and interior temperature, distance from it's parent star, even parent star's temperature or mass, combine to provide habitable conditions. With currently more than 1800 confirmed and more than 4000 unconfirmed discoveries[1], there is already enormous amount of accumulated data, where the challenge lies in the selection of how much to study about each planet, and which parameters are of the higher priority to evaluate.

Several important characteristics were introduced to address the habitability question. [Schulze-Makuch et al.2011] first addressed this issue through two indices, the Planetary

[1] Extrasolar Planets Encyclopedia, http://exoplanet.eu/catalog/

Habitability Index (PHI) and the Earth Similarity Index (ESI), where maximum, by definition, is set as 1 for the Earth, PHI=ESI=1.

ESI represents a quantitative measure with which to assess the similarity of a planet with the Earth on the basis of mass, size and temperature. But ESI alone is insufficient to conclude about the habitability, as planets like Mars have ESI close to 0.8 but we cannot still categorize it as habitable. There is also a possibility that a planet with ESI value slightly less than 1 may harbor life in some form which is not there on Earth, i.e. unknown to us. PHI was quantitatively defined as a measure of the ability of a planet to develop and sustain life. However, evaluating PHI values for large number of planets is not an easy task. In [Irwin et al.2014], another parameter was introduced to account for the chemical composition of exoplanets and some biology-related features such as substrate, energy, geophysics, temperature and age of the planet — the Biological Complexity Index (BCI). Here, we briefly describe the mathematical forms of these parameters.

Earth Similarity Index (ESI) ESI was designed to indicate how Earth-like an exoplanet might be [Schulze-Makuch et al.2011] and is an important factor to initially assess the habitability measure. Its value lies between 0 (no similarity) and 1, where 1 is the reference value, i.e. the ESI value of the Earth, and a general rule is that any planetary body with an ESI over 0.8 can be considered an Earth-like. It was proposed in the form

$$ESI_x = \left(1 - \left|\frac{x - x_0}{x + x_0}\right|\right)^w , \tag{33}$$

where ESI_x is the ESI value of a planet for x property, and x_0 is the Earth's value for that property. The final ESI value of the planet is obtained by combining the geometric means of individual values, where w is the weighting component through which the sensitivity of scale is adjusted. Four parameters: surface temperature T_s, density D, escape velocity V_e and radius R, are used in ESI calculation. This index is split into interior ESI_i (calculated from radius and density), and surface ESI_s (calculated from escape velocity and surface temperature). Their geometric means are taken to represent the final ESI of a planet. However, ESI in the form (33) was not introduced to define habitability, it only describes the similarity to the Earth in regard to some planetary parameters. For example, it is relatively high for the Moon.

Planetary Habitability Index (PHI) To actually address the habitability of a planet, [Schulze-Makuch et al.2 defined the PHI as

$$PHI = (S \cdot E \cdot C \cdot L)^{1/4} , \tag{34}$$

where S defines a substrate, E – the available energy, C – the appropriate chemistry and L – the liquid medium; all the variables here are in general vectors, while the corresponding scalars represent the norms of these vectors. For each of these categories, the PHI value is divided by the maximum PHI to provide the normalized PHI in the scale between 0 to 1. However, PHI in the form (34) lacks some other properties of a planet which may be necessary for determining its present habitability. For example, in Shchekinov et al. (2013) it was suggested to complement the original PHI with the explicit inclusion of the age of the planet (see their Eq. 6).

3.1.0.1 Biological Complexity Index (BCI) To come even closer to defining habitability, yet another index was introduced, comprising the above mentioned four parameters of the PHI and three extra parameters, such as geophysical complexity G, appropriate temperature T and age A [Irwin et al.2014]. Therefore, the total of seven parameters were initially considered to be important for the BCI. However, due to the lack of information on chemical composition and the existence of liquid water on exoplanets, only five were retained in the final formulation,

$$BCI = (S \cdot E \cdot T \cdot G \cdot A)^{1/5} . \tag{35}$$

It was found in [Irwin et al.2014] that for 5 exoplanets the BCI value is higher than for Mars, and that planets with high BCI values may have low values of ESI.

All previous indicators for habitability assume a planet to reside within in a classical HZ of a star, which is conservatively defined as a region where a planet can support liquid water on the surface [Huang1959, Kasting1993]. The concept of an HZ is, however, a constantly evolving one, and it has have been since suggested that a planet may exist beyond the classical HZ and still be a good candidate for habitability [Irwin & Schulze-Makuch2011, Heller & Armstrong2014]. Though presently all efforts are in search for the Earth's twin where the ESI is an essential parameter, it never tells that a planet with ESI close to 1 is habitable. Much advertised recent hype in press about finding the best bet for life-supporting planet – Gliese 832c with ESI = 0.81 [Wittenmyer et al.2014], was thwarted by the realization that the planet is more likely to be a super-Venus, with large thick atmosphere, hot surface and probably tidally locked with its star.

We present here the novel approach to determine the habitability score of all confirmed exoplanets analytically. Our goal is to determine the likelihood of an exoplanet to be habitable using the newly defined habitability score (CDHS) based on Cobb-Douglas habitability production function (CD-HPF), which computes the habitability score by using measured

and calculated planetary input parameters. Here, the PHI in its original form turned out to be a special case. We are looking for a feasible solution that maximizes habitability scores using CD-HPF with some defined constraints. In the following sections, the proposed model and motivations behind our work are discussed along with the results and applicability of the method. We conclude by listing key takeaways and robustness of the method. The related derivations and proofs are included in the appendices.

3.2 CD-HPF: Cobb-Douglas Habitability Production Function

We first present key definitions and terminologies that are utilized in this paper. These terms play critical roles in understanding the method and the algorithm adopted to accomplish our goal of validating the habitability score, **CDHS**, by using CD-HPF eventually.

Key Definitions

- **Mathematical Optimization**

  Optimization is one of the procedures to select the best element from a set of available alternatives in the field of mathematics, computer science, economics, or management science [Hájková & Hurnik2007]. An optimization problem can be represented in various ways. Below is the representation of an optimization problem. Given a function $f : A \to R$ from a set A to the real numbers R. If an element x_0 in A is such that $f(x_0) \leq f(x)$ for all x in A, this ensures minimization. The case $f(x_0) \geq f(x)$ for all x in A is the specific case of maximization. The optimization technique is particularly useful for modeling the habitability score in our case. In the above formulation, the domain A is called a search space of the function f, CD-HPF in our case, and elements of A are called the candidate solutions, or feasible solutions. The function as defined by us is a utility function, yielding the habitability score CDHS. It is a feasible solution that maximizes the objective function, and is called an optimal solution under the constraints known as **Returns to scale**.

- **Returns to scale** measure the extent of an additional output obtained when all input factors change proportionally. There are three types of returns to scale:

  1. **Increasing returns to scale (IRS)**. In this case, the output increases by a larger proportion than the increase in inputs during the production process. For example, when we multiply the amount of every input by the number N, the factor by which output increases is more than N. This change occurs as

     [(i)]

(a) Greater application of the variable factor ensures better utilization of the fixed factor.

(b) Better division of the variable factor.

(c) It improves coordination between the factors.

The 3-D plots obtained in this case are neither concave nor convex.

2. **Decreasing returns to scale (DRS)**. Here, the proportion of increase in input increases the output, but in lower ratio, during the production process. For example, when we multiply the amount of every input by the number N, the factor by which output increases is less than N. This happens because:
   [(i)]

   (a) As more and more units of a variable factor are combined with the fixed factor, the latter gets over-utilized. Hence, the rate of corresponding growth of output goes on diminishing.

   (b) Factors of production are imperfect substitutes of each other. The divisibility of their units is not comparable.

   (c) The coordination between factors get distorted so that marginal product of the variable factor declines.

   The 3-D plots obtained in this case are concave.

3. **Constant returns to scale (CRS)**. Here, the proportion of increase in input increases output in the same ratio, during the production process. For example, when we multiply the amount of every input by a number N, the resulting output is multiplied by N. This phase happens for a negligible period of time and can be considered as a passing phase between IRS and DRS. The 3-D plots obtained in this case are concave.

- **Computational Techniques in Optimization**. There exist several well-known techniques including Simplex, Newton-like and Interior point-based techniques [Nemirovski & Todd2008]. One such technique is implemented via MATLAB's optimization toolbox using the function **fmincon**. This function helps find the global optima of a constrained optimization problem which is relevant to the model proposed and implemented by the authors. Illustration of the function and its syntax are provided in Appendix D.

- **Concavity**. Concavity ensures global maxima. The implication of this fact in our case is that if CD-HPF is proved to be concave under some constraints (this will be elaborated

later in the paper), we are guaranteed to have maximum habitability score for each exoplanet in the global search space.

- **Machine Learning**. Classification of patterns based on data is a prominent and critical component of machine learning and will be highlighted in subsequent part of our work where we made use of a standard K-NN algorithm. The algorithm is modified to tailor to the complexity and efficacy of the proposed solution. Optimization, as mentioned above, is the art of finding maximum and minimum of surfaces that arise in models utilized in science and engineering. More often than not, the optimum has to be found in an efficient manner, i.e. both the speed of convergence and the order of accuracy should be appreciably good. Machines are trained to do this job as, most of the times, the learning process is iterative. Machine learning is a set of methods and techniques that are intertwined with optimization techniques. The learning rate could be accelerated as well, making optimization problems deeply relevant and complementary to machine learning.

3.3 Cobb-Douglas Habitability Production Function CD-HPF

The general form of the Cobb-Douglas production function CD-PF is

$$Y = k \cdot (x_1)^{\alpha} \cdot (x_2)^{\beta}\,, \tag{36}$$

where k is a constant that can be set arbitrarily according to the requirement, Y is the total production, i.e. output, which is homogeneous with the degree 1; x_1 and x_2 are the input parameters (or factors); α and β are the real fixed factors, called the elasticity coefficients. The sum of elasticities determines returns to scale conditions in the CDPF. This value can be less than 1, equal to 1, or greater than 1.

What motivates us to use the Cobb-Douglas production function is its properties. Cobb-Douglas production function (Cobb & Douglas, 1928) was originally introduced for modeling the growth of the American economy during the period of 1899–1922, and is currently widely used in economics and industry to optimize the production while minimizing the costs [Wu2001, Hossain et al.2012, Hassani2012, Saha et al.2016]. Cobb-Douglas production function is concave if the sum of the elasticities is not greater than one (see the proof in Bergstrom 2010). This gives global extremum in a closed interval which is handled by constraints in elasticity (Felipe & Adams, 2005). The physical parameters used in the Cobb-Douglas model may change over time and, as such, may be modeled as continuous entities. A functional

representation, i.e response, Y, is thus a continuous function, and may increase or decrease in maximum or minimum value as these parameters change (Hossain et al., 2012). Our formulation serves this purpose, where elasticities may be adjusted via *fmincon* or fitting algorithms, in conjunction with the intrinsic property of the CD-HPF that ensures global maxima for concavity. Our simulations, that include animation and graphs, support this trend (see Figures 1 and 2 in Section 3). As the physical parameters change in value, so do the function values and its maximum for all the exoplanets in the catalog, and this might rearrange the CDHS pattern with possible changes in the parameters, while maintaining consistency with the database.

The most important properties of this function that make it flexible to be used in various applications are:

- It can be transformed to the log-linear form from its multiplicative form (non-linear) which makes it simple to handle, and hence, linear regression techniques can be used for estimation of missing data.
- Any proportional change in any input parameter can be represented easily as the change in the output.
- The ratio of relative inputs x_1 and x_2 to the total output Y is represented by the elasticities α and β.

The analytical properties of the CDPF motivated us to check the applicability in our problem, where the four parameters considered to estimate the habitability score are surface temperature, escape velocity, radius and density. Here, the production function Y is the habitability score of the exoplanet, where the aim is to maximize Y, subject to the constraint that the sum of all elasticity coefficients shall be less than or equal to 1. Computational optimization is relevant for elasticity computation in our problem. Elasticity is the percentage change in the output Y (Eq. 4), given one percent change in the input parameter, x_1 or x_2. We assume k is constant. In other words, we compute the rate of change of output Y, the CDPF, with respect to one unit of change in input, such as x_1 or x_2. As the quantity of x_1 or x_2 increases by one percent, output increases by α or β percent. This is known as the elasticity of output with respect to an input parameter. As it is, values of the elasticity, α and β are not ad-hoc and need to be approximated for optimization purpose by some computational technique. The method, *fmincon* with interior point search, is used to compute the elasticity values for CRS, DRS and IRS. The outcome is quick and accurate. We elaborate the significance of the scales and elasticity in the context of CDPF and CDHS below.

- **Increasing returns to scale (IRS):** In Cobb-Douglas model, if $\alpha + \beta > 1$, the case is called an IRS. It improves the coordination among the factors. This is indicative of boosting the habitability score following the model with one unit of change in respective predictor variables.

- **Decreasing returns to scale (DRS):** In Cobb-Douglas model, if $\alpha + \beta < 1$, the case is called a DRS, where the deployment of an additional input may affect the output with diminishing rate. This implies the habitability score following the model may decrease with the one unit of change in respective predictor variables.

- **Constant returns to scale (CRS):** In Cobb-Douglas model, if $\alpha + \beta = 1$, this case is called a CRS, where increase in α or/and β increases the output in the same proportion. The habitability score, i.e the response variable in the Cobb-Douglas model, grows proportionately with changes in input or predictor variables.

The range of elasticity constants is between 0 and 1 for DRS and CRS. This will be exploited during the simulation phase (Section 3). It is proved in Appendices B and C that the habitability score (CDHS) maximization is accomplished in this phase for **DRS and CRS**, respectively.

The impact of change in the habitability score according to each of the above constraints will be elaborated in Sections 4 and 5. Our aim is to optimize elasticity coefficients to maximize the habitability score of the confirmed exoplanets using the CD-HPF .

3.4 Cobb-Douglas Habitability Score estimation

We have considered the same four parameters used in the ESI metric (Eq. 33), i.e. surface temperature, escape velocity, radius and density, to calculate the Cobb-Douglas Habitability Score (CDHS). Analogous to the method used in ESI, two types of Cobb-Douglas Habitability Scores are calculated – the interior CDHS_i and the surface CDHS_i. The final score is computed by a linear convex combination of these two, since it is well known that a convex combination of convex/concave function is also convex/concave. The interior CDHS_i, denoted by $Y1$, is calculated using radius R and density D,

$$Y1 = CDHS_i = (D)^{\alpha} \cdot (R)^{\beta}. \tag{37}$$

The surface CDHS_s, denoted by $Y2$, is calculated using surface temperature T_s and escape velocity V_e,

$$Y2 = CDHS_s = (T_s)^{\gamma} \cdot (V_e)^{\delta}. \tag{38}$$

The final CDHS Y, which is a convex combination of $Y1$ and $Y2$, is determined by

$$Y = w' \cdot Y1 + w'' \cdot Y2\,, \tag{39}$$

where the sum of w' and w'' equals 1. The values of w' and w'' are the weights of the interior CDHS_i and surface CDHS_s, respectively. These weights depend on the importance of individual parameters of each exoplanet. The $Y1$ and $Y2$ are obtained by applying CDPF (Eq. 36) with $k = 1$. Finally, the Cobb-Douglas habitability production function (CD-HPF) can be formally written as

$$\mathbb{Y} = f\,(R, D, T_s, V_e) = (R)^{\alpha} \cdot (D)^{\beta} \cdot (T_s)^{\gamma} \cdot (V_e)^{\delta}\,. \tag{40}$$

For a 3-D interpretation of the CDPF model with elasticities α and β, Appendix A contains brief discussion on manipulating α and β algebraically. The goal is to maximize Y, iff $\alpha + \beta + \gamma + \delta < 1$. It is possible to calculate the CDHS by using both Eqs. (39) and (50), however there is hardly any difference in the final value. Equation (50) is impossible to visualize since it is a 5-dimensional entity. Whereas, Eq. (39) has 3-dimensional structure.The ease of visualization is the reason **CDHS** is computed by splitting into two parts $Y1$ and $Y2$ and combining by using the weights w' and w''. Individually, each of $Y1$ and $Y2$ are sample 3-D models and, as such, are easily comprehensible via surface plots as demonstrated later (see Figs. 1 and 2 in Section 3). The authors would like to emphasize that instead of splitting and computing CDHS as a convex combination of $Y1$ and $Y2$, a direct calculation of CDHS through Eq. (50) is possible, which does not alter the final outcome. It is avoided here, since using the product of all four parameters with corresponding elasticities α, β, γ and δ would make rendering the plots impossible for the simple reason of dimensionality being too high, 5 instead of 3. We reiterate that the scalability of the model from α, β to α, β, γ and δ does not suffer due to this scheme. The proof presented in Appendix B bears testimony to our claim.

3.5 The Theorem for Maximization of Cobb-Douglas habitability production function

Statement: CD-HPF attains global maxima in the phase of DRS or CRS [Saha et al.2016].
Sketch of proof: Generally profit of a firm can be defined as

$$\text{profit} = \text{revenue} - \text{cost} = \big(\text{price of output} \times \text{output}\big) - \big(\text{price of input} \times \text{input}\big)\,.$$

Let $p_1, p_2, \ldots, p_n$ be a vector of prices for outputs, or products, and $w_1, w_2, \ldots, w_m$ be a vector of prices for inputs of the firm, which are always constants; and let the input levels be $x_1, x_2, \ldots, x_m$, and the output levels be $y_1, y_2, \ldots, y_n$. The profit, generated by the production plan, $(x_1, \ldots, x_m, y_1, \ldots, y_n)$ is

$$\pi = \left(p_1 \cdot y_1 + \ldots + p_n \cdot y_n - w_1 \cdot x_1 - \ldots - w_m \cdot x_m\right).$$

Suppose the production function for m inputs is

$$Y = f\left(x_1, x_2, ..., x_m\right),$$

and its profit function is

$$\pi = p \cdot Y - w_1 \cdot x_1 - \ldots - w_m \cdot x_m.$$

A single output function needs p as the price, while multiple output functions will require multiple prices $p_1, p_2, \ldots, p_n$. The profit function in our case, which is a single-output multiple-inputs case, is given by

$$\pi = p f\left(R, D, T_s, V_e\right) - w_1 R - w_2 D - w_3 T_s - w_4 V_e, \tag{41}$$

where w_1, w_2, w_3, w_4 are the weights chosen according to the importance for habitability for each planet. Maximization of CD-HPF is achieved when

$$(1)\ p\frac{\partial f}{\partial R} = w_1, \quad (2)\ p\frac{\partial f}{\partial D} = w_2, \quad (3)\ p\frac{\partial f}{\partial T_s} = w_3, \quad (4)\ p\frac{\partial f}{\partial V_e} = w_4. \tag{42}$$

The habitability score is conceptualized as a profit function where the cost component is introduced as a penalty function to check unbridled growth of CD-HPF. This bounding framework is elaborated in the proofs of concavity, the global maxima and computational optimization technique, and function *fmincon* in Appendices B, C and D, respectively.

Remark: If we consider the case of CRS, where all the elasticities of different cost components are equal, the output is $Y = \prod_{i=1}^{n} x_i^{\alpha_i}$, where all α_i are equal and $\sum \alpha_i = 1$. In such scenario, $Y \equiv G.M.$ (Geometric Mean) of the cost inputs. Further scrutiny reveals that the geometric mean formalization is nothing but the representation of the PHI, thus establishing our framework of CD-HPF as a broader model, with the PHI being a corollary for the CRS case.

Once we compute the habitability score, Y, the next step is to perform clustering of the Y

values. We have used K-nearest neighbor (K-NN) classification algorithm and introduced probabilistic herding and thresholding to group the exoplanets according to their Y values. The algorithm finds the exoplanets for which Y values are very close to each other and keeps them in the same group, or cluster. Each CDHS value is compared with its K (specified by the user) nearest exoplanet's (closer Y values) CDHS value, and the class which contains maximum nearest to the new one is allotted as a class for it.

3.6 Implementation of the Model

We applied the CD-HPF to calculate the Cobb-Douglas habitability score (CDHS) of exoplanets. A total of 664 confirmed exoplanets are taken from the Planetary Habitability Laboratory Exoplanets Catalog (PHL-EC)[2]. The catalog contains observed and estimated stellar and planetary parameters for a total of 3415 (July 2016) currently confirmed exoplanets, where the estimates of the surface temperature are given for 1586 planets. However, there are only 586 rocky planets where the surface temperature is estimated, using the correction factor of 30-33 K added to the calculated equilibrium temperature, based on the Earth's greenhouse effect (Schulze-Makuch et al. 2011a; Volokin & ReLlez 2016). For our dataset, we have taken all rocky planets plus several non-rocky samples to check the algorithm. In machine learning, such random samples are usually used to check for the robustness of the designed algorithm and to add variations in the training and test samples. Otherwise, the train and test samples would become heavily biased towards one particular trend. As mentioned above, the CDHS of exoplanets are computed from the interior CDHS_i and the surface CDHS_s. The input parameters radius R and density D are used to compute the values of the elasticities α and β. Similarly, the input parameters surface temperature T_S and escape velocity V_e are used to compute the elasticities γ and δ. These parameters, except the surface temperature, are given in Earth Units (EU) in the PHL-EC catalog. We have normalized the surface temperatures T_s of exoplanets to the EU, by dividing each of them with Earth's mean surface temperature, 288 K.

The Cobb-Douglas function is applied on varying elasticities to find the CDHS close to Earth's value, which is considered as 1. As all the input parameters are represented in EU, we are looking for the exoplanets whose CDHS is closer to Earth's CDHS. For each exoplanet, we obtain the optimal elasticity and the maximum CDHS value. The results are demonstrated graphically using 3-D plot. All simulations were conducted using the MATLAB software for the cases of DRS and CRS. From Eq. (B.38), we can see that for CRS Y will grow asymptotically,

[2]provided by the Planetary Habitability Laboratory @ UPR Arecibo, accessible at `http://phl.upr.edu/projects/habitable-exoplanets-catalog/data/database`

if

$$\alpha + \beta + \gamma + \delta = 1\,. \tag{43}$$

Let us set

$$\alpha = \beta = \gamma = \delta = 1/4\,. \tag{44}$$

In general, the values of elasticities may not be equal but the sum may still be 1. As we know already, this is CRS. A special case of CRS, where the elasticity values are made to be equal to each other in Eq. (12), turns out to be structurally analogous to the PHI and BCI formulations. Simply stated, the CD-HPF function satisfying this special condition may be written as

$$Y = f = k\,(R \cdot D \cdot T_s \cdot V_e)^{1/4}\,. \tag{45}$$

The function is concave for CRS and DRS (Appendices B and C).

3.7 Computation of CDHS in DRS phase

We have computed elasticities separately for interior CDHS_i and surface CDHS_s in the DRS phase. These values were obtained using function *fmincon*, a computational optimization technique explained in Appendix D. Tables 1 through 3 show a sample of computed values. Table 26 shows the computed elasticities α, β and CDHS_i. The optimal interior CDHS_i for most exoplanets are obtained at $\alpha = 0.8$ and $\beta = 0.1$. Table 2 shows the computed elasticities γ, δ and CDHS_s. The optimal surface CDHS are obtained at $\gamma = 0.8$ and $\delta = 0.1$. Using these results, 3-D graphs are generated and are shown in Figure 1. The X and Y axes represent elasticities and Z-axis represents CDHS of exoplanets. The final CDHS, Y, calculated using Eq. (7) with $w' = 0.99$ and $w'' = 0.01$, is presented in Table 3.

3.8 Computation of CDHS in CRS phase

The same calculations were carried out for the CRS phase. Tables 4, 5 and 6 show the sample of computed elasticities and habitability scores in CRS. The convex combination of CDHS_i and CDHS_s gives the final CDHS (Eq. 7) with $w' = 0.99$ and $w'' = 0.01$. The optimal interior CDHS_i for most exoplanets were obtained at $\alpha = 0.9$ and $\beta = 0.1$, and the optimal surface CDHS_s were obtained at $\gamma = 0.9$ and $\delta = 0.1$. Using these results, 3-D graphs were generated and are shown in Figure 2.

Tables 1, 2 and 3 represent CDHS for DRS, where the corresponding values of elasticities were found by *fmincon* to be 0.8 and 0.1, and the sum= $0.9 < 1$ (The theoretical proof is

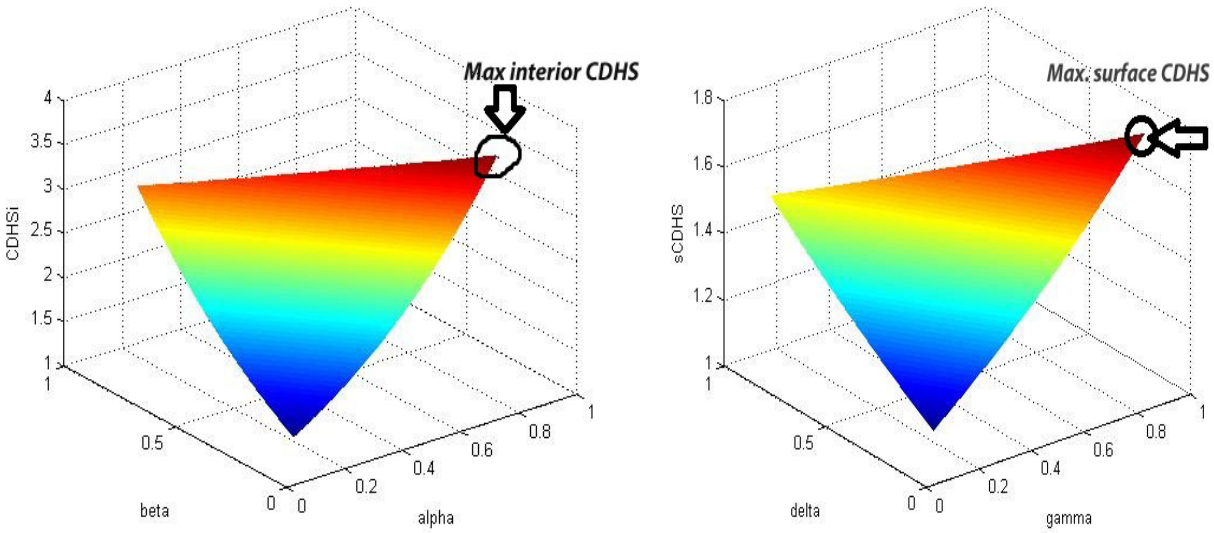

Figure 12: Plot of interior CDHS$_i$ (*Left*) and surface CDHS$_s$ (*Right*) for DRS

given in Appendix B). Tables 4, 5 and 6 show results for CRS, where the sum of the elasticities = 1 (The theoretical proof is given in Appendix C). The approximation algorithm *fmincon* initiates the search for the optima by starting from a random initial guess, and then it applies a step increment or decrements based on the gradient of the function based on which our modeling is done. It terminates when it cannot find elasticities any better for the maximum

Table 26: Sample simulation output of interior CDHS$_i$ of exoplanets calculated from radius and density for DRS

Exoplanet	Radius	Density	Elasticity(α)	Elasticity (β)	CDHS$_i$
GJ 163 c	1.83	1.19	0.8	0.1	1.65012
GJ 176 b	1.9	1.23	0.8	0.1	1.706056
GJ 667C b	1.71	1.12	0.8	0.1	1.553527
GJ 667C c	1.54	1.05	0.8	0.1	1.4195
GJ 667C d	1.67	1.1	0.8	0.1	1.521642
GJ 667C e	1.4	0.99	0.8	0.1	1.307573
GJ 667C f	1.4	0.99	0.8	0.1	1.307573
GJ 3634 b	1.81	1.18	0.8	0.1	1.634297
Kepler-186 f	1.11	0.9	0.8	0.1	1.075679
Gl 15 A b	1.69	1.11	0.8	0.1	1.537594
HD 20794 c	1.35	0.98	0.8	0.1	1.26879
HD 40307 e	1.5	1.03	0.8	0.1	1.387256
HD 40307 f	1.68	1.11	0.8	0.1	1.530311
HD 40307 g	1.82	1.18	0.8	0.1	1.641517

Table 27: Sample simulation output of surface CDHS of exoplanets calculated from escape velocity and surface temperature for DRS

Exoplanet	Escape Velocity	Surface temperature	Elasticity (γ)	Elasticity (δ)	$CDHS_s$
GJ 163 c	1.99	1.11146	0.8	0.1	1.752555
GJ 176 b	2.11	1.67986	0.8	0.1	1.91405
GJ 667C b	1.81	1.49063	0.8	0.1	1.672937
GJ 667C c	1.57	0.994	0.8	0.1	1.433764
GJ 667C d	1.75	0.71979	0.8	0.1	1.51409
GJ 667C e	1.39	0.78854	0.8	0.1	1.27085
GJ 667C f	1.39	0.898958	0.8	0.1	1.287614
GJ 3634 b	1.97	2.1125	0.8	0.1	1.946633
Kepler-186 f	1.05	0.7871	0.8	0.1	1.015213
Gl 15 A b	1.78	1.412153	0.8	0.1	1.641815
HD 40307 e	1.53	1.550694	0.8	0.1	1.482143
HD 40307 f	1.76	1.38125	0.8	0.1	1.623444
HD 40307 g	1.98	0.939236	0.8	0.1	1.716365
HD 20794 c	1.34	1.89791667	0.8	0.1	1.719223

Table 28: Sample simulation output of CDHS with $w' = 0.99$ and $w'' = 0.01$ for DRS

Exoplanet	$CDHS_i$	$CDHS_s$	CDHS
GJ 163 c	1.65012	1.752555	1.651144
GJ 176 b	1.706056	1.91405	1.708136
GJ 667C b	1.553527	1.672937	1.554721
GJ 667C c	1.4195	1.433764	1.419643
GJ 667C d	1.521642	1.514088	1.521566
GJ 667C e	1.307573	1.27085	1.307206
GJ 667C f	1.307573	1.287614	1.307373
GJ 3634 b	1.634297	1.946633	1.63742
Gl 15 A b	1.537594	1.641815	1.538636
Kepler-186 f	1.075679	1.015213	1.075074
HD 20794 c	1.26879	1.719223	1.273294
HD 40307 e	1.387256	1.482143	1.388205
HD 40307 f	1.530311	1.623444	1.531242
HD 40307 g	1.641517 7	1.716365	1.642265

CDHS. The plots in Figures 1 and 2 show all the elasticities for which *fmincon* searches for the global maximum in CDHS, indicated by a black circle. Those values are read off from the code (given in Appendix E) and printed as 0.8 and 0.1, or whichever the case may be. A minimalist web page is designed to host all relevant data and results: sets, figures, animation video and a graphical abstract. It is available at `https://habitabilitypes.wordpress.com/`.

Table 29: Sample simulation output of interior CDHS$_i$ of exoplanets calculated from radius and density for CRS

Exoplanet	Radius	Density	Elasticity(α)	Elasticity (β)	$CDHS_i$
GJ 163 c	1.83	1.19	0.9	0.1	1.752914
GJ 176 b	1.9	1.23	0.9	0.1	1.819151
GJ 667C b	1.71	1.12	0.9	0.1	1.639149
GJ 667C c	1.54	1.05	0.9	0.1	1.482134
GJ 667C d	1.67	1.1	0.9	0.1	1.601711
GJ 667C e	1.4	0.99	0.9	0.1	1.352318
GJ 667C f	1.4	0.99	0.9	0.1	1.352318
GJ 3634 b	1.81	1.18	0.9	0.1	1.734199
Kepler-186 f	1.11	0.9	0.9	0.1	1.086963
Gl 15 A b	1.69	1.11	0.9	0.1	1.62043
HD 20794 c	1.35	0.98	0.9	0.1	1.307444
HD 40307 e	1.5	1.03	0.9	0.1	1.444661
HD 40307 f	1.68	1.11	0.9	0.1	1.611798
HD 40307 g	1.82	1.18	0.9	0.1	1.74282

Table 30: Sample simulation output of surface CDHS of exoplanets calculated from escape velocity and surface temperature for CRS

Exoplanet	Escape Velocity	Surface temperature	Elasticity (γ)	Elasticity (δ)	CDHS$_s$
GJ 163 c	1.99	1.11146	0.9	0.1	1.877401
GJ 176 b	2.11	1.67986	0.9	0.1	2.062441
GJ 667C b	1.81	1.49063	0.9	0.1	1.775201
GJ 667C c	1.57	0.994	0.9	0.1	1.499919
GJ 667C d	1.75	0.71979	0.9	0.1	1.601234
GJ 667C e	1.39	0.78854	0.9	0.1	1.313396
GJ 667C f	1.39	0.898958	0.9	0.1	1.330722
GJ 3634 b	1.97	2.1125	0.9	0.1	2.097798
Kepler-186 f	1.05	0.7871	0.9	0.1	1.020179
Gl 15 A b	1.78	1.412153	0.9	0.1	1.739267
HD 40307 e	1.53	1.550694	0.9	0.1	1.548612
HD 40307 f	1.76	1.38125	0.9	0.1	1.717863
HD 40307 g	1.98	0 .939236	0.9	0.1	1.837706
HD 20794 c	1.34	1.89791667	0.9	0.1	1.832989

The animation video, available at the website, demonstrates the concavity property of CD-HPF and CDHS. The animation comprises 664 frames (each frame is a surface plot essentially), corresponding to 664 exoplanets under consideration. Each frame is a visual representation of the outcome of CD-HPF and CDHS applied to each exoplanet. The X and Y axes of the 3-D plots represent elasticity constants and Z-axis represents the CDHS. Simply

Table 31: Sample simulation output of CDHS with $w' = 0.99$ and $w'' = 0.01$ for CRS

Exoplanet	$CDHS_i$	$CDHS_s$	CDHS
GJ 163 c	1.752914	1.877401	1.754159
GJ 176 b	1.819151	2.062441	1.821584
GJ 667C b	1.639149	1.775201	1.64051
GJ 667C c	1.482134	1.499919	1.482312
GJ 667C d	1.601711	1.601234	1.601706
GJ 667C e	1.352318	1.313396	1.351929
GJ 667C f	1.352318	1.330722	1.352102
GJ 3634 b	1.734199	2.097798	1.737835
Kepler-186 f	1.086963	1.020179	1.086295
GI 15 A b	1.62043	1.739267	1.621618
HD 40307 e	1.444661	1.548612	1.445701
HD 40307 f	1.611798	1.717863	1.612859
HD 40307 g	1.74282	1.837706	1.743769
HD 20794 c	1.307444	1.832989	1.312699

stated, each frame, demonstrated as snapshots of the animation in Figs. 1 and 2, is endowed with a maximum CDHS and the cumulative effect of all such frames is elegantly captured in the animation.

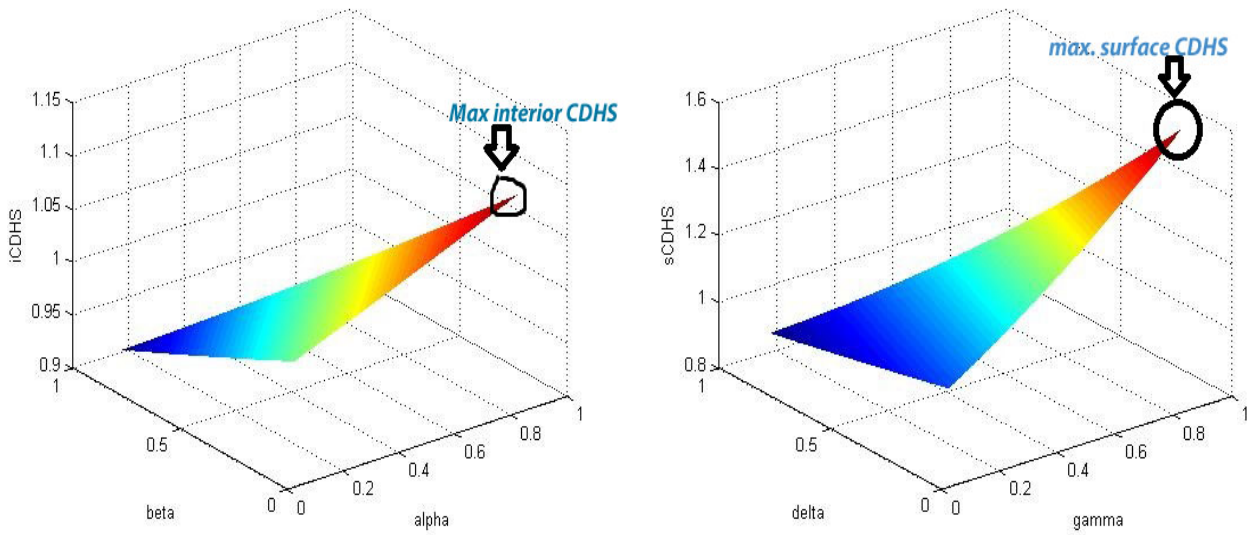

Figure 13: Plot of interior $CDHS_i$ (*Left*) and surface $CDHS_s$ (*Right*) for CRS

3.9 Attribute Enhanced K-NN Algorithm: A Machine learning approach

K-NN, or K-nearest neighbor, is a well-known machine learning algorithm. Attribute-enhanced K-NN algorithm is used to classify the exoplanets into different classes based on the computed CDHS values. 80% of data from the Habitable Exoplanets Catalog (HEC)[3]) are used for training, and remaining 20% for testing. Training–testing process is integral to machine learning, where the machine is trained to recognize patterns by assimilating a lot of data and, upon applying the learned patterns, identifies new data with a reasonable degree of accuracy. The efficacy of a learning algorithm is reflected in the accuracy with which the test data is identified. The training data set is uniformly distributed between 5 classes, known as balancing the data, so that bias in the training sample is eliminated. The algorithm produces 6 classes, wherein each class carries exoplanets with CDHS values close to each other, a first condition for being called as "neighbours". Initially, each class holds one fifth of the training data and a new class, i.e. Class 6, defined as Earth's Class (or "Earth-League"), is derived by the proposed algorithm from first 5 classes where it contains data based on the two conditions.
The two conditions that our algorithm uses to select exoplanets into Class 6 are defined as:

1. Thresholding: Exoplanets with their CDHS minus Earth's CDHS being less than or equal to the specified boundary value, called threshold. We have set a threshold in such a way that the exoplanets with CDHS values within the threshold of 1 (closer to Earth) fall in Earth's class. The threshold is chosen to capture proximal planets as the CDHS of all exoplanets considered vary greatly However, this proximity alone does not determine habitability.

2. Probabilistic Herding: if exoplanet is in the HZ of its star, it implies probability of membership to the Earth-League, Class 6, to be high; probability is low otherwise. Elements in each class in K-NN get re-assigned during the run time. This automatic re-assignment of exoplanets to different classes is based on a weighted likelihood concept applied on the members of the initial class assignment.

Consider K as the desired number of nearest neighbors and let $S := p_1, \ldots, p_n$ be the set of training samples in the form $p_i = (x_i, c_i)$, where x_i is the d-dimensional feature vector of the point p_i and c_i is the class that p_i belongs to. In our case, dimension, $d = 1$. We fix $S' := p_{1'}, \ldots, p_{m'}$ to be the set of testing samples. For every sample, the difference in CDHS

[3]The Habitable Exoplanets Catalog (HEC) is an online database of potentially habitable planets, total 32 as on January 16, 2016; maintained by the Planetary Habitability LaboratoryUPR Arecibo, and available at `http://phl.upr.edu/projects/habitable-exoplanets-catalog`

between Earth and the sample is computed by looping through the entire dataset containing the 5 classes. Class 6 is the offspring of these 5 classes and is created by the algorithmic logic to store the selected exoplanets which satisfy the conditions of the K-NN and the two conditions – thresholding and probabilistic herding defined above. We train the system for 80% of the data-points based on the two constraints, prob($habitability_i$) = 'high' and CDHS(p_i)−CDHS(**Earth**)≤ threshold. These attributes enhance the standard K-NN and help the re-organization of $exoplanet_i$ to Class 6.

If CDHS of $exoplanet_i$ falls with a certain range, K-NN classifies it accordingly into one of the remaining 5 classes. For each $p' = (x', c')$, we compute the distance $d(x', x_i)$ between p' and all p_i for the dataset of 664 exoplanets from the PHL-EC, S. Next, the algorithm selects the K nearest points to p' from the list computed above. The classification algorithm, K-NN, assigns a class c' to p' based on the condition prob($habitability_i$) = 'high' plus the thresholding condition mentioned above. Otherwise, K-NN assigns p' to the class according to the range set for each class. Once the "Earth-League" class is created after the algorithm has finished its run, the list is cross-validated with the habitable exoplanet catalog HEC. It must be noted that Class 6 not only contains exoplanets that are similar to Earth, but also the ones which are most likely to be habitable. The algorithmic representation of K-NN is presented in Appendix E.

3.10 Results and Discussion

The K-NN classification method has resulted in "Earth-league", Class 6, having 14 and 12 potentially habitable exoplanets by DRS and CRS computations, respectively. The outcome of the classification algorithm is shown in Tables 7 and 8.

There are 12 common exoplanets in Tables 7 and 8. We have cross-checked these planets with the Habitable Exoplanets Catalog and found that they are indeed listed as potentially habitable planets. Class 6 includes all the exoplanets whose CDHS is proximal to Earth. As explained above, classes 1 to 6 are generated by the machine learning technique and classification method. Class 5 includes the exoplanets which are likely to be habitable, and planets in Classes 1, 2, 3 & 4 are less likely to be habitable, with Class 1 being the least likely to be habitable. Accuracy achieved here is 92% for $K = 1$, implying 1-nearest neighbor, and is 94% for $K = 7$, indicating 7 nearest neighbors.

In Figure 3 we show the plots of K-NN algorithm applied on the results in DRS (top plot) and CRS (bottom plot) cases. The X-axis represents CDHS and Y-axis – the 6 dif-

Table 32: Potentially habitable exoplanets in Earth's class using DRS: Outcome of CDHS and K-NN

Exoplanet	CDH Score
GJ 667C e	1.307206
GJ 667C f	1.307373
GJ 832 c	1.539553
HD 40307 g	1.642265
Kapteyn's b	1.498503
Kepler-61 b	1.908765
Kepler-62 e	1.475502
Kepler-62 f	1.316121
Kepler-174 d	1.933823
Kepler-186 f	1.07507
Kepler-283 c	1.63517
Kepler-296 f	1.619423
GJ 667C c	1.419643
GJ 163 c	1.651144

Table 33: Potentially habitable exoplanets in Earth's class using CRS: Outcome of CDHS and K-NN

Exoplanet	CDH Score
GJ 667C e	1.351929
GJ 667C f	1.352102
GJ 832 c	1.622592
HD 40307 g	1.743769
Kapteyn's b	1.574564
Kepler-62 e	1.547538
Kepler-62 f	1.362128
Kepler-186 f	1.086295
Kepler-283 c	1.735285
Kepler-296 f	1.716655
GJ 667C c	1.482312
GJ 163 c	1.754159

ferent classes assigned to each exoplanet. The figure is a schematic representation of the outcome of our algorithm. The color points, shown in circles and boxes to indicate the membership in respective classes, are representative of membership only and do not indicate a quantitative equivalence. The numerical data on the number of the exoplanets in each class is provided in Appendix F. A quantitative representation of the figures may be found at `https://habitabilitypes.wordpress.com/`.

We also normalized CDHS of each exoplanet, dividing by the maximum score in each category, for both CRS and DRS cases (with Earth's normalized score for CRS = 0.003176 and DRS = 0.005993). This resulted in CDHS of all 664 exoplanets ranging from 0 to 1. Analogous to the case of non-normalized CDHS, these exoplanets have been assigned equally to 5 classes. K-NN algorithm was then applied to all the exoplanets' CDHS for both CRS and DRS cases. Similar to the method followed in non-normalized CDHS for CRS and DRS, K-NN has been applied to "dump" exoplanets which satisfy the criteria of being members of Class 6. Table 9 shows the potentially habitable exoplanets obtained from classification on normalized data for both CRS and DRS. This result is illustrated in Figs. 3c and 3d. In this figure, Class 6 contains 16 exoplanets generated by K-NN and which are considered to be potentially habitable according to the PHL-EC. The description of the remaining classes is

the same as in Figs. 3a and 3b.

Table 34: The outcome of K-NN on normalized dataset: potentially habitable exoplanets in Class 6 (Earth-League).

Exoplanet	DRSnormCDHS	CRSnormCDHS
GJ 667C e	0.007833698	0.004294092
GJ 667C f	0.007834698	0.004294642
GJ 832 c	0.009226084	0.005153791
HD 40307 g	0.009841607	0.005538682
Kapteyn's b	0.008980084	0.00500124
Kepler-22 b	0.01243731	0.007181929
Kepler-61 b	0.011438662	0.006546287
Kepler-62 e	0.008842245	0.004915399
Kepler-62 f	0.007887122	0.004326487
Kepler-174 d	0.011588827	0.006641471
Kepler-186 f	0.006442599	0.003450367
Kepler-283 c	0.009799112	0.005511735
Kepler-296 f	0.009704721	0.005452561
Kepler-298 d	0.013193284	0.007666263
GJ 667C c	0.007028218	0.00775173
GJ 163 c	0.022843579	0.005571684

As observed, the results of classification are almost similar for non-normalized (Figs. 3a & 3b) and normalized (Figs. 3c & 3d) CDHS. Both methods have identified the exoplanets that were previously assumed as potentially habitable (listed in the HEC database) with comparable accuracy. However, after normalization, the accuracy increases from 94% for $K = 1$ to above 99% for $K = 7$. All our results for confirmed exoplanets from PHL-EC, including DRS and CRS habitability CDHS scores and classes assignations, are presented in the catalog at `https://habitabilitypes.wordpress.com/`. CRS gave better results compared to DRS case in the non-normalized dataset, therefore, the final habitability score is considered to be the CDHS obtained in the CRS phase.

Remark: Normalized and non-normalized CDHS are obtained by two different methods. After applying the K-NN on the non-normalized CDHS, the method produced 12 and 14 habitable exoplanets in CRS and DRS cases, respectively, from a list of 664 exoplanets. The "Earth-League", Class 6, is the class where the algorithm "dumps" those exoplanets which satisfy the conditions of K-NN and threshold and probabilistic herding as explained in Sections 3.1, 3.2 and 3.3. We applied this algorithm again to the normalized CDHS of 664 exoplanets under the same conditions. It is observed that the output was 16 exoplanets that

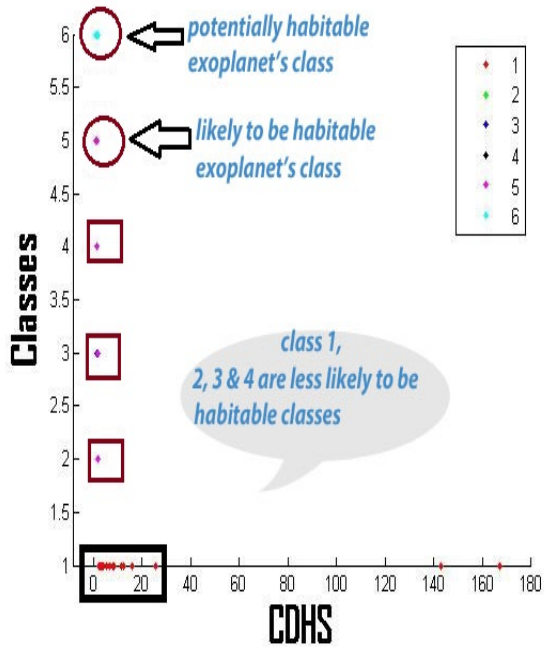

(a) for DRS on non-normalized data set

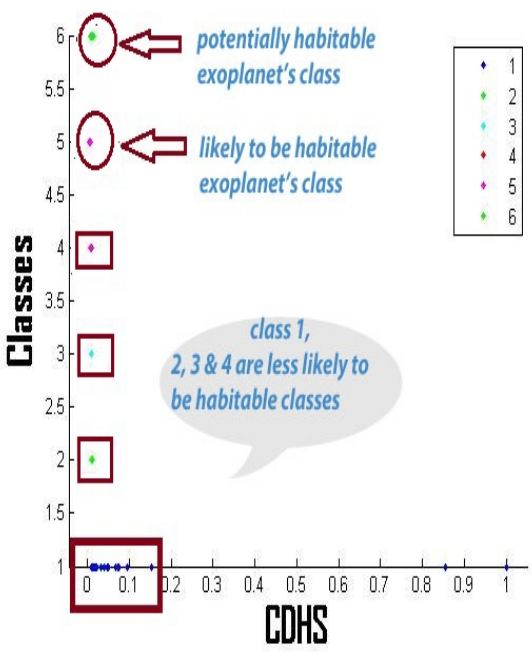

(c) for DRS on normalized data set

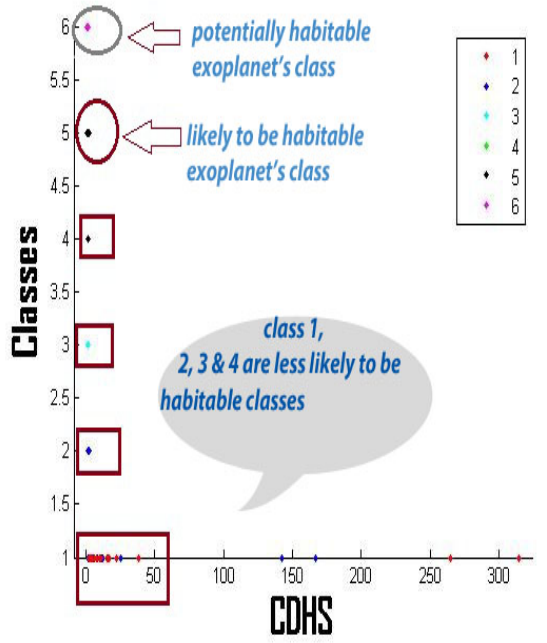

(b) for CRS on non-normalized data set

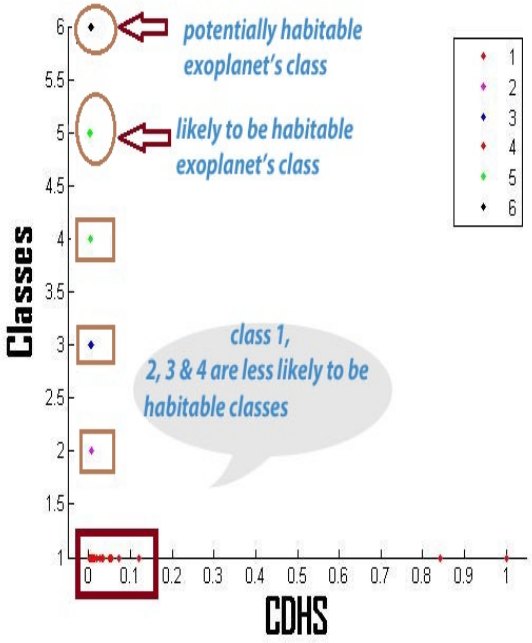

(d) for CRS on normalized data set

Figure 14: Results of attribute enhanced K-NN algorithm. The X-axis represents the Cobb-Douglas habitability score and Y-axis – the 6 classes: schematic representation of the outcome of our algorithm. The points in circles and boxes indicate membership in respective classes. These points are representative of membership only and do not indicate a quantitative equivalence of the exact representation. Full catalog is available at our website `https://habitabilitypes.wordpress.com/`

satisfied the conditions of being in Class 6, the "Earth-league", irrespective of CRS or DRS conditions. The reason is that the normalized scores are tighter and much closer to each other compared to the non-normalized CDHS, and that yielded a few more exoplanets in Class 6.

ESI is a metric that tells us whether an exoplanet is similar to Earth in some parameters. However, it may have nothing to do with habitability, and a planet with an ESI of 0.5 can be as habitable as a planet with an ESI of 0.99, since essentially only three Earth comparison points enter the ESI index: mass, radius and surface temperature (both density and escape velocity are calculated from mass and radius). Another metric, PHI, also cannot be used as a single benchmark for habitability since many other physical conditions have to be checked before a conclusion is drawn, such as existence of a magnetic field as a protector of all known forms of life, or stellar host variability, among others. Our proposed novel method of computing habitability by CD-HPF and CDHS, coupled with K-NN with probabilistic herding, estimates the habitability index of exoplanets in a statistically robust way, where optimization method is used for calculation. K-NN algorithm has been modified as an attribute-enhanced voting scheme, and the probabilistic proximity is used as a checkpoint for final class distribution. For large enough data samples, there are theoretical guarantees that the algorithm will converge to a finite number of discriminating classes. The members of the “Earth-League" are cross-validated with the list of potentially habitable exoplanets in the HEC database. The results (Table 9) render the proposed metric CDHS to behave with a reasonable degree of reliability.

Currently existing habitability indices ESI and PHI are restricted to only few parameters. At any rate, any one single benchmark for habitability may sound ambitious at present state of the field, given also the perpetual complexity of the problem. It is possible that developing the metric flexible enough to include any finite number of other planetary parameters, such as, e.g. orbital period, eccentricity, planetary rotation, magnetic field etc. may help in singling out the planets with large enough probability of potential habitability to concentrate the observational efforts. This is where the CD-HPF model has an advantage. The model generates 12 potentially habitable exoplanets in Class 6, which is considered to be a class where Earth-like planets reside. We have added several non-rocky samples to the dataset so that we could validate the algorithm. In machine learning, such random samples are usually used to check for the robustness of the designed algorithm. For example, if a non-rocky planet were classified by our algorithm as a member of the Earth-class, it would mean that the algorithm (and model) is wrong. However, it has not happened, and all the results of the Earth-league were verified to be rocky and potentially habitable. All these 12 exoplanets are identified as potentially habitable by the PHL.

The score generated by our model is a single metric which could be used to classify habitability of exoplanets as members of the "Earth League", unlike ESI and PHI. Attribute-enhanced K-NN algorithm, implemented in the paper, helps achieve this goal and the assignment of exoplanets to different classes of habitability may change as the input parameters of Cobb-Douglas model change values.

We would like to note that throughout the paper we equate habitability with Earth-likeness. We are searching for life as we know it (as we do not know any other), hence, the concept of an HZ and the “follow the water" directive. It is quite possible that this concept of habitability is too anthropocentric, and can be challenged, but not at present when we have not yet found any extraterrestrial life. At least, being anthropocentric allows us to know exactly what we can expect as habitable conditions, to know what we are looking for (e.g. biomarkers). In this process, we certainly will come across “exotic” and unexpected finds, but the start has to be anthropocentric.

3.11 Conclusion and Future Work

CD-HPF is a novel metric of defining habitability score for exoplanets. It needs to be noted that the authors perceive habitability as a probabilistic measure, or a measure with varying degrees of certainty. Therefore, the construction of different classes of habitability 1 to 6 is contemplated, corresponding to measures as “most likely to be habitable" as Class 6, to “least likely to be habitable" as Class 1. As a further illustration, classes 6 and 5 seem to represent the identical patterns in habitability, but they do not! Class 6 – the "Earth-League", is different from Class 5 in the sense that it satisfies the additional conditions of thresholding and probabilistic herding and, therefore, ranks higher on the habitability score. This is in stark contrast to the binary definition of exoplanets being “habitable or non-habitable", and a deterministic perception of the problem itself. The approach therefore required classification methods that are part of machine learning techniques and convex optimization — a sub-domain, strongly coupled with machine learning. Cobb-Douglas function and CDHS are used to determine habitability and the maximum habitability score of all exoplanets with confirmed surface temperatures in the PHL-EC. Global maxima is calculated theoretically and algorithmically for each exoplanet, exploiting intrinsic concavity of CD-HPF and ensuring "no curvature violation". Computed scores are fed to the attribute enhanced K-NN algorithm — a novel classification method, used to classify the planets into different classes to determine how similar an exoplanet is to Earth. The authors would like to emphasize that, by using classical K-NN algorithm and not exploiting the probability of habitability

criteria, the results obtained were pretty good, having 12 confirmed potentially habitable exoplanets in the "Earth-League". We have created a web page for this project to host all relevant data and results: sets, figures, animation video and a graphical abstract. It is available at `https://habitabilitypes.wordpress.com/`. This page contains the full customized catalog of all confirmed exoplanets with class annotations and computed habitability scores. This catalog is built with the intention of further use in designing statistical experiments for the analysis of the correlation between habitability and the abundance of elements (this work is briefly outlined in Safonova et al., 2016). It is a very important observation that our algorithm and method give rise to a score metric, CDHS, which is structurally similar to the PHI as a corollary in the CRS case (when the elasticities are assumed to be equal to each other). Both are the geometric means of the input parameters considered for the respective models.

CD-HPF uses four parameters (radius, density, escape velocity and surface temperature) to compute habitability score, which by themselves are not sufficient to determine habitability of exoplanets. Other parameters, such as e.g. orbital period, stellar flux, distance of the planet from host star, etc. may be equally important to determine the habitability. Since our model is scalable, additional parameters can be added to achieve better and granular habitability score. In addition, out of all confirmed exoplanets in PHL-EC, only about half have their surface temperatures estimated. For many expolanets, the surface temperature, which is an important parameter in this problem, is not known or not defined. The unknown surface temperatures can be estimated using various statistical models. Future work may include incorporating more input parameters, such as orbital velocity, orbital eccentricity, etc. to the Cobb-Douglas function, coupled with tweaking the attribute enhanced K-NN algorithm by checking an additional condition such as, e.g. distance to the host star. Cobb-Douglas, as proved, is a scalable model and doesn't violate curvature with additional predictor variables. However, it is pertinent to check for the dominant parameters that contribute more towards the habitability score. This can be accomplished by computing percentage contributions to the response variable – the habitability score. We would like to conclude by stressing on the efficacy of the method of using a few of the parameters rather than sweeping through a host of properties listed in the catalogs, effectively reducing the dimensionality of the problem. To sum up, CD-HPF and CDHS turn out to be self-contained metrics for habitability.

4 THEORETICAL VALIDATION OF POTENTIAL HABITABILITY VIA ANALYTICAL AND BOOSTED TREE METHODS: AN OPTIMISTIC STUDY ON RECENTLY DISCOVERED EXOPLANETS

4.1 Introduction

With discoveries of exoplanets pouring in hundreds, it is becoming necessary to develop some sort of a quick screening tool – a ranking scale – for evaluating habitability perspectives for the follow-up targets. One such scheme was proposed recently by us – the Cobb-Douglas Habitability Score (CDHS; [Bora et al.2016]). While our paper "CD-HPF: New Habitability Score Via Data Analytic Modeling" was in production, the discovery of an exoplanet Proxima b orbiting the nearest star (Proxima Centauri) to the Sun was announced [Anglada-EscudÃl'2016]. This planet generated a lot of stir in the news [Witze2016] because it is located in the habitable zone and its mass is in the Earth's mass range: $1.27-3\ M_{\oplus}$, making it a potentially habitable planet (PHP) and an immediate destination for the Breakthrough Starshot initiative [Starshot].

This work is motivated by testing the efficacy of the suggested model, CDHS, in determining the habitability score of Proxima b. The habitability score model has been found to work well in classifying exoplanets in terms of potential habitability. Therefore it was natural to test whether the model can also classify Proxima b as potentially habitable by computing its habitability score. This could indicate whether the model may be extended for a quick check of the potential habitability of newly discovered exoplanets in general. As we discover in ***Section VI***, this is indeed the case with the newly announced TRAPPIST-1 system [Trappist-1].

CDHS does encounter problems commonly found in convex functional modeling, such as scalability and curvature violation. Scalability is defined as the condition on the global maximum of the function; the global maximum is adjusted as the number of parameters entering the function (elasticity) increases, i.e if a global maximum is ensured for n parameters, it will continue to hold for $n+1$ parameters. The flowchart in Fig. 1 summarizes our approach to the habitability investigation of Proxima b. A novel inductive approach inspired by the Cobb-Douglas model from production economics [cobb-douglas] was proposed to verify theoretical conditions of global optima of the functional form used to model and compute the habitability score of exoplanets in [**?**]. The outcome of classification of exoplanets based on the score (Method 1) is then tallied with another classification method which discriminates samples (exoplanets) into classes based on the features/attributes of the samples (Method 2).

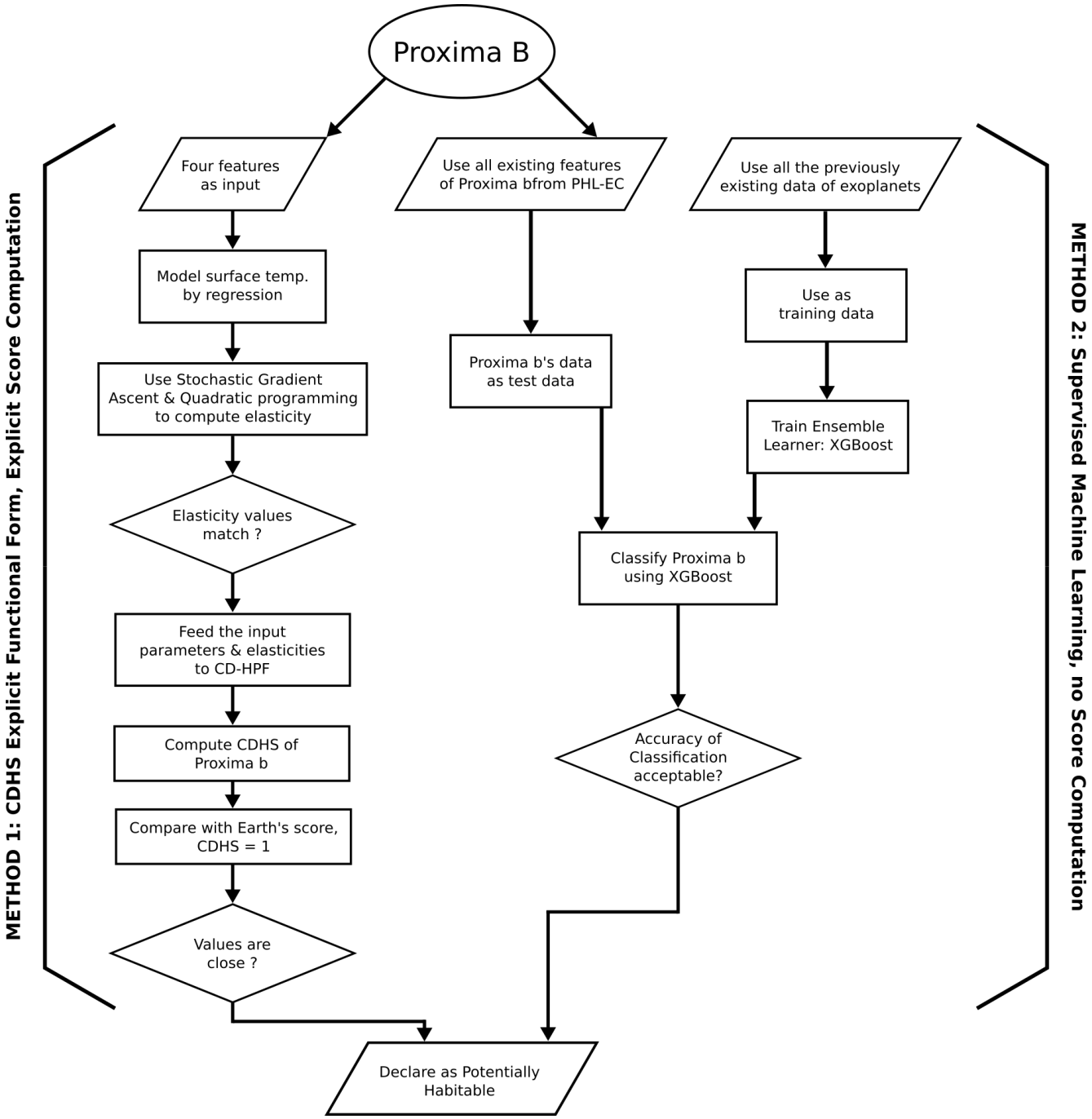

Figure 15: The convergence of two different approaches in investigation of the potential habitability of Proxima b. The outcome of the explicit scoring scheme for Proxima b places it in the “Earth-League", which is synonymous to being classified as potentially habitable.

The similar outcome from both approaches (the exoplanets are classified in the same habitability class), markedly different in structure and methodology, fortifies the growing advocacy of using machine learning in astronomy.

The habitability score model considers four parameters/features, namely mass, radius, density and surface temperature of a planet, extracted from the PHL-EC (Exoplanet Catalog hosted by the Planetary Habitability Laboratory (PHL); http://phl.upr.edu/projects). Though the catalog contains 68 observed and derived stellar and planetary parameters, we have currently considered only four for the CDHS model. However, we show here that the CDHS model is scalable, i.e. capable of accommodating more parameters (see Section IV on model scalability, and Appendix I for the proof of the theorem). Therefore, we may use more parameters in future to compute the CDHS. The problem of curvature violation in tackled in Sec. II.A later in the paper.

PHL classifies all discovered exoplanets into five categories based on their thermal characteristics: non-habitable, and potentially habitable: psychroplanet, mesoplanet, thermoplanet and hypopsychroplanet. Proxima b is one of the recent additions to the catalog with recorded features. Here, we employ a non-metric classifier to predict the class label of Proxima b. We compute the accuracy of our classification method, and aim to reconcile the result with the habitabilty score of Proxima b, which may suggest its proximity to "Earth-League". We call this an investigation in the optimistic determination of habitabilty. The hypothesis is the following: a machine learning-based classification method, known as boosted trees, classifies exoplanets and returns some with the class by mining the features present in the PHL-EC (Method 2 in Fig. 1). This process is independent of computing an explicit habitability score for Proxima b (aka Method 1 in Fig. 1), and indicates habitability class by learning attributes from the catalog. This implicit method should match the outcome suggested by the CDHS, i.e. that Proxima b score should be close to the Earth's CDHS habitability score (with good precision), computed explicitly.

The second approach is based on XGBoost – a statistical machine-learning classification method used for supervised learning problems, where the training data with multiple features is used to predict a target variable. Authors intend to test whether the two different approaches to investigate the habitability of Proxima b, analytical and statistical, converge with a reasonable degree of confidence.

4.2 Analytical Approach via CDHS: Explicit Score Computation of Proxima b

We begin by discussing the key elements of the analytical approach. The parameters of the planet (Entry #3389 in the dataset) for this purpose were extracted from the PHL-EC: minimal mass 1.27 EU, radius 1.12 EU, density 0.9 EU, surface temperature 262.1 K, and escape velocity 1.06 EU, where EU is the Earth Units. The Earth Similarity Index (ESI) for this new planet, estimated using a simplified version of ESI[4], is 0.87. By definition, ESI ranges from 0 (totally dissimilar to Earth) to 1 (identical to Earth), and a planet with ESI ≥ 0.8 is considered an Earth-like.

4.2.1 Earth Similarity Index

In general, the ESI value of any exoplanet's planetary property is calculated using the following expression [Schulze-Makuch et al.2011],

$$ESI_x = \left(1 - \left|\frac{x - x_0}{x + x_0}\right|\right)^{w_x}, \tag{46}$$

where x is a planetary property – radius, surface temperature, density, or escape velocity, x_0 is the Earth's reference value for that parameter – 1 EU, 288 K, 1 EU and 1 EU, respectively, and w_x is the weighted exponent for that parameter. After calculating ESI for each parameter by Eq. (1), the global ESI is found by taking the geometric mean (G.M.) of all four ESI_x,

$$ESI = \left(\prod_{x=1}^{n} ESI_x\right)^{\frac{1}{n}}. \tag{47}$$

The problem in using Eq. (2) to obtain the global ESI is that sometimes there no available data to obtain all input parameters, such as in the case of Proxima b – only its mass and the distance from the star are known. Due to that, a simplified expression was proposed by the PHL for ESI calculation in terms of only radius and stellar flux,

$$ESI = 1 - \sqrt{\frac{1}{2}\left(\frac{R - R_0}{R + R_0}\right)^2 + \left(\frac{S - S_0}{S + S_0}\right)^2}, \tag{48}$$

where R and S represent radius and stellar flux of a planet, and R_0 and S_0 are the reference values for the Earth. Using 1.12 EU for the radius and 0.700522 EU for the stellar flux, we

[4] http://phl.upr.edu/projects/earth-similarity-index-esi

obtain ESI = 0.8692. It is worth mentioning that once we know one observable – the mass – other planetary parameters used in the ESI computation (radius, density and escape velocity) can be calculate based on certain assumptions. For example, the small mass of Proxima b suggests a rocky composition. However, since 1.27 EU is only a low limit on mass, it is still possible that its radius exceeds 1.5 – 1.6 EU, which would make Proxima b not rocky [rogers2014]. In the PHL-EC, its radius is estimated using the mass-radius relationship -

$$R = \begin{cases} M^{0.3} & M \leq 1 \\ M^{0.5} & 1 \leq M < 200 \\ (22.6)\, M^{(-0.0886)} & M \geq 200 \end{cases} \tag{49}$$

Since Proxima b mass is 1.27 EU, the radius is $R = M^{0.5} \equiv 1.12$ EU. Accordingly, the escape velocity was calculated by $V_e = \sqrt{2GM/R} \equiv 1.065$ (EU), and the density by the usual $D = 3M/4\pi R^3 \equiv 0.904$ (EU) formula. If we use all four parameters provided in the catalog, the global ESI becomes 0.9088.

4.2.2 Cobb Douglas Habitability Score (CDHS)

We have proposed the new model of the habitability score in [Bora et al.2016] using a convex optimization approach [Saha et al.2016]. In this model, the Cobb Douglas function is reformulated as Cobb-Douglas habitability production function (CD-HPF) to compute the habitability score of an exoplanet,

$$\mathbb{Y} = f(R, D, T_s, V_e) = (R)^{\alpha} \cdot (D)^{\beta} \cdot (T_s)^{\gamma} \cdot (V_e)^{\delta}\,, \tag{50}$$

where the same planetary parameters are used – radius R, density D, surface temperature T_s and escape velocity V_e. $\mathbb{Y}$ is the habitability score CDHS, and f is defined as CD-HPF. The goal is to maximize the score, $\mathbb{Y}$, where the elasticity values are subject to the condition $\alpha + \beta + \gamma + \delta < 1$. These values are obtained by a computationally fast algorithm Stochastic Gradient Ascent (SGA) described in Section 3. We calculate CDHS score for the constraints known as returns to scale: Constant Return to Scale (CRS) and Decreasing Return to Scale (DRS) cases; for more details please refer to [Bora et al.2016].

As Proxima b is considered an Earth-like planet, we endeavored to cross-match the observation via the method explained in the previous section. The analysis of CDHS will help to explore how this method can be effectively used for newly discovered planets. The eventual classification of any exoplanet is accomplished by using the proximity of CDHS

of that planet to the Earth, with additional constraints imposed on the algorithm termed "probabilistic herding". The algorithm works by taking a set of values in the neighborhood of 1 (CDHS of Earth). A threshold of 1 implies that CDHS value between 1 and 2 is acceptable for membership in "Earth-League", pending fulfillment of further conditions. For example, the CDHS of the most potentially habitable planet before Proxima b, Kepler-186 f, is 1.086 (the closest to the Earth's value), though its ESI is only 0.64. While another PHP GJ-163 c has the farthest score (1.754) from 1; and though its ESI is 0.72, it may not be even a rocky planet as its radius can be between 1.8 to 2.4 EU, which is not good for a rocky composition theory, see e.g. [rogers2014].

4.2.3 CDHS calculation using radius, density, escape velocity and surface temperature

Using the estimated values of the parameters from the PHL-EC, we calculated CDHS score for the CRS and DRS cases, and obtained optimal elasticity and maximum CDHS value. The CDHS values in CRS and DRS cases were 1.083 and 1.095, respectively. The degree/extent of closeness is explained in [Bora et al.2016] in great detail.

Table 35: Rocky planets with unknown surface temperature:*Oversampling, attribute mining and using association rules for missing value imputation: cf. subsection 1*

P.Name	*P.Composition Class*
Kepler-132 e	rocky-iron
Kepler-157 d	rocky-iron
Kepler-166 d	rocky-iron
Kepler-176 e	rocky-iron
Kepler-192 d	rocky-iron
Kepler-217 d	rocky-iron
Kepler-271 d	rocky-iron
Kepler-398 d	rocky-iron
Kepler-401 d	rocky-iron
Kepler-403 d	rocky-iron
WD 1145+017 b	rocky-iron

4.2.4 Missing attribute values: Surface Temperature of 11 rocky planets (Table I)

We observed missing values of surface temperature in Table I. The values of equilibrium temperature of those entries are also unknown. Imputation of missing values is commonly done by filling in the blanks by computing the mean of continuous valued variables in the same column, using other entries of the same type, rocky planets in this case. However, this

method has demerits. We propose the following method to achieve the task of imputing missing surface temperature values.

Data imputation using Association Rules: A more sophisticated method of data imputation is that of *rule based learning*. Popularized by Agrawal et al. [Agrawal1993] through their seminal paper in 1993, it is a robust approach in Data Mining and Big Data Analytics for the purpose of filling in missing values. The original approach was inspired by unexpected correlations in items being purchased by customers in markets. An illustrative example making use of samples and features from the PHL-EC dataset is presented here.

Any dataset has samples and features. Say, we have n samples $S = \{s_1, s_2, ..., s_n\}$ and m features, $X = \{X_1, X_2, ..., X_m\}$, such that each sample is considered to be a $1 \times m$ vector of features, $s_i = \{x_{i1}, x_{i2}, ..., x_{im}\}$. Here, we would like to find out if the presence of any feature set A amongst all the samples in S implies the presence of a feature set B.

Table 36: Table of features used to construct the association rule for missing value imputation

P.Name	*P.Zone Class*	*P.Mass Class*	*P.Composition Class*	*P.Atmosphere Class*	Class Label
8 Umi b	Hot	Jovian	gas	hydrogen-rich	non-habitable
GJ 163 c	Warm	Superterran	rocky-iron	metals-rich	psychroplanet
GJ 180 b	Warm	Superterran	rocky-iron	metals-rich	mesoplanet
GJ 180 c	Warm	Superterran	rocky-iron	metals-rich	mesoplanet
14 Her b	Cold	Jovian	gas	hydrogen-rich	non-habitable

Consider Table 36. An interesting observation is that all the planets with *P.Zone Class* = *Warm, P.Mass Class* = *Superterrain* and *P. Composition Class* = *rocky-iron* (the planets GJ 163 c, GJ 180 b and GJ 180 c) also have *P. Atmosphere Class* as *metals-rich.* Here, if we consider conditions A = *{P.Zone Class = Warm, P.Mass Class = Superterran, P.Composition Class = rocky-iron}* and B = *{P.Atmosphere Class = metals-rich}*, then $A \Rightarrow B$ holds true. But what does it mean in for data imputation? If there exists a sample s_k in the dataset such that condition A holds good for s_k but the value of *P.Atmosphere Class* is missing, then by the association rule $A \Rightarrow B$, we can impute the value of *P.Atmosphere Class* for s_k as metals rich. Similarly, if A' = *{P.Mass Class = Jovian, P.Composition Class = gas}* and B' = *{P.Atmosphere Class = hydrogen-rich}*, then $A' \Rightarrow B'$ becomes another association rule which may be used to impute vales of *P.Atmosphere Class.* Note here the exclusion of the variable *P.Zone Class.* In the two samples which satisfy A', the value of *P.Zone Class* are not the same and hence they do not make for a strong association with B'.

In Table 36, we have mentioned the class labels alongside the samples. However this is just indicative; the class labels should not be used to form associations (if they are used, then

some resulting associations might become similar to a traditional classification problem!) Different metrics are used to judge how interesting a rule is, i.e., the goodness of a rule. Two of the fundamental metrics are:

1. **Support**: It is an indicator of how frequently a condition A appears in the database. Here, t is the set of samples in S which exhibit the condition A.

$$supp(A) = \frac{|t \in S; A \subseteq t|}{|S|} \tag{51}$$

   In the example considered, A = *{P.Zone Class = Warm, P.Mass Class = Superterran, P.Composition Class = rocky-iron}* has a support of $3/5 = 0.6$.

2. **Confidence**: It is an indication of how often the rule was found to be true. For the rule $A \Rightarrow B$ in S, the confidence is defined as:

$$conf(A \Rightarrow B) = \frac{supp(A \cup B)}{supp(A)} \tag{52}$$

   For example, the rule $A \Rightarrow B$ considered in our example has a confidence of $0.6/0.6 = 1$, which means 100% of the samples satisfying A = *{P.Zone Class = Warm, P.Mass Class = Superterran, P.Composition Class = rocky-iron}* will also satisfy B = *{P.Atmosphere Class = metals-rich}*.

Association rules must satisfy thresholds set for support and confidence in order to be accepted as rules for data imputation. The example illustrated is a very simple one. In practice, association rules need to be considered over thousands or millions of samples. From one dataset, millions of association rules may arise. Hence, the support and confidence thresholds must be carefully considered. The example makes use of only categorical variables for the sake of simplicity. However, association rules may be determined for continuous variables by considering bins of values. Algorithms exist that are used for discovering association rules, amongst which *a priori* [Agrawal 1994] is the most popular.

In the original text, the features considered here are called *items* and each sample is called a *transaction*.

4.2.5 CDHS calculation using stellar flux and radius

Following the simplified version of the ESI on the PHL website, we repeated the CDHS computation using only radius and stellar flux (1.12 EU and 0.700522 EU, respectively). Using

the scaled down version of Eq. (5), we obtain CDHS_{DRS} and CDHS_{CRS} as 1.168 and 1.196, respectively. These values confirm the robustness of the method used to compute CDHS and validate the claim that Proxima b falls into the "Earth-League" category.

4.2.6 CDHS calculation using stellar flux and mass

The habitability score requires the use of available physical parameters, such as radius, or mass, and temperature, and the number of parameters is not extremely restrictive. As long as we have the measure of the interior similarity – the extent to which a planet has a rocky interior, and exterior similarity – the location in the HZ, or the favorable range of surface temperatures, we can reduce the number of parameters (or increase). Since radius is calculated from an observable parameter – mass, we decided to use the mass directly in the calculation. We obtained CDHS_{DRS} as 1.168 and CDHS_{CRS} as 1.196. The CDHS achieved using radius and stellar flux (Section 2.3) and the CDHS achieved using mass and stellar flux have the same values.

Remark: *Does this imply that the surface temperature and radius are enough to compute the habitability score as defined by our model? It cannot be confirmed until enough number of clean data samples are obtained containing the four parameters used in the original ESI and CDHS formulation. We plan to perform a full-scale dimensionality analysis as future work*

The values of ESI and CDHS using different methods as discussed above are summarized in Table 37.

Table 37: ESI and CDHS values calculated for different parameters

Parameters Used	ESI	CDHS_{CRS}	CDHS_{DRS}
R, D, T_s, V_e	0.9088	1.083	1.095
Stellar Flux, R	0.869	1.196	1.168
Stellar Flux, M	0.849	1.196	1.167

NOTE: The nicety in the result, i.e. little difference in the values of CDHS, is due to the flexibility of the functional form in the model proposed in [Ginde2016], and the computation of the elasticities by the Stochastic Gradient Ascent method. Using this method led to the fast convergence of the elasticities α and β. Proxima b passed the scrutiny and is classified as a member of the "Earth-league".

4.3 Elasticity computation: Stochastic Gradient Ascent (SGA)

[Bora et al.2016] used a library function **fmincon** to compute the elasticity values. Here, we have implemented a more efficient algorithm to perform the same task. This was done for two reasons: to be able to break free from the in-built library functions, and to devise a sensitive method which would mitigate oscillatory nature of Newton-like methods around the local minima/maxima. There are many methods which use gradient search including the one proposed by Newton. Although theoretically sound, algorithmic implementations of most of these methods faces convergence issues in real time due to the oscillatory nature. Stochastic Gradient Descent was used to find the minimal value of a multivariate function, when the input parameters are known. We tried to identify the elasticities for mass, radius, density and escape velocity. We do this separately for interior CDHS and surface CDHS, and use a convex combination to compute the final CDHS (for detail, see [Bora et al.2016]) for which the maximum value is attained under certain constraints. Our objective is to maximize the final CDHS. We have employed a modified version of the descent, a Stochastic Gradient Ascent algorithm, to calculate the optimum CDHS and the elasticity values α, β, etc. As opposed to the conventional Gradient Ascent/Descent method, where the gradient is computed only once, stochastic version recomputes the gradient for each iteration and updates the elasticity values. Theoretical convergence, guaranteed otherwise in the conventional method, is though sometimes slow to achieve. Stochastic variant of the method speeds up the convergence, justifying its use in the context of the problem (the size of data, i.e. the number of discovered exoplanets, is increasing every day).

Output elasticity of Cobb-Douglas habitability function is the accentual change in the output in response to a change in the levels any of the inputs. α and β are the output elasticity of density and radius respectively. Accuracy of α and β values is crucial in deciding the right combination for the optimal CDHS, where different approaches are analyzed before arriving at final decision.

4.3.1 Computing Elasticity via Gradient Ascent

Gradient Ascent algorithm is used to find the values of α and β. Gradient Ascent is an optimization algorithm used for finding the local maximum of a function. Given a scalar function $F(x)$, gradient ascent finds the $\max_x F(x)$ by following the slope of the function. This algorithm selects initial values for the parameter x and iterates to find the new values of x which maximizes $F(x)$ (here CDHS). Maximum of a function $F(x)$ is computed by iterating

through the following step,

$$x_{n+1} \leftarrow x_n + \chi \frac{\partial F}{\partial x}, \tag{53}$$

where x_n is an initial value of x, x_{n+1} the new value of x, $\frac{\partial F}{\partial x}$ is the slope of function $Y = F(x)$ and χ denotes the step size, **which is greater than** 0 **and forces the algorithm make a small jump (descent or ascent algorithms are trained to make small jumps in the direction of the new update)** . Note that the interior CDHS_i, denoted by $Y1$, is calculated using radius R and density D, while the surface CDHS_s, denoted by $Y2$, is calculated using surface temperature T_s and escape velocity V_e. The objective is to find elasticity value that produces the optimal habitability score for the exoplanet, i.e. to find $Y_1 = \max_{\alpha,\beta} Y(R,D)$ such that, $\alpha > 0$, $\beta > 0$ and $\alpha + \beta \leq 1$. (Please note that $\alpha + \beta < 1$ is the DRS condition for elasticity which may be scaled to $\alpha_1 + \alpha_2 + \ldots + \alpha_n < 1$). Similarly, we need to find $Y_2 = \max_{\gamma,\delta} Y(T, V_e)$ such that $\gamma > 0$, $\delta > 0$ and $\delta + \gamma \leq 1$. (Analogously, $\delta + \gamma < 1$ is the DRS condition for elasticity which may be scaled to $\delta_1 + \delta_2 + \ldots + \delta_n < 1$).

Stochastic variant thus mitigates the oscillating nature of the global optima – a frequent malaise in the conventional Gradient Ascent/Descent and Newton-like methods, such as **fmincon** used in [**?**]. At this point of time, without further evidence of recorded/measured parameters, it may not be prudent to scale up the CD-HPF model by including more parameters other than the ones used by either ESI or our model. But if it ever becomes a necessity (to utilize more than the four parameters), the algorithm will come in handy and multiple optimal elasticity values may be computed fairly easily.

4.3.2 Computing Elasticity via Constrained Optimization

Let the assumed parametric form be $\log(y) = \log(K) + \alpha \log(S) + \beta \log(P)$. Consider a set of data points,

$$\begin{array}{ccccccc} \ln(y_1) & = & K' & + & \alpha S'_1 & + & \beta P'_1 \\ \vdots & & \vdots & & \vdots & & \vdots \\ \ln(y_N) & = & K' & + & \alpha S'_N & + & \beta P'_N \end{array} \tag{54}$$

where

$$\begin{aligned} K' &= \log(K), \\ S'_i &= \log(S'_i), \\ P'_i &= \log(P'_i). \end{aligned}$$

If $N > 3$, this is an over-determined system, where one possibility to solve it is to apply a least squares method. Additionally, if there are constraints on the variables (the parameters to be solved for), this can be posed as a constrained optimization problem. These two cases are discussed below.

No constraints: This is an ordinary least squares solution. The system is in the form $y = Ax$, where

$$x = \begin{bmatrix} K' & \alpha & \beta \end{bmatrix}^T, \tag{55}$$

$$y = \begin{bmatrix} y_1 \\ . \\ . \\ y_N \end{bmatrix} \tag{56}$$

and

$$A = \begin{bmatrix} 1 & S'_1 & P'_1 \\ & \dots & \\ 1 & S'_N & P'_N \end{bmatrix}. \tag{57}$$

The least squares solution for x is the solution that minimizes

$$(y - Ax)^T (y - Ax). \tag{58}$$

It is well known that the least squares solution to Eq. (54) is the solution to the system

$$A^T y = A^T A x, \tag{59}$$

i.e.

$$x = (A^T A)^{-1} A^T y. \tag{60}$$

In *Matlab*, the least squares solution to the overdetermined system $y = Ax$ can be obtained by $x = A \backslash y$. Table II presents the results of least squares (**No constraints**) obtained for the elasticity values after performing the least square fitting, while Table III displays the results obtained for the elasticity values after performing the constrained least square fitting.

Table 38: Elasticity values for IRS, CRS & DRS cases after performing the least square test (**No constraints**): elasticity values α and β satisfy the theorem $\alpha+\beta<1, \alpha+\beta=1$, and $\alpha+\beta>1$ for DRS, CRS and IRS, respectively, and match the values reported previously [Bora et al.2016].

	IRS	CRS	DRS
α	1.799998	0.900000	0.799998
β	0.100001	0.100000	0.099999

Constraints on parameters: this results in a constrained optimization problem. The objective function to be minimized (maximized) is still the same, namely,

$$(y-Ax)^T(y-Ax). \tag{61}$$

This is a quadratic form in x. If the constraints are linear in x, then the resulting constrained optimization problem is a quadratic program (QP). A standard form of a QP is

$$\max x^T Hx + f^T x, \tag{62}$$

such that

Suppose the constraints are $\alpha, \beta > 0$ and $\alpha+\beta \leq 1$. The QP can be written as (neglecting the constant term $y^T y$)

$$\max x^T(A^T A)x - 2y^T Ax, \tag{63}$$

such that

$$\begin{aligned} &\alpha > 0, \\ &\beta > 0, \\ &\alpha+\beta \leq 1. \end{aligned} \tag{64}$$

For the standard form as given in Eq. (16), Eqs. (63)-(64) can be represented by rewriting the objective function as

$$x^T Hx + f^T x, \tag{65}$$

where

$$H = A^T A \text{ and } f = -2A^T y. \tag{66}$$

The inequality constraints can be specified as

$$C = \begin{bmatrix} 0 & -1 & 0 \\ 0 & 0 & -1 \\ 0 & 1 & 1 \end{bmatrix}, \tag{67}$$

and

$$b = \begin{bmatrix} 0 \\ 0 \\ 1 \end{bmatrix}. \tag{68}$$

SUPERNOVA CLASSIFICATION

4.4 Introduction

This work describes the classification of supernova into various types. The focus is given on the classification of Type-Ia supernova. But the question is why we need to classify supernovae or why is it important? Astronomers use Type-Ia supernovae as âĂIJstandard candlesâĂİ to measure distances in the Universe. Classification of supernovae is mainly a matter of concern for the astronomers in the absence of spectra.

A supernova is a violent explosion of a star, whose brightness for an amazingly short period of time, matches that of the galaxy in which it occurs. This explosion can be due to the nuclear fusion in a degenerated star or by the collapse of the core of a massive star, both leads in the generation of massive amount of energy. The shock waves due to explosion can lead to the formation of new stars and also helps astronomers indicate the astronomical distances. Supernovae are classified according to the presence or absence of certain features in their orbital spectra. According to Rudolph Minkowski there are two main classes of supernova, the Type-I and the Type-II. Type-I is further subdivided into three classes i.e. the Type-Ia, the Type-Ib and the Type-Ic. Similarly, Type II supernova are further sub-classified as Type IIP and Type IIn. Astronomers face lot of problem in classifying them because a supernova changes itself over the time. At one instance a supernovae belonging to a particular type, may get transformed into the supernovae of other type. Hence, at different time of observation, it may belong to different type. Also, when this spectra is not available, it poses a great challenge to classify them. They have to rely only on photometric measurements for their classification which poses a big challenge in front of astronomers to do their studies.

Machine learning methods help researchers to analyze the data in real time. Here, we build a model from the input data. A learning algorithm is used to discover and learn knowledge from the data. These methods can be supervised (that rely on training set of objects for which target property is known) or unsupervised (require some kind of initial input data but unknown class).

In this chapter, classification of Type Ia supernova are taking in considerations from a supernova dataset defined in [Davis et al.2007],[Riess et al.2007] and [Wood-Vassey et al.2007] using several machine learning algorithms. To solve this problem, the dataset is classified in two classes which may aid astronomers in the classification of new supernovae with high

accuracy.

4.5 Categorization of Supernova

The basic classification of supernova is done depending upon the shape of their light curves and the nature of their spectra. But there are different ways of classifying the supernovae-
a) Based on presence of hydrogen in spectra If hydrogen is not present in the spectra then it belongs to the Type I supernova; otherwise, it is the Type II.
b) Based on type of explosion There are two types of explosions that may takes place in the star- thermonuclear and core-collapse . Core collapse, happens at the final phase in the evolution of a massive star , whereas thermonuclear explosions are found in white dwarfs.

The detailed classification of supernova is given below where both types are discussed in correspondence to each other. The classification is the basic classification depending on Type I and Type II .

4.6 Type I supernova

Supernova are classified as Type I if their light curves exhibit sharp maxima and then die away smoothly and gradually. The spectra of Type I supernovae are hydrogen poor. As discussed earlier they have three more types- Type-Ia, Type-Ib and Type-Ic. According to [Fraser] and [supernova tutorial], Type Ia supernova are created when we have binary star where one star is a white dwarf and the companion can be any other type of star, like a red giant, main sequence star, or even another white dwarf. The white dwarf pulls off matter from the companion star and the process continues till the mass exceeds the **Chandrasekhar limit** of 1.4 solar masses (According to [Philipp], the Chandrasekhar limit/mass is the maximum mass at which a self gravitating object with zero temperature can be supported by electron degeneracy method). This causes it to explode. Type-Ia is due to the thermonuclear explosion and has strong silicon absorption lines at 615 nm and this type is mainly used to measure the astronomical distances. This is the only supernova that appears in all type of galaxies. Type-Ib have strong helium absorption lines and no silicon lines, Type-Ic have no silicon and no helium absorption lines. Type Ib and Type Ic are core collapse supernova like Type II without hydrogen lines. The reason of Type-Ib and Type-Ic to fall in core collapse is that they produce little Ni [Phillips93] and are found within or near star formation regions. Core

collapse explosion mechanism happens in massive stars for which hydrogen is exhausted and sometimes even He (as in case of Type-Ic). Both the mechanisms are shown in Figure 16

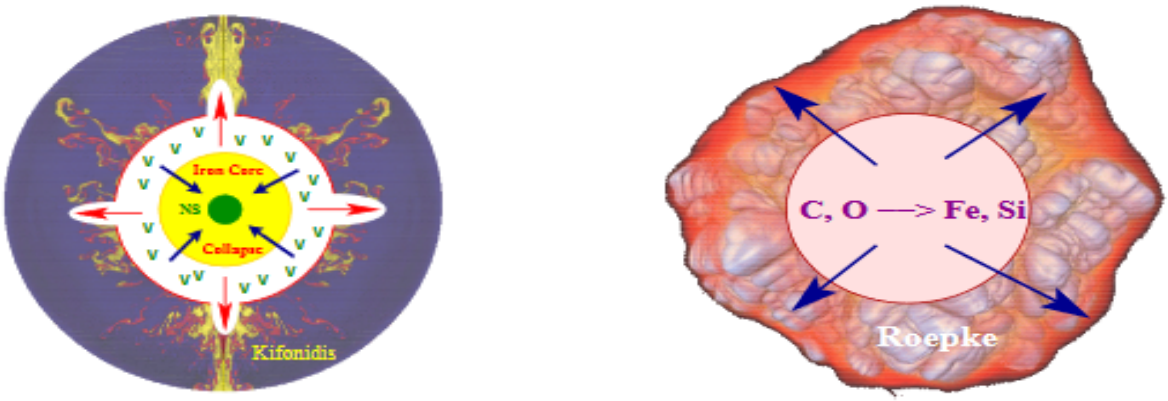

Figure 16: Core collapse supernova (*Left*) and Thermonuclear Mechanism(*Right*)

4.7 Type II supernova

Type-II is generally due to core collapse explosion mechanism. These supernovae are modeled as implosion-explosion events of a massive star. An evolved massive star is organized in the manner of an onion, with layers of different elements undergoing fusion. The outermost layer consists of hydrogen, followed by helium, carbon, oxygen, and so forth. According to [Fraser], a massive star, with 8-25 times the mass of the Sun, can fuse heavier elements at its core. When it runs out of hydrogen, it switches to helium, and then carbon, oxygen, etc, all the way up the periodic table of elements. When it reaches iron, however, the fusion reaction takes more energy than it produces. The outer layers of the star collapses inward in a fraction of a second, and then detonates as a Type II supernova. Finally the process left with a dense neutron star as a remnant. This show a characteristic plateau in their light curves a few months after initiation. They have less sharp peaks at maxima and peak at about 1 billion solar luminosity. They die away more sharply than the Type I. It has visible strong hydrogen and helium absorption lines. If the massive star have more than 25 times mass of the Sun, the force of the material falling inward collapses the core into a black hole. The main characteristics of Type II supernova is the presence of hydrogen lines in itâĂŹs spectra. These lines have P Cygni profiles and are usually very broad, which indicates rapid expansion velocities for the material in the supernova.
Type II supernova are sub-divided based on the shape of their light curves. Type II-Linear

(Type II-L) supernova has fairly rapid, linear decay after maximum light. Type II-plateau (Type II-P) remains bright for a certain period of time after maximum light i.e. they shows a long phase that lasts approximately 100d and here light curves are almost constant(plateau phase). TypeII-L is rarely found and doesnâĂŹt show the plateau phase, but decreases logarithmically after their light curve is peaked. As they drops on logarithmic scale, more or less linearly , hence L stands for âĂIJLinearâĂİ. In Type II-narrow (Type IIn) supernova, hydrogen lines had a vague or no P Cygni profile, and instead displayed a narrow component superimposed on a much broader base. Some type Ib/Ic and IIn supernova with explosion energies E >1052 erg are often called **hypernovae**. The classification of supernova is shown in Figure 17 with the flowchart as-

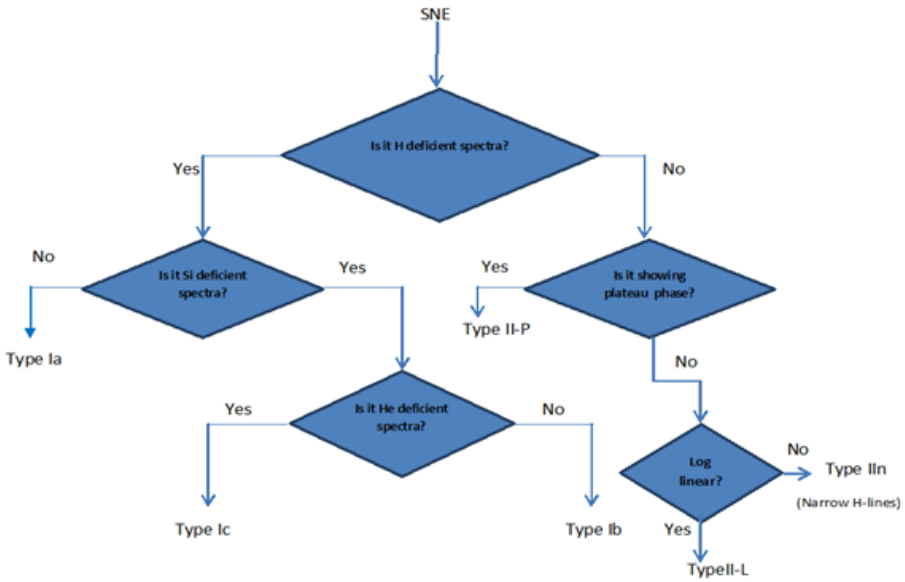

Figure 17: Classification of Supernova

4.8 Machine Learning Techniques

Machine learning is a discipline that constructs and study algorithms to build a model from input data. The type and the volume of the dataset will affect the learning and prediction performance. Machine learning algorithms are classified into supervised and unsupervised methods, also known as predictive and descriptive, respectively. Supervised methods are

also known as classification methods. For them class labels or category is known. Through the data set for which labels are known, machine is made to learn using a learning strategy, which uses parametric or non-parametric approach to get the data. In parametric model, there are fixed number of parameters and the probability density function is specified as p(x|θ) which determines the probability of pattern x for the given parameter θ (generally a parameter vector). In nonparametric model, there are no fixed number of parameters, hence cannot be parameterized. Parametric models are basically probabilistic models like Bayesian model, Maximum Aposteriori Classifiers etc. and non- parametric where directly decision boundaries are determined like Decision Trees, KNN etc. These models (parametric and nonparametric) mainly talks about the distribution of data in the data set, which helps to take the decision upon the use of appropriate classifiers.

If class labels are not known (unsupervised case), and data is taken from different distributions it is hard to assess. In these cases, some distance measure, like Euclidean distance, is considered between two data points, and if this distance is 0 or nearly 0, the two points are considered as similar. All the similar points are kept in the same group, which is called as cluster. Likewise the clusters are devised. While clustering main aim is to keep high intracluster similarity and low intercluster similarity. There are several ways in which clustering can be done. It can be density based, distance based, grid based etc. Shapes of the cluster also can be spherical, ellipsoidal or any other based on the type of clustering being performed. Most basic type of clustering is distance based, on the basis of which K-means algorithm is devised which is most popular algorithm. Other clustering algorithms to name a few are K-medoids, DB Scan, Denclue etc. Each has its own advantages and limitations. They have to be selected based on the dataset for which categorization has to be performed. Data analytic uses machine learning methods to make decision for a system.

According to [Nicholas et al.2010], supervised methods rely on a training set of objects for which the target property, for example a classification, is known with confidence. The method is trained on this set of objects, and the resulting mapping is applied to further objects for which the target property is not available. These additional objects constitute the testing set. Typically in astronomy, the target property is spectroscopic, and the input attributes are photometric, thus one can predict properties that would normally require a spectrum for the generally much larger sample of photometric objects.

On the other hand, unsupervised methods do not require a training set. These algorithms usually require some prior information of one or more of the adjustable parameters, and the solution obtained can depend on this input.

In between supervised and unsupervised algorithms there is one more type of model-

semi-supervised method is there that aims to capture the best from both of the above methods by retaining the ability to discover new classes within the data, and also incorporating information from a training set when available.

4.9 Supernovae Data source and classification

The selection of classification algorithm not only depends on the dataset, but also the application for which it is employed. There is, therefore, no simple method to select the best optimal algorithm. Our problem is to identify Type Ia supernova from the given dataset in [Davis et al.] which contains 292 different supernova information. Since the classification is binary classification, as one need to identify Type Ia supernova from the list of 292 supernovas, the best resulting algorithms are used for this purpose. The algorithms used for classification are NaÃŕve Bayes, LDA, SVM, KNN, Random Forest and Decision Tree.

The dataset used is retrieved from [Davis et al.]. These data are a combination of the ESSENCE, SNLS and nearby supernova data reported in Wood-Vasey et al. (2007) and the new Gold dataset from Riess et al.(2007). The final dataset used is combination of ESSENCE / SNLS / nearby dataset from **Table 4** of Wood-Vasey et al. (2007), using only the supernova that passed the light-curve-fit quality criteria. It has also considered the HST data from **Table 6** of Riess et al. (2007), using only the supernovae classified as gold. These were combined for Davis et al. (2007) and the data are provided in 4 columns: redshift, distance modulus, uncertainty in the distance modulus and quality as âĂIJGoldâĂİ or âĂIJSilverâĂİ. The supernova with quality labeled as âĂIJGoldâĂİ are Type Ia with high confidence and those with label âĂIJSilverâĂİ are Likely but uncertain SNe Ia. In the dataset, all the supernova with redshift value less than 0.023 and quality value Silver are discarded.

4.10 Results and Analysis

The experimental study was setup to evaluate performance of various machine learning algorithms to identify Type-Ia supernova from the above mentioned dataset. The data set mentioned above is tested on 6 major classification algorithms namely NaÃŕve Bayes, Decision tree, LDA, KNN, Random Forest and SVM respectively. A ten-fold cross validation procedure was carried out to make the best use of data, that is, the entire data was divided into ten bins in which one of the bins was considered as test-bin while the remaining 9 bins were taken as training data. We observe the following results and conclude that the outcome of the experiment is encouraging, considering the complex nature of the data. Table 39 shows the result of classification.

Table 39: Results of Type -Ia supernova classification

Algorithm	Accuracy (%)
NaÃŕve Bayes	98.86
Decision Tree	98.86
LDA	65.90
KNN	96.59
Random Forest	97.72
SVM	65.90

Performance analysis of the algorithms on the dataset is as follows.
1. NaÃŕve BayesâĂŹ and Decision Tree top the accuracy table with the accuracy of 98.86%.
2. Random Forest ranks 2 with accuracy of 97.72% and KNN occupies 3rd position with 96.59% accuracy.
3. The dramatic change was observed in the case of SVM, which occupied the last position with LDA with an accuracy of 65.9%. The geometric boundary constraints inhibit the performance of the two classifiers.

Overall, we can conclude NaÃŕve BayesâĂŹ, Decision Tree and Random Forest perform exceptionally well with the dataset, while KNN acts as an average case.

4.11 Conclusion

In this chapter, we have compared few classification techniques to identify Type Ia supernova. Here it is seen that Naive Bayes, Decision Tree and Random Forest algorithms gave best result among all. This work is relevant to astroinformatics, especially for classification of supernova, star-galaxy classification etc. The dataset used is a well-known which is the combination of ESSENCE, SNLS and nearby supernova data.

4.12 Future Research Directions

Supernova classification is an emerging problem that scientists, astronomers and astrophysicists are working on to solve using various statistical techniques. In the absence of spectra, how this problem can be solved. In this chapter, Type-Ia supernova are classified

using machine learning techniques based on redshift value and distance modulus. The same techniques can be applied to solve the overall supernova classification problem. It can help us to differentiate Type I supernova from Type II, Type Ib from Type Ic or so on. Machine learning techniques along with various statistical methods help us to solve such problems.

MACHINE LEARNING DONE RIGHT: A CASE STUDY IN QUASAR-STAR CLASSIFICATION

4.13 Introduction

Quasars are *quasi-stellar radio sources*, which were first discovered in 1960. They emit radio waves, visible light, ultraviolet rays, infrared rays, X-rays and gamma rays. They are very bright and the brightness causes the light of all the other stars becoming relatively faint in that galaxy which houses these quasars. The source of their brightness is generally the massive black hole present in the center of the host galaxy. Quasars are many light-years away from the Earth and the energy from quasars takes billions of years to reach the earth's atmosphere; they may carry signatures of the early stages of the universe. This information gathering exercise and subsequent physical analysis of quasars pose strong motivation for the study. It is difficult for astronomers to study quasars by relying on telescopic observations alone since quasars are not distinguishable from the stars due to their great distance from Earth. Evolving some kind of semi-automated or automated technique to classify quasars from stars is a pressing necessity.

Identification of large numbers of quasars/active galactic nuclei (AGN) over a broad range of redshift and luminosity has compelled astronomers to distinguish them from stars. Historically, quasar candidates have been identified by virtue of color, variability, and lack of proper motion but generally not all of these combined. The standard way of identifying large numbers of candidate quasars is to make *color cuts* using optical or infrared photometry. This is because the majority of quasars at $z < 2.5$ emit light that mostly falls in the frequencies corresponding to blue than the majority of stars in the optical range, and light whose frequencies are much lower than infrared. This establishes the inadequacy to distinguish stars from quasars based on color, variability, and proper motion. Machine learning techniques have turned out to be extremely effective in performing classification of various celestial objects.

Machine Learning (ML) [Basak et al.(2016)] is a sub-field of computer science which relies on statistical methods for predictive analysis. Machine learning algorithms broadly fall into two categories: *supervised* and *unsupervised methods*. In supervised methods, target values are assigned to every entity in the data set. These may be class labels for *classification*, and continuous values for *regression*. In unsupervised methods, there are no target values associated with entities and thus the algorithms must find similarities between different entities. *Clustering* is an unsupervised machine learning approach. ML algorithms may broadly make use of one *strong* classifier, or a combination of *weak* classifiers. A *strong*

classifier or a strong learner is a single model implementation which may effectively be able to predict the outcome of an input, based on training samples. A weak learner, on the contrary, is not a robust classifier itself and may be only slightly better than a random guess. Combinations of weak learners may be used to make strong predictions. Namely two broad approaches exist for this: bootstrap aggregation (*bagging*) and *boosting*. In bagging [Breiman(1996)], the attribute set of a training sample is a subset of all the attributes. Often, successive learners complement each other for making a prediction. In boosting, each learner makes a prediction, usually on the entire attribute set, which is very close to a random guess: based on accuracy of each weak learner, a weight for each class is assigned to the weak learner successively constructed; the contribution of each weak learner to the final prediction depends on these weights. Consequently, the model is built based on a scheme of checks-and-balances to get the best results over many learners. AdaBoost was introduced by Freund and Schapire [Freund & Schapire(1996)], which is based on the aforementioned principles of boosting. Over time, many variations of the original algorithm have been suggested which take into consideration biases present in the data set and uneven costs of misclassification such as AdaCost, AdaBoost. MH, Sty-P Boost, Asymmetric AdaBoost etc.

Machine learning algorithms have been used in various fields of astronomy. In this manuscript, the strength of such algorithms has been utilized to classify quasars or stars to complement the astronomers' task of distinguishing them. Some evidence of data classification methods for quasar-star classification such as Support Vector Machines [Gao et al.(2008), Elting et al.(2008)] and SVM-kNN [Peng et al.(2013)] is available in the existing literature. However, there is room for critical analysis and re-examination of the published work and significant amendments are not redundant! Machine learning has the potential to provide good predictions (in this case, determining whether the class a stellar object belongs to is that of a star or a quasar): but only if aptly and correctly applied; otherwise, it may lead to wrong classifications or predictions. For example, a high *accuracy* may not necessarily be an indication of a proper application of machine learning as these statistical indicators themselves may lead to controversial results when improperly used. The presentation of the results, inclusive of appropriate validation methods depending on the nature of data, may reveal the correctness of the methods used. Incorrect experimental methods and critical oversight of nuances in data may not be a faithful representation of the problem statement; this is elaborated in Sections 4.16 to **??**.

The remainder of the paper is organized as follows: Section 4.14 presents the motivation behind re-investigating the problems and the novel contribution in the solution scheme. This is followed by a literature survey where the existing methods are highlighted Section 4.15.

Section 4.16 discusses the data source, acquisition method, and nuances present in data, used in existing work. Section 4.17 discusses a few machine learning methods that are used with emphasis on the effectiveness of a particular approach bolstered by the theoretical analysis of the methods employed by the authors of this paper. Section **??** of the paper discusses various metrics used for performance analysis of the given classification approaches. Section **??** presents and analyzes the results obtained using the approaches used in Section 4.17; this section elaborates on the comparison between the work surveyed and the work presented in this paper. In Section **??**, a discussion reconciles all the facts discovered while exploring the dataset and various methods, and our ideas on an appropriate workflow in any data analytic pursuit. We conclude in Section **??** by reiterating and fortifying the motivation for the work presented and document a workflow thumb rule (Figure **??**) for the benefit of the larger readership.

4.14 Motivation and Contribution

The contribution of this paper is two-fold: novelty and critical scrutiny. Once the realization about data imbalance dawned upon us, we proposed a method, Asymmetric Adaboost, tailor made to handle such imbalance. This has not been attempted before in star-quasar classification, the problem under consideration. Secondly, the application of this method makes it imperative to critically analyze other methods reported in the existing literature and this exercise helped unlock the nuances of this problem, otherwise unknown. This exercise sheds some light on the distinction between classical pattern recognition and machine learning. The former typically assumes that data are balanced across the classes and the algorithms and methods are written to handle balanced data. However, the latter is designed to tackle data cleaning and preparation issues within the algorithmic framework. Thus, beneath the hype, the rationality, and science behind choosing machine learning over classical pattern recognition emerges; machine learning is more convenient and powerful. The problem turns out to be a case study for investigating such a paradigm shift. This has been highlighted by the authors through critical mathematical and computational analysis and should serve as another significant contribution.

Different algorithms are not just explored on a random basis but are chosen carefully in cognizance of papers available in the public domain. Extremely high accuracy reported in the papers surveyed (refer to Section 4.15), not consistent with the data distribution raised reasonable doubt. Hence the authors decided to adopt careful scrutiny of the work accomplished in the literature, having set the goals on falsification; scientific validation of

those results required re-computation and investigative analysis of the ML methods used in the past. This has brought up several anomalies in the published work. The authors intend to highlight those in phases throughout the remainder of the text. AstroInformatics is an emerging field and is thus prone to erroneous methods and faulty conclusions. Correcting and re-evaluating those are important contributions that the community should not ignore! This is the cornerstone of the work presented apart from highlighting the correct theory behind ML methods in astronomy and science. The detailed technical contributions made by authors are summarized as follows:

- We have attempted to demonstrate the importance of linear separability tests. This is done to check whether the data points are linearly separable or not. Certain algorithms like SVM with linear kernel cannot be used if data is not linearly separable. The implications of a separability test, an explanation for which has been given in Section **??**, has been overlooked in the available literature.

- A remarkable property of this particular data set, the presence of data bias, has been identified. If the classification is performed without considering the bias in the data set, it may lead to biased results; for example, if two classes C_1 and C_2 are present in the dataset and one class is dominating in the dataset then directly applying any classification algorithm may return results which are biased by the dominating class. We argue that a dataset must be balanced i.e. the selected training set for classification must contain almost the same amount of data belonging to both classes. This is presented in Section 4.17.1 as the concept of artificial balancing of the dataset.

- We have also proposed an approach which mathematically handles the bias in the dataset. This approach can be used directly in the presence of inherent data bias. Known as Asymmetric AdaBoost, this has been discussed in Section **??**.

It is important to note that the authors have used the same datasets from previous work by other researchers. Also, the paper is not only about highlighting the efficacy of a method by exhibiting marginal improvements in accuracy. Astronomy is becoming increasingly data driven and it is imperative that such new paradigms be embraced by the leaders of the astronomical community. However, such endeavor should be carefully pursued because of the possible loopholes that can arise due to oversight or lack of adequate foundation in data science. Through this paper, apart from demonstrating effective methods for automatic classification of stars and quasars, the authors laid down some fundamental ideas that should be kept in mind and adhered to. The ideas/working rules are for anyone wishing to pursue

astroInformatics or data analytics in any area. A flowchart presenting the knowledge base is presented in the conclusion section (Figure **??**).

All the experiments were performed in Python3, using the machine learning toolkit *scikit-learn* [Pedregosa et al.(2011)].

4.15 Star-Quasar Classification: Existing Literature

Support Vector Machine (SVM) is one of the most powerful machine learning methods, discussed in detail in Section 4.17. It is used generally for binary classification. However, variants of this method can also be applied for multi-class classification. Since the classification is based on two classes, namely stars and quasars, SVM has been widely used in the existing literature to classify quasars and stars.

[Gao et al.(2008)] used SVM to separate quasars from stars listed in the Sloan Digital Sky Survey (SDSS) database (refer to Section 4.16 for details on data acquisition). Four colors: $u-g$, $g-r$, $r-i$, and $i-z$ are used for photometric classification of quasars from stars. SVM was used for the classification of quasars and stars. A non-linear radial basis function (RBF) kernel was used for SVM. The main reason for the usage of RBF kernels was to tune the parameters γ and c (trade-off) to increase the accuracy. The highest accuracy of classification obtained was equal to 97.55%. However, the manuscript fails to check for linear separability of the two classes. [Elting et al.(2008)] used SVM for the classification of stars, galaxies, and quasars. A data set comprising the $u-g$, $g-r$, $r-i$ and $i-z$ colors is used for the prediction on unbalanced data set. A non-linear RBF kernel was used for classification and an accuracy of 98.5% was obtained.

The aforementioned papers used non-linear RBF kernel which is commonly used when data distribution is Gaussian. It is imprudent to cite increase the accuracy as the reason for using any kernel. The choice of kernel depends on the data. Therefore, authors in the present manuscript have performed a linear separability test on the data set, discussed in Section 4.17, which clearly shows that the data is mostly linearly separable and hence, a linear kernel should be used. [Peng et al.(2013)] used an SVM-KNN method which is a combination of SVM and KNN. SVM-KNN strengthens the generalization ability of SVM and applies KNN to correct some forecasting errors of SVM and improve the overall forecast accuracy. SVM-KNN was applied for classification using a linear kernel. SVM-KNN (the ratio of the number of samples in the training set to the testing set as 9:1) was applied on the unbalanced SDSS data set which was dominated by the "star" class. This gave an overall accuracy of 98.85% as the data was unbalanced and the classes were biased. The total percentage of stars and quasars

which were classified using this method was 99.41% and 98.19% respectively.

SVM should not be used without performing a separability test and therefore, choice of linear or RBF kernel depends on the linear separability of data. If data is linearly separable, then SVM may be implemented using a linear kernel. The absence of linear separability and evidence of a normal trend in data may justify SVM implementation in conjunction with the RBF kernel. However, that evidence was not forthcoming in the works by [Gao et al.(2008)], [Elting et al.(2008)] or [Peng et al.(2013)]. In fact, one should select the kernel and then accordingly should apply SVM depending on the data distribution. There was no evidence of a separability analysis being performed by [Gao et al.(2008)], [Elting et al.(2008)] or [Peng et al.(2013)], thus forcing the conclusion that the kernel was chosen without proper examination. [Gao et al.(2008)] and [Elting et al.(2008)] used a non-linear RBF kernel is used along with SVM. Similarly, in [Peng et al.(2013)] used a linear kernel in SVM-KNN without a proper justification. Moreover, the class dominance was ignored in [Gao et al.(2008), Elting et al.(2008), Peng et al.(2013)]. Class dominance must be considered, otherwise, the accuracy of classification obtained will be biased by the dominant class and it will always be numerically very high. We have performed *artificial balancing* of data to counter the effects of class bias; the process of artificial balancing has been elaborated in 4.17.1.

The authors would like to emphasize that the manuscript is not a *black-box assembly* of several ML techniques but a careful study of those methods, eventually picking the right classifier based on the nature of data (such as Asymmetric Adaboost, as discussed in Section **??**). The algorithm's ability to handle class imbalance, and establishing the applicability of such an algorithm to solve similar kind of problems have been addressed in our work.

Sensitivity and *specificity* are measures of performance for binary classifiers. The accuracy obtained without calculating sensitivity and specificity is not always meaningful. Sensitivity and specificity are used to check the correctness of the obtained accuracy but were not reported in [Gao et al.(2008), Elting et al.(2008), Peng et al.(2013)]. This makes accuracy validation difficult.

The comparison of the results obtained from these [Gao et al.(2008), Elting et al.(2008), Peng et al.(2013)] are presented in Table 40.

4.16 Data Acquisition

The Sloan Digital Sky Survey (SDSS) [Adelman-McCarthy et al.(2008)] has created the most detailed three-dimensional maps of the Universe ever made, with deep multi-color images of

Table 40: Results of classification obtained by [Gao et al.(2008), Elting et al.(2008), Peng et al.(2013)]: the critical and challenging issues not addressed in the cited literature are tabulated as well.

Methods	Accuracy (%)	Class Bias	Data Imbalance	Linear Separability Test Done
[Gao et al.(2008)]	97.55	YES	YES	NO
[Elting et al.(2008)]	98.5	YES	YES	NO
[Peng et al.(2013)]	98.85	YES	YES	NO

one-third of the sky and spectra for more than three million astronomical objects. It is a major multi-filter imaging and spectroscopic redshift survey using a dedicated 2.5m wide-angle optical telescope at the Apache Point Observatory in New Mexico, USA. Data collection began in 2000 and the final imaging data release covers over 35% of the sky, with photometric observations of around 500 million objects and spectra for more than 3 million objects. The main galaxy sample has a median redshift of $z = 0.1$; there are redshifts for luminous red galaxies as far as $z = 0.7$, and for quasars as far as $z = 5$; and the imaging survey has been involved in the detection of quasars beyond a redshift $z = 6$. Stars have a redshift of $z = 0$.

SDSS makes the data releases available over the Internet. Data release 7 (DR7) [Abazajian et al.(2009)], released in 2009, includes all photometric observations taken with SDSS imaging camera, covering 14,555 square degrees of the sky. Data Release 9 (DR9) [Ahn et al.(2013)], released to the public on 31 July 2012, includes the first results from the Baryon Oscillations Spectroscopic Survey (BOSS) spectrograph, including over 800,000 new spectra. Over 500,000 of the new spectra are of objects in the Universe 7 billion years ago (roughly half the age of the universe). Data release 10 (DR10), released to the public on 31 July 2013. DR10 is the first release of the spectra from the SDSS-III's Apache Point Observatory Galactic Evolution Experiment (APOGEE), which uses infrared spectroscopy to study tens of thousands of stars in the Milky Way. The SkyServer provides a range of interfaces to an underlying Microsoft SQL Server. Both spectra and images are available in this way, and interfaces are made very easy to use. The data are available for non-commercial use only, without written permission. The SkyServer also provides a range of tutorials aimed at everyone from school children up to professional astronomers. The tenth major data release, DR10, released in July 2013, provides images, imaging catalogs, spectra, and redshifts via a variety of search interfaces. The datasets are available for download from the casjobs website (`http://skyserver.sdss.org/casjobs`).

The spectroscopic data is stored in the *SpecObj* table in the SkyServer. Casjobs is a flexible and advanced SQL-based interface to the Catalog Archive Server (CAS), for all data releases. It is used to download the SDSS DR6 [Elting et al.(2008)] data set which contains spectral information of 74463 quasars and 430827 stars. Spectral information like the colors $u - g$,

$g-r$, $r-i$, $i-z$ and redshift are obtained by running a SQL query. The output obtained from running the query is downloaded in the form of a comma-separated value (CSV) file.

4.17 Methods

4.17.1 Artificial Balancing of Data

Since the dataset is dominated by a single class (stars), it is essential for the training sets used for training the algorithms to be artificially balanced. In the data set, the number of entities in the stars' class is about six times greater than the number of entities in the quasars' class; it is a cause of concern as a data bias is imminent. In such a case, voting for the dominating class naturally increases as the number of entities belonging to this class is greater. The number of entities classified as stars is far greater than the number of entities classified as quasars. The extremely high accuracy reported by [Gao et al.(2008)], [Elting et al.(2008)], and, [Peng et al.(2013)] is because of the dominance of one class and not because the classes are correctly identified. In such cases, the sensitivity and specificity are also close to 1.

Artificial balancing of data needs to be performed such that the classes present in the dataset used for training a model don't present a bias to the learning algorithm. In quasar-star classification, the stars' class dominates the quasars' class. This causes an increase in the influence of the stars' class on the learning algorithm and results in a higher accuracy of classification. Algorithms like SVM cannot handle the imbalance in classes if the separating boundary between the two classes is thin, or slightly overlapping (which is often the case in many datasets) and end up classifying more number of samples as belonging to the dominant class, thereby increasing the accuracy of classification, numerically. It is found that the accuracy of classification decreases with the artificial balancing of the dataset as shown in Section **??**. In artificial balancing, an equal number of samples from both the classes are taken for training the classifier. This eliminates the class bias and the data imbalance. The dataset used for analysis has a larger number of samples belonging to the stars' class as compared to the number of samples in the quasars' class. The samples that are classified as belonging to the stars' class are more when compared to the number of sampled classified as belonging to the quasars' class as the voting for the dominating class increases with imbalance and results in a higher accuracy of classification. Hence, the voting for the stars' class was found to be 99.41% which is higher than the voting of quasars, which is 98.19%, by [Peng et al.(2013)]. The accuracy claimed is doubtful as there data imbalance and class bias is prevalent.

5 AN INTRODUCTION TO IMAGE PROCESSING

5.1

6 PYTHON CODES

REFERENCES

[Asimov1989] Asimov I., The Relativity of Wrong, 1989, p121-198, ISBN-13:9781558171695

[Anglada-Escudé et al.2016] Anglada-Escudé G. et al., 2016, A terrestrial planet candidate in a temperate orbit around Proxima Centauri, Nature, Vol. 536, Number 7617, p.437-440, doi:10.1038/nature19106

[Ball & Brunner2010] Ball N. M., Brunner R. J., 2010, Data Mining and Machine Learning in Astronomy, International Journal of Modern Physics D, Vol. 19, Number 7, p. 1049-1106, doi:10.1142/s0218271810017160

[Batalha 2014] Batalha, N. M., 2014, Exploring exoplanet populations with NASA's Kepler Mission, Proceedings of the National Academy of Sciences, Vol. 111, Number 35, p. 12647-12654, doi:10.1073/pnas.1304196111

[Bora et al.2016] Bora K., Saha S., Agrawal S., Safonova M., Routh S., Narasimhamurthy A. M., CD-HPF: New Habitability Score Via Data Analytic Modeling, 2016, Journal of Astronomy and Computing, Vol. 17, p. 129-143, doi:10.1016/j.ascom.2016.08.001

[Abraham2014] Botros A., Artificial Intelligence on the Final Frontier: Using Machine Learning to Find New Earths, 2014, Planet Hunter: http://www.abrahambotros.com/src/docs/AbrahamBotros

[Breiman2001] Breiman L., 2001, Random Forests, Machine Learning, Vol. 45, Number 1, p. 5-32, doi:10.1023/a:1010933404324

[Bylander & Hanzlik1999] Bylander T., Hanzlik D., 1999, Estimating generalization error using out-of-bag estimates. In Proceedings of the National Conference on Artificial Intelligence. AAAI, pp. 321-327, Proceedings of the 1999 16th National Conference on Artificial Intelligence (AAAI-99), 11th Innovative Applications of Artificial Intelligence Conference (IAAI-99), Orlando, FL, USA, 18-22 July.

[Cai, Duo & Cai2010] Cai Y. L., Duo J., Cai D., 2010, A KNN Research Paper Classification Method Based on Shared Nearest Neighbor, Proceedings of the 8th NTCIR Workshop Meeting on Evaluation of Information Access Technologies: Information Retrieval, Question Answering and Cross-Lingual Information Access, NTCIR-8, National Center of Sciences, Tokyo, Japan, June 15-18, p. 2010, 336-340

[Chawla et al.2002] Chawla N. V., Bowyer K. W., Hall L. O., 2002, Kegelmeyer W. P., SMOTE: Synthetic Minority Over-sampling Technique, Journal of Artificial Intelligence Research, Vol. 16, p. 321-357, doi:10.1613/jair.953

[Chen & Guestrin2016] Chen T., Guestrin C., 2016, XGBoost: A Scalable Tree Boosting System, Proceedings of the 22nd ACM SIGKDD International Conference on Knowledge Discovery and Data Mining - KDD '16, doi:10.1145/2939672.2939785

[Danielski2014] Danielski C., 2014, Optimal Extraction Of Planetary Signal Out Of Instrumental and Astronphysical Noise, PhD Thesis, University of London(UCL)

[Dayal et al.2015] Dayal P., Cockell C., Rice K., Mazumdar A., 2015, The Quest for Cradles of Life: Using the Fundamental Metallicity Relation to Hunt for the Most Habitable Type of Galaxy, apjl, Vol. 810, Number 1, p. L2, doi:10.1088/2041-8205/810/1/L2

[Debray & Wu2013] Debray A., Wu R., 2013, Astronomical Implications of Machine Learning, http://cs229.stanford.edu/proj2013

[Eckart & Young1936] Eckart C., Young G., 1936, The approximation of one matrix by another of lower rank, Psychometrika Vol. 1, Number 3, p. 211-218, doi:10.1007/BF02288367

[Fischer et al.2014] Fischer D. A., Howard A. W., Laughlin G. P., Macintosh B., Mahadevan S., Sahlmann J., Yee J. C., 2014, Exoplanet Detection Techniques, Protostars and Planet VI, University of Arizona Press, Tucson, p.715-737, doi:10.2458/azu_uapress_9780816531240-ch031

[Gonzalez, Brownlee & Ward2001] Gonzalez G., Brownlee D., Ward P., 2001, The Galactic Habitable Zone: Galactic Chemical Evolution, Icarus, Vol. 152, Number 1, p. 185-200, doi:10.1006/icar.2001.6617

[Green et al.2015] Green G. M. et al., 2015, A Three-dimensional Map of Milky Way Dust, apjl, Vol. 810, Number 1, p. 25, doi:10.1088/0004-637x/810/1/25

[Heller & Armstrong2014] Heller R., Armstrong J., 2014, Superhabitable Worlds, Astrobiology, Volume 14, Issue 1, p. 50-66, doi:10.1089/ast.2013.1088

[Hestenes1958] Hestenes M. R., 1958, Inversion of Matrices by Biorthogonalization and Related Results, Journal of the Society for Industrial and Applied Mathematics, Vol. 6, Number 1, p. 51-90, doi:10.1137/0106005

[Hassanat et al.2014] Hassanat A. B., Abbadi M. A., Altarawaneh G. A., Alhasnat A. A., 2014, Solving the Problem of the K Parameter in the KNN Classifier Using an Ensemble Learning Approach, preprint(arxiv:1409.0919v1)

[Kaltenegger et al.2011] Kaltenegger L, Udry S., Pepe F, A Habitable Planet around HD 85512?, preprint(arXiv:1108.3561)

[Hsu, Chang & Lin2016] Hsu C. W., Chang C. C., Lin C. J., 2016, A Practical Guide to Support Vector Classification, url:http://www.csie.ntu.edu.tw/ cjlin/papers/guide/guide.pdf

[Huang1959] Huang, S. S., 1959, The Problem of Life in the Universe And the Mode of Star Formation, Publications of the Astronomical Society of the Pacific, Vol. 71, Number 422, p. 421, url:http://stacks.iop.org/1538-3873/71/i=422/a=421

[Irwin et al.2014] Irwin L. N., Méndez A., Fairén A. G., Schulze-Makuch D., 2014, Assessing the Possibility of Biological Complexity on Other Worlds, with an Estimate of the Occurrence of Complex Life in the Milky Way Galaxy, Challenges, Vol. 5, Number 1, p. 159-174, doi:10.3390/challe5010159

[Irwin & Schulze-Makuch2011] Irwin L. N., Schulze-Makuch D., 2011, Cosmic Biology: How Life Could Evolve on Other World, Springer-Praxis, New York, ISBN-13:978-1441916464

[Kasting1993] Kasting, J. F., 1993, Earth's Early Atmosphere, Science, Vol. 259, Number 5097, p. 920-926, doi:10.1126/science.11536547

[Ridden-Harper et al.2016] Ridden-Harper A. R. et al., 2016, Search for an exosphere in sodium and calcium in the transmission spectrum of exoplanet 55 Cancri e, A&A, Vol. 593, p. A129, doi:10.1051/0004-6361/201628448

[McCauliff et al.2014] McCauliff S. D. et.al., 2015, Automatic Classification of Kepler Planetary Transit Candidates, apjl, Vol. 806, Number 1, p. 6, doi:10.1088/0004-637X/806/1/6

[Méndez2011] Méndez A., 2011, A Thermal Planetary Habitability Classification for Exoplanets, University of Puerto Rico at Arecibo, url:http://phl.upr.edu/library/notes/athermalplanetaryhabitabilityclassi ficationforexoplanets

[Méndez2015] Méndez A. et al., 2015, PHL's Exoplanet Catalog of the Planetary Habitability Laboratory at University of Puerto Rico at Arecibo,

http://phl.upr.edu/projects/habitable-exoplanets-catalog/data/database, as accessed in June 2015

[Méndez2016] Méndez A. et al., 2016, PHL's Exoplanet Catalog of the Planetary Habitability Laboratory at University of Puerto Rico at Arecibo, http://phl.upr.edu/projects/habitable-exoplanets-catalog/data/database, as accessed on 20th May 2016

[Parzen1962] Parzen E., 1962, On Estimation of a Probability Density Function and Mode. Annals of Mathematical Statistics, 33, no. 3, 1065-1076. doi:10.1214/aoms/1177704472

[Pedregosa et al.2011] Pedregosa F. et al., 2011, Scikit-learn: Machine Learning in Python, Journal of Machine Learning Research, Vol. 12, p. 2825-2830

[Peng, Zhang & Zhao2013] Peng N., Zhang Y., Zhao Y., 2013, A SVM-kNN method for quasar-star classification, Science China Physics, Mechanics and Astronomy, Volume 56, Number 6, p. 1227-1234, doi:10.1007/s11433-013-5083-8

[Powell1977] Powell M. J. D., 1977, Restart procedures for the conjugate gradient method, Mathematical Programming, Vol. 12, Number 1, p. 241-254, doi:10.1007/BF01593790

[Quinlan1986] Quinlan J. R., Induction Of Decision Trees, Machine Learning, Vol. 1, Number 1, p. 81-106, doi:10.1007/BF00116251

[Rish2001] Rish I., An Empirical Study Of Naive Bayes Classifier, In IJCAI 2001 Workshop on Empirical Methods in Artificial Intelligence, New York: IBM, Vol. 3, Number 22, p. 41-46

[Roesnblatt1956] Rosenblatt M., 1956, Remarks on some nonparametric estimates of a density function, Annals of Mathematical Statistics, 27: 832-837.

[Saha et al.2015] Saha S., Agrawal S., Manikandan R., Bora K., Routh S., Narasimhamurthy A., 2015, ASTROMLSKIT: A New Statistical Machine Learning Toolkit: A Platform for Data Analytics in Astronomy, preprint(arXiv:1504.07865)

[Saha et al.2016] Saha S., Sarkar J., Dwivedi A., Dwivedi N., Narasimhamurthy A. M., Roy R., 2016, A novel revenue optimization model to address the operation and maintenance cost of a data center, Journal of Cloud Computing, Vol. 5, Number 1, doi: 10.1186/s13677-015-0050-8

[Sale2015] Sale S. E., 2015, Three-dimensional extinction mapping and selection effects, MNRAS, Vol. 452, No. 3, p. 2960-2972, doi:10.1093/mnras/stv1459

[Schulze-Makuch et al.2011] Schulze-Makuch D. et al., 2011, A Two-Tiered Approach to Assessing the Habitability of Exoplanets, Astrobiology, Vol. 11, Number 10, p. 1041-1052, doi:10.1089/ast.2010.0592

[Soutter2012] Soutter J. L., 2012, Finding Exoplanets Around Eclipsing Binaries: A Feasibility Study using Mt Kent and Moore Observations, thesis, University of Southern Queensland, url:https://eprints.usq.edu.au/23220/

[Strigari et al.(2012)] Strigari L. E., Barnabè M., Marshall P. J., Blandford R. D., 2012, Nomads of the Galaxy, mnras, Vol. 423, Number 2, p. 1856-1865, doi:10.1111/j.1365-2966.2012.21009.x

[Theophilus, Reddy & Basak2016] Theophilus A. J., Reddy M., Basak S., ExoPlanet, Astrophysics Source Code Library (submitted), url:http://ascl.net/code/v/1475

[Swift et al.2013] Swift J. J., Johnson J. A., Morton T. D., Crepp J. R., Montet B. T., Fabrycky D. C., Muirhead P. S., 2013, Characterizing the Cool KOIs IV: Kepler-32 as a prototype for the formation of compact planetary systems throughout the Galaxy, apj, Vol. 764, Number 1, p. 105, doi:10.1088/0004-637X/764/1/105

[Waldmann & Tinetti2012] Waldmann I. P., Tinetti G., 2012, Exoplanetary spectroscopy using unsupervised machine learning, European Planetary Science Congress, EPSC2012-195

[Welling2005] Welling M., 2005, Fischer Linear Discriminant Analysis, Department Of Computer Science, University Of Toronto, url:https://www.ics.uci.edu/ welling/teaching/273ASpring09/Fisher-LDA.pdf

[Öberg et al.2015] Öberg, K. I., Guzmán, V. V., Furuya, K., et al., 2015. The comet-like composition of a protoplanetary disk as revealed by complex cyanides. nat, 520, 198

[Cassan et al.2012] Cassan, A., Kubas, D., Beaulieu, J.-P., et al., 2012. One or more bound planets per Milky Way star from microlensing observations. nat, 481, 167

[Huang1959] Huang, S.-S., 1959. The Problem of Life in the Universe And the Mode of Star Formation. *Publications of the Astronomical Society of the Pacific*, 71, 421

[Wittenmyer et al.2014] Wittenmyer, R. A., Tuomi, M., Butler, R. P., et al., 2014. GJ 832c: A Super-Earth in the Habitable Zone. apj, 791, 114

[Nemirovski & Todd2008] Nemirovski, Arkadi S., and Todd, M. J., 2008. Interior-point methods for optimization. *Acta Numerica*, 17, 191. doi:10.1017/S0962492906370018.

[Hájková & Hurnik2007] Hájková, D. and Hurnik, J., 2007. Cobb-Douglas: The Case of a Converging Economy, *Czech Journal of Economics and Finance (Finance a uver)*, 57, 465

[Wu2001] Wu, D.-M., 1975. Estimation of the Cobb-Douglas Production Function. *Econometrica*, 43, 739. http://doi.org/10.2307/1913082

[Hossain et al.2012] Hossain, M., Majumder,A. & Basak, T., 2012. An Application of Non-Linear Cobb-Douglas Production Function to Selected Manufacturing Industries in Bangladesh. *Open Journal of Statistics*, 2, 460, doi: 10.4236/ojs.2012.24058

[Hassani2012] Hassani, A., 2012. Applications of Cobb-Douglas Production Function in Construction Time-Cost Analysis (M.Sc. thesis). University of Nebraska, Lincoln.

[Anglada-EscudÃl'2016] Anglada-Escudé G. et al., 2016. A terrestrial planet candidate in a temperate orbit around Proxima Centauri. *Nature*, 536, 437-440.

[Witze2016] Witze, A. 2016. Earth-sized planet around nearby star is astronomy dream come true. *Nature*, 536, 381-382.

[Starshot] Breakthrough Starshot. "A Russian billionaire has a crazy plan to reach a nearby planet that might harbor life". http://www.businessinsider.in. Retrieved 12 2016.

[Trappist-1] http://exoplanet.eu/catalog/trappist-1_c/, as accessed on Feb 25, 2017.

[cobb-douglas] Cobb, C. W. and Douglas, P. H., 1928. A Theory of Production. *American Economic Review*, 18 (Supplement), 139.

[rogers2014] Rogers, L. A., 2014. Most 1.6 Earth-radius Planets are Not Rocky. *Ap. J.*, 801:1, 41.

[Agrawal1993] Agrawal, R., Imielinski, T. and Swami A., Mining Association Rules between Sets of Items in Large Databases. In Proc. 1993 ACM SIGMOD International Conference on Management of Data, Washington DC (USA), pp. 207-216.

[Agrawal 1994] Agrawal, R., Srikant, R.1994. Fast Algorithms for Mining Association Rules in Large Databases. In Proc. 20th International Conference on Very Large Data Bases (VLDB '94), Jorge B. Bocca, Matthias Jarke, and Carlo Zaniolo (Eds.). (Morgan Kaufmann Publishers Inc., San Francisco, CA, USA), 487-499.

[Ginde2016] Ginde, G., Saha, S., Mathur, A., Venkatagiri, S., Vadakkepat, S., Narasimhamurthy, A., B.S. Daya Sagar., 2016. ScientoBASE: A Framework and

Model for Computing Scholastic Indicators of Non-Local Influence of Journals via Native Data Acquisition Algorithms. *J. Scientometrics*, 107:1, 1-51

[Nicholas et al.2010] Nicholas M. Ball & Robert J. Brunner 2010, Overview of Data Mining and Machine Learning methods. Retrieved on 25-04-16, from http://ned.ipac.caltech.edu/level5/March11/Ball/Ball2.html

[Davis et al.2007] T. M. Davis, E. Mortsell, J. Sollerman, A. C. Becker, S. Blondin, P. Challis, A. Clocchiatti, A. V. Filippenko, R. J. Foley, P. M. Garnavich, S. Jha, K. Krisciunas, R. P. Kirshner, B. Leibundgut, W. Li, T. Matheson, G. Miknaitis, G. Pignata, A. Rest, A. G. Riess, B. P. Schmidt, R. C. Smith, J. Spyromilio, C. W. Stubbs, N. B. Suntzeff, J. L. Tonry and W. M. Wood-Vasey 2007, Scrutinizing Exotic Cosmological Models Using ESSENCE Supernova Data Combined with Other Cosmological Probes. Astrophys.J, 666:716-725, DOI: 10.1086/519988

[Riess et al.2007] Riess et al. 2007, New Hubble Space Telescope Discoveries of Type Ia Supernovae at z > 1: Narrowing Constraints on the Early Behavior of Dark Energy. Astrophys.J, 659:98-121, DOI: 10.1086/510378

[Wood-Vassey et al.2007] Wood-Vassey et al. 2007, âĂIJObservational Constraints on the Nature of the Dark Energy: First Cosmological Results from the ESSENCE Supernova SurveyâĂİ, Astrophys.J, 666:694-715, DOI: 10.1086/518642

[Davis et al.] Type Ia supernova data used by Davis, MÃűrtsell, Sollerman, et al. 2007, Retrieved from http://dark.dark-cosmology.dk/ tamarad/SN/

[Fraser] Fraser Cain 2016, What are the Different Kinds of Supernovae?, retrieved on 20-04-2016, from http://www.universetoday.com/127865/what-are-the-different-kinds-of-supernovae/

[supernova tutorial] Type I and Type II Supernovae, retrieved on 20-04-2016, from http://hyperphysics.phy-astr.gsu.edu/hbase/astro/snovcn.html#c3

[Philipp] Philipp Podsiadlowski, Supernovae and Gamma Ray Bursts, Department of Astrophysics, University of Oxford, Oxford, OX1 3RH, UK retrieved from http://www-astroṗhysicsȯxȧcůk/ podsi/sn_podsiṗdf

[Phillips93] Phillips, M.M. The absolute magnitudes of Type IA supernovae. Astrophys. J, 413 , L105 1993

[Abazajian et al.(2009)] Abazajian KN, Adelman-McCarthy JK, Agüeros MA, et al. 2009, apjs, 182, 543-558

[Adelman-McCarthy et al.(2008)] Adelman-McCarthy JK, Agüeros MA., Allam SS, et al. 2008, apjs, 175, 297-313

[Ahn et al.(2013)] Ahn CP, Alexandroff R, Prieto CA, Anderson SF, Anderton T and Andrews BH. 2013, The ninth data release of the Sloan Digital Sky Survey: first spectroscopic data from the SDSS-III Baryon Oscillation Spectroscopic Survey, 203, 1-14.

[Basak et al.(2016)] Basak S, Saha S et al., 2016, Star Galaxy Separation using Adaboost and Asymmetric Adaboost, DOI: 10.13140/RG.2.2.20538.59842, 10/2016.

[Breiman(1996)] Breiman L, 1996, Bagging predictors. In Machine Learning, pages 123-140.

[Elting et al.(2008)] Elting C, Bailer-Jones CAL and Smith KW, 2008, Photometric Classification of Stars, Galaxies and Quasars in the Sloan Digital Sky Survey DR6 Using Support Vector Machines, AIP Conference Proceedings, Volume 1082, Issue 1.

[Freund & Schapire(1996)] Freund Y and Schapire RE, 1996, Experiments with a New Boosting algorithm. In Proceedings of the Thirteenth International Conference on Machine Learning, Page 148 - 156.

[Gao et al.(2008)] Gao D, Zhang Y and Zhao Y, 2008, Support vector machines and kd-tree for separating quasars from large survey data bases. Monthly Notices of the Royal Astronomical Society, 386: 1417-1425.

[Pedregosa et al.(2011)] Pedregosa F et al., 2011, Scikit-learn: Machine Learning in Python, Journal of Machine Learning Research, 12, 2825-2830.

[Peng et al.(2013)] Peng N, Zhang Y & Zhao Y, 2013, Sci. China Phys. Mech. Astron., 56: 1227.

[Vázquez & Alba-Castro(2015)] Vázquez IL and Alba-Castro JL, 2015, Revisiting AdaBoost for Cost-Sensitive Classification. Part I: Theoretical Perspective. CoRR, abs/1507.04125.

[Vázquez & Alba-Castro(2012)] Vázquez IL and Alba-Castro JL, 2012, Shedding light on the asymmetric learning capability of adaboost. Pattern Recogn. Lett., 33(3):247-255.